LBL-21896 c.2
Preprint

Lawrence Berkeley Laboratory
UNIVERSITY OF CALIFORNIA

Materials & Molecular Research Division

RECEIVED
LAWRENCE
BERKELEY LABORATORY

SEP 3 1986

LIBRARY AND
DOCUMENTS SECTION

Submitted to Journal of Chemical Physics

THE ELECTRONIC STATE-SELECTIVE PHOTODISSOCIATION OF CH_2BrI AT 248, 210, AND 193 nm

L.J. Butler, E.J. Hintsa, S.F. Shane and Y.T. Lee

July 1986

TWO-WEEK LOAN COPY
This is a Library Circulating Copy
which may be borrowed for two weeks.

LBL-21896 c.2

Prepared for the U.S. Department of Energy under Contract DE-AC03-76SF00098

DISCLAIMER

This document was prepared as an account of work sponsored by the United States Government. While this document is believed to contain correct information, neither the United States Government nor any agency thereof, nor the Regents of the University of California, nor any of their employees, makes any warranty, express or implied, or assumes any legal responsibility for the accuracy, completeness, or usefulness of any information, apparatus, product, or process disclosed, or represents that its use would not infringe privately owned rights. Reference herein to any specific commercial product, process, or service by its trade name, trademark, manufacturer, or otherwise, does not necessarily constitute or imply its endorsement, recommendation, or favoring by the United States Government or any agency thereof, or the Regents of the University of California. The views and opinions of authors expressed herein do not necessarily state or reflect those of the United States Government or any agency thereof or the Regents of the University of California.

THE ELECTRONIC STATE-SELECTIVE PHOTODISSOCIATION OF CH_2BrI AT 248, 210, AND 193 nm

L. J. Butler,* E. J. Hintsa, S. F. Shane, and Y. T. Lee

Materials and Molecular Research Division
Lawrence Berkeley Laboratory and
Department of Chemistry, University of California
Berkeley, California 94720 USA

ABSTRACT

The primary photodissociation channels of CH_2BrI following excitation at 193.3, 210, and 248.5 nm have been studied with the crossed laser-molecular beam technique. Product translational energy distributions and polarization dependences were derived for the primary dissociation processes observed. The data demonstrate bond selective photochemistry as well as some selective formation of electronically excited photofragments in bond fission and concerted dissociation. Excitation at 248.5 nm, which is assigned to excitation of primarily a n(I) $\rightarrow$ σ^*(C-I) transition with some contribution from an overlapping n(Br) $\rightarrow$ σ^*(C-Br) transition, results in both C-I and C-Br bond fission. C-I bond fission is the dominant channel, producing I atoms in both the $^2P_{3/2}$ and spin-orbit excited $^2P_{1/2}$ states in a ratio of 1.0:0.75. Excitation at 193.3 nm, assigned to a transition to primarily predissociated Rydberg levels on the I atom, leads to C-Br bond fission, some

*Present Address: Department of Chemistry, University of Wisconsin, Madison, WI 53706 USA.

C-I bond fission, and significant concerted elimination of IBr. Analysis of the product translational energy distributions for the dissociation products indicates that the IBr is formed electronically excited and that the halogen atom products are spin-orbit excited. Excitation at 210 nm, of the transition assigned as n(Br) $\rightarrow$ σ^*(C-Br) based on comparison with CH_3Br, results in selective breaking of the stronger C-X bond in the molecule, the C-Br bond, and no fission of the C-I bond. Some concerted elimination of IBr also occurs; the IBr velocity distribution indicates it is probably formed electronically excited as in photolysis at 193.3 nm. The selective breaking of the C-Br bond over the weaker C-I bond is discussed in contrast to previous photolysis studies of polyhalomethanes.

INTRODUCTION

The photodissociation of CH_2BrI was undertaken to investigate how the electronic nature of a particular state excited in a molecule influences the product channels by which the molecule dissociates. CH_2BrI has three distinct types of electronic transitions at wavelengths longer than 190 nm which are separated in frequency as shown in Figure 1. The spectrum consists of a broad band peaking near 270 nm which is assigned to the promotion of a nonbonding electron on the iodine to an antibonding orbital on the C-I bond, a broad band peaking near 215 nm assigned to promotion of a nonbonding electron on the Br atom to an antibonding orbital on the C-Br bond, and sharp features around 190 nm corresponding to Rydberg transitions on the I atom. These assignments are made based on comparison with the spectra of CH_3I and CH_3Br. The features of CH_2BrI are similar in shape to the analogous transitions observed in CH_3I and CH_3Br, but the broad bands are considerably more intense and shifted slightly to the red. The ultraviolet spectrum of CH_2BrI from 200 nm to 350 nm has been previously recorded by Lee and Bersohn.[1] They attributed the shift in the absorption bands to the fact that the central carbon atom has more positive charge than it does in a monohalomethane, thus stabilizing the antibonding orbitals.

Two recent studies of bromo-iodo alkanes are particularly relevant to this study. Lee and Bersohn[1] investigated the photodissociation of CH_2BrI with a broadband light source extending from 240 to 340 nm with a full width of half maximum (FWHM) of approximately 40 nm. They

measured the mass spectrum of dissociation fragments and reported signal at I^+, Br^+, CH_2Br^+, and CH_2I^+, but not at IBr^+. From their integrated signal at I^+ and Br^+, they derived the branching ratio between C-I and C-Br bond fission to be 6:1. The anisotropy of the I atom angular distribution showed a parallel dependence on the direction of the electric vector of the dissociating light. It was concluded that excitation in the n(I) $\rightarrow$ σ^*(C-I) band promotes only C-I bond fission; the C-Br fission was attributed to the bandwidth of the light partially overlapping the absorption band of the n(Br) $\rightarrow$ σ^*(C-Br) transition. The dissociation pathways were also suggested to be critically sensitive to the electronic nature of the initial excitation.

A recent study of the photodissociation of C_2F_5Br, C_2F_5I, and 1,2-C_2F_4BrI by Krajnovich et al.[2] investigated product channels resulting from excitation in the n(I) $\rightarrow$ σ^*(C-I) and in the n(Br) $\rightarrow$ σ^*(C-Br) absorption bands. When 1,2-C_2F_4BrI was excited at 248 nm and 266 nm, only C-I bond fission was observed as a primary dissociation channel as expected, and most or all of the iodine product was spin-orbit excited $I(^2P_{1/2})$. When the molecule was dissociated at 193 nm, some of the molecules underwent primary C-I bond fission and some underwent primary C-Br bond fission in a ratio of approximately 1.7:1. The results were interpreted in terms of a fast electronic energy transfer between the C-Br and C-I bonds after a local excitation of the C-Br bond at 193 nm. This interpretation was consistent with the polarization dependences, which showed that both bond fission channels resulted from a dipole transition moment aligned parallel to

the breaking bonds, because the C-I and C-Br bonds are nearly parallel in 1,2-C_2F_4BrI.[3]

CH_2BrI was chosen as a model system for three specific reasons. First, the n $\rightarrow$ σ^* transitions of the C-I and C-Br bonds are resolved despite the shared carbon. Second, the angle between the C-I and C-Br bond is strongly bent, potentially allowing us to use the polarization dependences of the dissociation channels to identify the particular electronic transition which resulted in each dissociation channel. Third, the molecule is small and the energetics relevant to the dissociation channels are fairly well known as shown in Figure 2,[4] so primary dissociation events can be distinguished from secondary or three-body dissociation events (where the final products are CH_2 + Br + I). Care should be taken in comparing the experimental results on CH_2BrI to those on 1,2-C_2F_4BrI. The absorption bands due to the n $\rightarrow$ σ^* transitions are shifted to longer wavelengths in CH_2BrI so, for instance, excitation at 193 nm promotes a n(Br) $\rightarrow$ σ^*(C-Br) transition in 1,2-C_2F_4BrI but promotes a Rydberg transition in CH_2BrI; one must excite CH_2BrI at 210 nm to excite the n(Br) $\rightarrow$ σ^*(C-Br) transition.

EXPERIMENTAL

The molecular beam photofragmentation apparatus has been previously described in detail.[5] The molecular beam was formed by bubbling argon through a reservoir of CH_2BrI (Fairfield Chemical) maintained at 18°C. A total stagnation pressure of 300 torr was used

(5 torr CH_2BrI, 295 torr Ar) behind a 0.125 mm diameter nozzle. The nozzle was heated to 135°-140°C to reduce the formation of clusters in the beam. The peak velocity of the molecular beam was typically 6.15 ± 0.07 x 10^4 cm/sec with a FWHM of about 10 percent. The beam passed through two skimmers and two differential pumping regions, the second skimmer defining the beam to a full angular divergence of 2.3° before the molecular beam crossed the laser 74 mm from the nozzle. At the crossing point the beam diameter was 3 mm. The beam source is rotatable in a plane containing the detector and perpendicular to the laser beam.

All the optical setups are described in detail in Reference 6. For the experiments at 193 and 248 nm using unpolarized light, the photodissociating light source was arranged as follows. The light from a Lambda Physik EMG 103MSC excimer laser operated at 100-150 Hz with ArF and KrF gas mixtures was focused onto the interaction region of the molecular beam to an oblong 3 mm by 1 mm spot with a 240 mm focal length (f.l.) magnesium fluoride lens. Since the electric vector of the laser is isotropic in the source detector plane, the c.m. angular distribution of scattered product must then by symmetry be isotropic in the source-detector plane, whether the absorption is anisotropic or not. Laser pulse energies at 193 nm were typically 100-150 mJ/pulse and at 248 nm were ~200 mJ/pulse, with specified pulse widths of 17 and 25 nsec respectively.

The photons for the 210 nm experiments were obtained by Raman shifting the 193 nm output of a Lambda Physik 102E excimer laser

equipped with unstable resonator optics using H_2 gas. The 210 nm Stokes shifted light, after dispersion with a quartz Pellin-Broca prism, was directed along the axis of rotation of the beam source and focused onto the interaction region with a 240 mm f.l. MgF_2 lens to a ~3 mm^2 spot. Typical pulse energies produced were 2 mJ/pulse of 210 nm light from 55 mJ/pulse of 193 nm input energy to the Raman cell. The 210 nm light is primarily unpolarized as is the fundamental, but the horizontal component is transmitted more easily through the entrance and exit surfaces of the Pellin-Broca resulting in the horizontal component having ~60 percent of the energy and the vertical having ~40 percent.

The excimer laser was polarized for the measurements of anisotropy at all three wavelengths by passing the beam through a birefringent prism. The two output beams were >99.9 percent linearly polarized in orthogonal directions. Light with the desired polarization was directed along the axis of rotation of the beam source with a prism. At 193 nm, data was obtained with both unpolarized and horizontally polarized light ($\vec{E}$ vector pointing along the line between the crossing point of the beams and the detector), allowing the anisotropy to be derived from the intensity of scattered product at each center-of-mass recoil angle within each photofragment time-of-flight spectrum. For the experiment at 210 nm, either the horizontally or the vertically polarized light could be directed to the interaction region of the laser and molecular beam while the apparatus was under vacuum. The data were thus taken with each polarization under exactly the same

experimental conditions. Because the horizontally polarized light is better transmitted by the Pellin-Broca, only the shapes of the time-of-flight data, not the total signal intensities, can be compared for the two polarizations unless one performs additional normalization to the photon intensity. For the anisotropy measurements at 248 nm, the two linearly polarized components of the excimer laser were dispersed by the quartz Pellin-Broca and the horizontal component was reoriented through a first-order half-wave retarder from Karl Lambrecht Co. The intensity of scattered product was measured as a function of the direction of the electric vector in the source detector plane. The purity of rotation of the light was checked by resolving the light after the rotator into its vertical and horizontal components with a MgF_2 prism. When the optical axis of the rotator was parallel with the electric vector ($\vec{E}$) of the horizontally polarized incoming light, the vertical component of the outgoing light completely disappeared. When the half wave retarder was rotated by 45° (rotates $\vec{E}$ vector by 90°) the horizontal component of the outgoing light disappeared completely.

Neutral dissociation products formed at the crossing point of the laser and molecular beam travel 36.6 cm to an electron bombardment ionizer. The products passed through a set of defining slits mounted on the walls of the differentially pumped detector chamber and were ionized by 120 eV electrons. The ions were mass selected with a quadrupole mass spectrometer and counted with a Daly detector and a multichannel scaler with respect to their flight time from the inter-

action region after the dissociating laser pulse. All time-of-flight (TOF) data presented for 248 nm unpolarized and 193 nm excitation wavelengths were signal averaged over at least 200,000 laser shots each. The TOF data taken with 210 nm and polarized 248 nm light (with the lower repetition 102E laser) were averaged for at least 50,000 counts each. Typical signal levels at 193 nm ranged from 0.008 counts/laser pulse at CH_2Br^+ to 2.2 counts/laser pulse at I^+.

The polarization dependence measurements at 248 nm of the I^+ and CH_2I^+ signals were carefully executed to average out laser power differences between laser gas fills and within each gas fill. Nine separate data averaging periods of 7,500 laser shots each for CH_2I^+ and 6,000 laser shots each for I^+ were summed for each of the nine electric vector positions to obtain the angular distibution data shown in this paper. The order of signal accumulation in the gas fill for each polarization angle was varied to average out the 2-15 percent change in laser power between the beginning and the end of each gas fill. Because of these averaging techniques, no additional normalization to laser power was needed at the various polarization angles.

RESULTS AND ANALYSIS:

I. Photodissociation of CH_2BrI at 248 nm

A. $$CH_2BrI \xrightarrow{248\ nm} CH_2Br + I(^2P_{3/2}) \quad (1a)$$
$$\rightarrow CH_2Br + I(^2P_{1/2}) \quad (1b)$$

The time-of-flight (TOF) spectra of m/e=95, $CH_2{}^{81}Br^+$, and m/e=127, I^+, are shown in Figures 3 and 4, respectively. Both sets of TOF spectra show two narrow and fast overlapping product distributions, as well as a slow hump with a peak flight time of ~650 μsec at small laboratory angles. The I^+ TOF spectra also show a broad underlying signal. The slow hump at 650 μsec is from dissociation of dimers in the molecular beam (see Section I.E) and the broad underlying signal in the I^+ TOF's is due to secondary photodissociation of CH_2I product (see Section I.G). The two sharp peaks in the I^+ and CH_2Br^+ TOF spectra are I and CH_2Br products from C-I bond fission, the faster of the pair being from bond fission producing $I(^2P_{3/2})$ and the slower one from fission producing $I(^2P_{1/2})$. This assignment follows from the fact that the products from fission giving spin-orbit excited iodine atoms must channel 21.7 kcal/mole (the spin-orbit splitting of iodine) of the total available energy into electronic energy. Hence, less energy is available for translation and internal motion and these products have smaller center-of-mass recoil velocities and longer arrival times in the TOF spectra.[7] Dissociation to each spin-orbit state is shown in Section I.H to have the same anisotropy in the product angular distribution.

The center-of-mass product recoil translational energy distribution, $P(E_T)$, for C-I bond fission in CH_2BrI excited at 248 nm can be derived from forward convolution fitting of either the CH_2Br^+ TOF or the sharp peaks in the I^+ TOF, as the CH_2Br and I center-of-mass (c.m.) product velocities are related simply by momentum conservation. The CH_2Br^+ TOF was used initially as it is not complicated by underlying signal from secondary dissociation. The $P(E_T)$ shown in Figure 5 gives the solid line fit shown in Figure 3. In order to determine a product channel branching ratio, this total $P(E_T)$ must be divided into two component translational energy distributions, one for production of each spin-orbit state of the I atom. This was done approximately by constraining the shape of each $P(E_T)$ to be similar. Although there is clearly uncertainty in the shape of the $P(E_T)$'s in the overlapping region, there is little uncertainty in the total area under each component $P(E_T)$, which determines the product channel branching ratio. Production of ground state iodine is clearly the favored channel. The $P(E_T)$'s and their fits shown in Figs. 3 and 4 give the relative probability of producing spin-orbit excited I atoms to ground state I atoms in the primary bond fission to be 0.75:1.

The derivation of the branching ratio between reactions 1a and 1b from the data is dependent on the ionization cross section of $I(^2P_{1/2})$ being the same as that of $I(^2P_{3/2})$. This was explicitly checked with our ionizer conditions by photodissociating CF_3I at 248 nm and checking that the same weighting of the two dissociation channels (~7 percent $I(^2P_{3/2})$ is formed) fit both the CF_3^+ and the I^+ TOF spec-

tra. Similar insensitivity of the ionization efficiency to the spin-orbit excitation of I has been noted by Gorry and coworkers.[8]

B. $CH_2BrI \xrightarrow{248\ nm} CH_2I + Br\ (^2P_{3/2}, {}^2P_{1/2})$ (2)

The TOF spectra of m/e=141, CH_2I^+, and m/e=81, $^{81}Br^+$, are shown in Figures 6 and 7 respectively. The spin-orbit splitting of Br atoms is 10.54 kcal/mole compared to 21.7 kcal/mole for I atoms, so it is much harder to resolve the two dissociation channels given the width of the product translational energy distribution. The total $P(E_T)$ for C-Br bond fission to CH_2I + Br was derived via fitting of the CH_2I^+ TOF spectrum and is shown in Figure 8. The corresponding fit obtained to the CH_2I product TOF is shown in solid line in Figure 6. There is clearly a little uncertainty in the low energy side of the $P(E_T)$ due to contamination of the CH_2I^+ TOF by signal from dimers (see section I.E). This $P(E_T)$ was then used to predict where signal from the momentum matched Br product would appear in the Br^+ TOF. The predicted Br^+ distribution shown in solid line in Figure 7 matches the shape and position of the spike in the Br^+ signal. Based on the amount of kinetic energy released for those Br atoms appearing in the leading edge of the broad underlying signal, we attribute the underlying signal in these TOF's to secondary photodissociation of some of the CH_2Br product from C-I bond fission. This secondary photodissociation will be discussed later (see Section I.F). It should be noted that some of the faster signal in the sharp peak of the Br^+

TOF spectra could be due to CH_2Br product giving Br^+ in the ionizer, but this contribution must be fairly small or the shape of the fits would not match the shape of the observed peaks.

The relative intensities of the Br atom signal from C-Br bond fission and the I atom signal from C-I bond fission suggest that C-Br bond fission is a minor channel. This will be quantified in Section I.I.

C. Absence of $CH_2BrI \xrightarrow{248\ nm} CHI + HBr$ (3) and

$CH_2BrI \xrightarrow{248\ nm} CHBr + HI$ (4)

Two independent techniques were used to check for the possibility of concerted dissociation channels forming HI or HBr. First we looked for signal at HI^+ and at $H^{81}Br^+$ (see ref. 6 for more detail). Second, we looked for differences in the spectra of CH_2I^+ and CHI^+ and of $CH_2{}^{81}Br^+$ and $CH^{81}Br^+$. CHBr would contribute to the $CH^{81}Br^+$ but not to the $CH_2{}^{81}Br^+$ TOF (and likewise for CHI). The TOF spectra taken at m/e=128, I^+, and m/e=82, $H^{81}Br^+$, show no appreciable signal at HI^+ and at HBr^+. The similarity of the CHI^+ spectrum (shown in Fig. 9) to the CH_2I^+ spectrum affirm that no HBr production is evident. Similarly there is no evidence for HI production, as there is no signal at HI^+ and the TOF spectra of $CH^{81}Br^+$ and $CH_2{}^{81}Br^+$ shown in Figures 9 and 3 are indistinguishable.

D. Search for $CH_2BrI \xrightarrow{248\ nm} CH_2 + IBr$

The TOF spectrum of m/e=206 and 208, IBr^+, is shown in Figure 10. The signal is so low that one cannot discount the possibility that this signal is due to dimers. We searched for evidence of this concerted reaction in two other ways. Fast signal arriving earlier than 100 μsec was observed in the CH^+ TOF, Figure 11, but it was not correctly related to the IBr^+ signal by momentum conservation (this signal is due to CH_2 from the secondary photodissociation of CH_2Br and CH_2I as will be shown in Sections I.F and I.G). One can predict where the CH_2 should appear in the CH^+ TOF via conservation of momentum with the observed IBr^+ signal; the predicted CH_2 arrival times are shown by the fastest broad hump between 100 and 200 usec in the CH^+ spectrum. There is no significant signal there. In addition, there is no evidence for IBr in the I^+ TOF spectra; at 10° (Figure 4) the peak would arrive at ~500 μsec, between the signal from C–I bond fission and the hump from dimer contamination. Thus the signal at IBr^+ is probably due to clusters in the beam. Note that if any IBr were formed with a total translational energy release of less than ~4.4 kcal/mole it would not recoil away from the molecular beam with a large enough velocity to be detected at angles larger than 10° from the beam. The CH_2 product from $CH_2BrI \rightarrow CH_2 + IBr$ could however be detected at 20° with as little as 0.04 kcal/mole release to translation, but might be difficult to pick out in the congested CH^+ spectrum.

E. Identification of Signal from Dissociation of Dimers in the Molecular Beam.

Although the fraction of CH_2BrI dimers in the molecular beam is probably very small as the nozzle was heated to 135°C, some contamination of the TOF spectra from dissociation of clusters can be observed at small angles. Molecular fragments from clusters usually recoil with small c.m. velocities and thus only appear in a small laboratory angular range about the molecular beam. Although their signal is often not observed at large angles, we are particularly sensitive to them at smaller angles because the products are concentrated in a small angular and velocity range.

TOF spectra of m/e=81 and 127 at 10° and m/e=94 at 20° obtained with a lower concentration of clusters in the beam by using a lower seeding ratio are shown in Figure 12. Under the new beam conditions all the signal is substantially reduced because the beam intensity is weaker, but the ratio of monomers to clusters in the molecular beam is significantly increased. Thus any signal from clusters will be reduced in relative intensity. Comparing the m/e=127 TOF at 10° in Figure 12 with that in Figure 4, one sees that the feature near 650 μsec is clearly due to dissociation of clusters. Likewise, comparison of Figure 9 and Figure 12 shows that the spectrum of m/e=94 in Figure 9 contains signal from dimers around 650 μsec. The m/e=81 spectrum shows no change, however. The slow signal in this spectrum, as will be shown in the next section, is due to Br from secondary dissociation of CH_2Br.

F. Secondary Photodissociation of $CH_2Br \xrightarrow{248\ nm} CH_2 + Br$ (5)

The TOF at m/e=81, $^{81}Br^+$ (Figure 7) shows broad signal at faster and slower times than the CH_2Br product arrival time (which is toward the fast side of the Br signal from primary C-Br bond fission indicated in solid line). Such a broad underlying signal is characteristic of secondary photodissociation. After primary C-I bond fission requiring 55 kcal/mole, the CH_2Br product cannot be left with enough internal energy to undergo unimolecular dissociation to form CH_2 + Br. Its secondary dissociation must occur via absorption of another photon. In a previous experiment on the photodissociation of CF_2Br_2 at 248 nm,[9] the CF_2Br product from C-Br fission absorbed another photon and dissociated to CF_2 + Br, thus it is not surprising that CH_2Br radicals also absorb at 248 nm and dissociate. When the laser power was reduced by a factor of 5.6 the relative intensity of the broad signal with respect to the primary signal decreased as shown in the low and high power TOF spectra of Br^+ at 20° in Figure 13, thus confirming that the signal is Br product from CH_2Br absorbing a photon and dissociating. The surprisingly small decrease of the broad signal also shows that the secondary absorption is strongly saturated as it was for CF_2Br.

A simple calculation was made to assure that the assignment of the underlying signal in the Br^+ TOF spectrum to reaction (5) is consistent with conservation of energy and momentum. If one asks how much energy would have to go into translation in the dissociation of $CH_2Br \rightarrow CH_2$ +

Br for the Br to reach the shortest observed arrival time of 180 μsec at 10°, one calculates 52 kcal/mole for Br originating from CH_2Br in the peak of the CH_2Br + I translational energy distribution. Whether the two photons absorbed can provide all the necessary energy is easily calculated:

$$\text{Required energy} = E_{T_{I+CH_2Br}} + D_{o_{I-CH_2Br}} + E_{T_{CH_2+Br}} + D_{o_{Br-CH_2}}$$

$$= 19 + 55 + 52 + (75) \approx 201 \text{ kcal/mole}$$

$$2E_{h\nu} = 230 \text{ kcal/mole} > 201 \text{ kcal/mole.}$$

One also calculates that the CH_2 product from the secondary dissociation of CH_2Br which releases 52 kcal/mole to translation would have a total flight time of 67 μsec. This corresponds to within a few μsec of the fast side of the previously unassigned sharp spike in the CH^+ TOF of Figure 11.

G. Secondary Photodissociation of $CH_2I \xrightarrow{248\ nm} CH_2 + I$ (6)

The TOF spectrum of m/e=127, I^+, contains a broad underlying signal which is mainly due to the secondary photodissociation of CH_2I. As was the case for CH_2Br secondary photodissociation, the CH_2I product cannot have enough internal energy after C-Br bond fission to dissociate spontaneously and must dissociate via absorption of another photon.

The shape of the secondary dissociation TOF signal was calculated from a $P(E_T)$ for reaction 6 by summing the recoil velocities of the

primary and secondary decompositions (see ref. 6). A broad $P(E_T)$ peaking at 18 kcal/mol with a full width at half maximum of 20 kcal and a total width ranging from 0 to 40 kcal/mol gave an acceptable fit to the underlying signal shown in Figure 4. Because there are other contributions to these spectra, uncertainty in what signal should be fit is evident. It is, however, certain that the secondary dissociation signal should extend underneath the primary I signal or the relative heights of the two components would not be well fit by the $P(E_T)$ derived for reactions 1a and 1b from the CH_2Br^+ spectra.

H. Anisotropy of the C-I and C-Br Bond Dissociation Channels

The dependence of the I^+ signal from primary C-I bond fission on the direction of the electric vector of the laser, at a molecular beam to detector angle of 20°, is shown in Figure 14a. A polarization angle of 0° corresponds to the $\vec{E}$ vector pointing from the interaction region to the centerline of the detector. The electric vector is rotated in the opposite direction as the source so a polarization angle of 20° at beam to detector angle of 10° corresponds to an angle of 30° with respect to the molecular beam direction. The Newton diagram in the corner of Figure 14a shows that for a given beam to detector angle the peak of the I^+ signal intensity vs polarization angle occurs when the $\vec{E}$ vector is parallel to the peak center-of-mass velocity vector of the I atom fragments which reach the detector.

Zare[10] has derived an expression for the center-of-mass (c.m.) angular distribution of the fragments formed when a molecule absorbs light via an electric dipole transition. The probability, $\omega(\theta)$, of a fragment recoiling in a direction θ from the electric vector of the laser is:

$$\omega(\theta) = {}^{1}/_{4\pi}(1 + \beta P_2(\cos\theta)) \tag{7}$$

The anisotropy parameter β can range from 2, corresponding to a parallel ($\cos^2\theta$) angular distribution, to -1, corresponding to a perpendicular ($\sin^2\theta$) angular distribution. More exact quantum mechanical expressions have followed;[11] in the limit of high relative translational energies of fragments, as is the case for the photodissociation of CH_2BrI at 248 nm, Zare's formula is recovered. If the molecule rotates during dissociation or if bending vibrations change the dissociation direction after absorption of the light, a purely parallel or perpendicular absorption will not result in anisotropies of 2 or -1; the β will be closer to zero.

The anisotropy parameter was derived from fitting of the data as follows. The $P(E_T)$ for each of the C-I bond fission channels is derived from the unpolarized light TOF data which is constrained by symmetry to be independent of the anisotropy. Only the relative heights of the $I(^2P_{1/2})$ and $I(^2P_{3/2})$ signals can be affected. A c.m. to lab transformation with β as the only variable parameter is used to calculate the variation in signal intensity integrated over a specific

range of arrival times as a function of the direction of the electric vector. This is compared to experimental data integrated over the same range of arrival times. For I^+, we integrated the signal between arrival times of 304.5 to 427.5 μsec and approximately subtracted the underlying secondary signal by averaging the secondary signal between 571.5 and 628.5 μsec.

The best fit to the total primary I atom product signal intensity versus polarization direction gives $\beta = 1.0 \pm 0.1$ (the calculated curves are shown in solid line in Figure 14a). It is easily determined that the production of $I(^2P_{1/2})$ and $I(^2P_{3/2})$ each independently has an anisotropy of $\beta = 1.0$. The I^+ TOF data taken with the laser light polarized at 0° and 100° are shown in Figures 14b and c respectively with fits calculated assuming that each channel has an anisotropy of 1.0. Beside them are shown fits assuming the anisotropy of the $I(^2P_{1/2})$ to be 2.0 and the $I(^2P_{3/2})$ to be 0.5 with the relative scaling constrained to also fit the unpolarized light data. Clearly, as shown in the fits, the $I(^2P_{1/2})$ channel with the more parallel angular distribution would be enhanced at a polarization angle of 0° and diminished at a polarization angle of 100° with respect to the less parallel $I(^2P_{3/2})$ channel, although the total intensity versus polarization angle dependence would still approximately fit Figure 14a. Thus, the relative intensities of the $I(^2P_{1/2})$ and $I(^2P_{3/2})$ signal in the polarized light data clearly show that both channels have the same polarization dependence and indicate that they both result

from excitation to an electronic state with the transition moment roughly parallel to the C-I bond.

The polarization dependence of the CH_2I^+ signal at a molecular beam to detector angle of 20° is shown in Figure 15a. The experimental signal was derived from the data by averaging the data between 6 and 150 μsec arrival times to obtain the background and subtracting it from the total signal intensity between 330 and 406 μsec to obtain the signal from CH_2I with the corresponding range of laboratory velocities. The expected signal from CH_2I as a function of the direction of the electric vector was then calculated as for the I^+ data and compared to the experimental data, with β again as the only variable parameter. The best fit was obtained with $\beta = 0.6 \pm 0.1$. As shown explicitly for the the I^+ polarized light data in Figures 14b and c, the good fit to the CH_2I^+ data using a uniform anisotropy of 0.6 over the entire distribution indicates that signal at the fast side and at the slow side of the distribution, which might contain various amounts of $Br(^2P_{1/2})$ and $Br(^2P_{3/2})$, have the same angular distribution. It is discussed in Ref. 6 that for C-Br bond fission this parallel anisotropy indicates that primarily $Br(^2P_{1/2})$ is formed in C-Br dissociation at 248 nm.

I. Branching Ratio Between C-I and C-Br bond fission at 248 nm

A lower bound to the relative number of molecules undergoing primary C-I bond fission to the number undergoing primary C-Br bond fission at 248 nm can be estimated from the relative signal intensities in the I^+ and $^{81}Br^+$ spectra assigned to I and Br atoms from primary dissociation events. The ratio obtained is a lower limit because Br^+ signal from CH_2Br would fall at arrival times in the fast part of the signal which is assumed to be only due to Br atoms. (The CH_2I product signal arrives at slower times than the sharp spikes in the I^+ spectra, so it introduces no error.)

The calculation of the branching ratio from the signal intensities proceeds in the manner described in detail by Krajnovich[12] with two additions, correction for the isotopic abundance of $^{81}Br^+$ and for our extra sensitivity to fragments recoiling with a more parallel angular distribution with respect to the electric vector of the dissociating light. Assuming the angular divergence of the beam and the finite angular acceptance of the detector are negligible, one is more sensitive to products with higher anisotropy parameters by a factor of $1 + \beta/4$. A lower limit of 1.2:1 for C-I:C-Br bond fission is thus obtained. At this excitation wavelength, which may contain contributions from both the $n(I) \rightarrow \sigma^*(C-I)$ and the $n(Br) \rightarrow \sigma^*(C-Br)$ transitions, both C-I and C-Br fission occur to a significant extent, with C-I fission being the dominant channel.

II. Photodissociation of CH_2BrI at 193 nm

A. Thermodynamic Constraint on the Stability of Dissociation Products

Identification of all the primary dissociation channels of CH_2BrI excited via absorption of a 193 nm photon is complicated by the fact that the photon energy of 147.9 kcal/mol is greater than the endoergicity of $CH_2BrI \rightarrow CH_2 + I + Br$ (see Figure 2). Thus it is possible that some of the products formed will spontaneously undergo secondary dissociation.

The secondary dissociation of CH_2I, CH_2Br, or IBr will occur if the internal energy of those products is greater than their dissociation energy. Their internal energy can be derived from knowledge of the translational energy and internal energy channeled to the partner fragment (Br, I, and CH_2 respectively) in each primary dissociation. The routes for net formation of $CH_2 + I + Br$ are:

$$CH_2BrI \xrightarrow{h\nu} \left[\begin{array}{ll} \text{a.} & CH_2I + Br \\ \text{b.} & CH_2Br + I \\ \text{c.} & CH_2 + IBr \\ \text{d.} & \text{(simultaneous 3-body)} \end{array}\right] \longrightarrow CH_2 + I + Br \qquad (8)$$

Assuming there is no barrier to dissociation beyond the endothermicity, the energy required for reaction 8 is 130.4 kcal/mol.[4] The CH_2Br, CH_2I, or IBr fragments will be observed only if the energy released to translation plus the spin-orbit excitation of the I or Br fragment or the internal energy of the CH_2 fragment for each respective

primary dissociation event is greater than $E(h\nu) - \Delta H$(reaction 8) = 147.9 - 130.4 = 17.5 kcal/mol. In special cases, CH_2Br, CH_2I, or IBr formed with internal energies above their dissociation limits may still survive secondary dissociation during the transit time to the detector. The fragment may be stable if, for instance, there is a rotational barrier to dissociation or if an electronically excited fragment fluoresces prior to dissociation, leaving it energetically stable. The contributing factors to the stability of the individual CH_2Br, CH_2I, and IBr fragments observed at 193 nm will be outlined in each section below.

B. $CH_2BrI \xrightarrow{193\ nm} CH_2I + Br$ (9)

The TOF spectrum of m/e = 141, CH_2I^+, is shown in Figure 16. The spectrum consists of a fast narrow signal peaking at 370 μsec corresponding to CH_2I product from C-Br bond fission that has not undergone secondary dissociation to CH_2 + I, and a small broad tail attributed to dissociation fragments of a small fraction of dimer contamination in the beam. The $P(E_T)$ derived from forward convolution fitting of the CH_2I signal is shown in Figure 17. The fit is shown in solid line in Figure 16. Below 6 kcal/mol the $P(E_T)$ is somewhat uncertain due to contamination of the CH_2I^+ TOF from dissociation of dimers. The $P(E_T)$ shows the distribution of translational energies released in C-Br fission for dissociation events that formed stable CH_2I radical product.

The analysis of the energetics in Section II.A. concluded that C-Br bond fission releasing less than 17.5 kcal/mol to translation would produce energetically unstable CH_2I unless the partner Br atom were spin-orbit excited. CH_2I produced with even a kcal/mol of energy above its dissociation limit would be expected to dissociate in much less than the > 350 μsec flight time to the detector. Thus, most of the observed reaction (9) with the $P(E_T)$ shown in Figure 17 must correspond to the process:

$$CH_2BrI \xrightarrow{193\ nm} CH_2I + Br\ (^2P_{1/2}) \qquad (10)$$

One would expect that if an appreciable fraction of C-Br bond fissions produced ground state Br atoms one would see a break in the $P(E_T)$ derived from the CH_2I^+ TOF near 17.5 kcal/mol, because the CH_2I from the ground state channel would be lost below that translational energy to secondary dissociation. There is no break observed. Normally one could compare the distribution of c.m. velocities of CH_2I and Br atom products to determine whether any CH_2I was being lost to secondary dissociation since the two fragment velocities are related by momentum conservation, but in this system, the Br^+ spectrum is too congested with signal from other dissociation pathways.

C. $CH_2BrI \xrightarrow{193\ nm} CH_2Br + I$ (11)

The TOF spectrum of m/e = 95, $CH_2{}^{81}Br^+$, is shown in Figure 18 (top frame). The spectrum shows a fast signal peaking near 300 μsec attributed to stable CH_2Br product from C-I bond fission, a small peak at 400 μsec and a broad slow peak at 650 μsec. The peaks at ~ 650 μsec and at 400 μsec were explicitly determined to be from dissociation of clusters in the beam by repeating the TOF measurement under conditions with smaller amounts of dimers as in I.E (bottom frame in Figure 18). The cluster dissociation signal is large in relation to the primary C-I dissociation channel signal because the fraction of C-I bond fission at 193 nm is so much smaller than at 248 nm.

An approximate $P(E_T)$ for C-I bond fission producing stable CH_2Br product was derived from forward convolution fitting of the CH_2Br^+ TOF. The $P(E_T)$ in Figure 19 gave the fit shown in solid line in Figure 18; the shape of the $P(E_T)$ below 10 kcal/mol is only approximate due to dimer contamination. By the same argument stated in Section II.A and applied in detail to the C-Br fission $P(E_T)$ in Section II.B, more than two thirds of the dissociation events that produced this stable CH_2Br product must have produced I atom in the $^2P_{1/2}$ state:

$$CH_2BrI \xrightarrow{193\ nm} CH_2Br + I(^2P_{1/2}) \quad (12)$$

Because the spin-orbit splitting of I is so large, 21.7 kcal/mol, all the CH_2Br produced via reaction (12) would be energetically stable and could be detected in the CH_2Br^+ spectrum, independent of the translational energy of the products. C-I bond fission producing ground state I atoms would not produce stable CH_2Br product unless more than 17.5 kcal/mol were released into translation. As in C-Br bond fission, most of the fast peak in the $CH_2{}^{81}Br^+$ spectrum must correspond to formation of spin-orbit excited $I(^2P_{1/2})$ product (reaction 12).

As with Br^+, the I^+ spectrum in this system is too congested with signal from other dissociation pathways to determine whether any of the CH_2Br product is being lost to secondary dissociation. It is clear, however, that if more than a small fraction of C-I bond fissions produced ground state I atoms one would see a break in the $P(E_T)$ derived from the CH_2Br TOF near 17.5 kcal/mol, because the CH_2Br from the ground state channel would be lost below that translational energy to secondary dissociation.

D. $CH_2BrI \xrightarrow{193\ nm} CH_2 + IBr$ (13)

The TOF spectra of m/e = 206,208, IBr^+, at source to detector angles of 10° and 20° are shown in Figure 20. The signal is easily assigned to IBr product from the primary three-center elimination of IBr from CH_2BrI. It was explicitly determined that the signal was not due to dissociation of dimers by identifying the I^+ and Br^+

signal from IBr through their arrival times and checking those spectra for contribution from dimers. The times of arrival of I^+ and Br^+ from IBr (corrected for ion flight time) are shown in the left frames of Figure 21 in solid line. The signal from IBr is evident in both the I^+ and Br^+ TOF's. The data taken under reduced dimer conditions are shown in the right frames of Figure 21 for comparison. Any signal from dissociation of dimers in the beam should decrease substantially with respect to monomer signal, as measured at 248 nm (see Section I.E.). Because signal attributed to IBr did not decrease in intensity relative to the monomer dissociation signal at shorter arrival times, the IBr product observed must be from the concerted elimination of IBr from CH_2BrI monomer excited at 193 nm.

The $P(E_T)$ shown in Figure 22 is derived from fitting the IBr^+ TOF shown in Figure 20. Neglecting the small fraction of IBr that might be formed in an excited electronic state which fluoresces on a time scale faster than predissociation, the stable IBr product must have been formed in dissociation events which channelled at least 17.5 kcal/mol of energy into translation and internal excitation of the CH_2 partner fragment. At lower and lower translational energies, the partner CH_2 to the IBr product must be more and more internally excited for the IBr product to be stable. Thus one would expect the $P(E_T)$ for formation of all IBr product including that which subsequently dissociates to show a lower average translational energy than the $P(E_T)$ derived from stable IBr in Figure 22. The IBr that undergoes secondary dissociation to I + Br would contribute to the

signal peaking at ~ 600 and ~ 500 μsec in the I^+ and Br^+ TOF's respectively, as discussed in Section II.E.

The $P(E_T)$ for production of stable IBr also suggests the nature of the IBr electronic state. The maximum energy released to translation is a very sharp 23.5 ± 1.0 kcal/mol. This energy corresponds very closely to the maximum available energy for translation if electronically excited IBr ($^3\Pi_1$) is formed:

$$CH_2BrI \rightarrow IBr\ (^3\Pi_1) + CH_2 \qquad \Delta E = 88.46 + 35.12^{13} = 123.58 \qquad (14)$$

$$E_{avail} = 147.9 - 123.58 = 24.3 \text{ kcal/mol}$$

Because the CH_2 has so few degrees of freedom one would expect that some of the fragments would recoil with very close to the total available energy. Apparently the I atom Rydberg state formed by exciting CH_2BrI at 193 nm is predissociated by a state that correlates specifically to electronically excited IBr product and ground state $CH_2(^3B_1)$. It is not clear whether the broad and flat translational energy distribution is due to the fact that a channel producing $IBr(^3\Pi_1)$ + $CH_2(^1A_1)$ (9.05 kcal/mol above $CH_2(^3B_1)$) is also involved.

E. Anisotropy of Primary Processes and Secondary Dissociation of Fragments

Two sets of TOF spectra of m/e = 127, I^+, and m/e = 81, Br^+, are shown in Figures 23 and 24 respectively. The TOF spectra in the first column are taken with the photolyzing laser unpolarized and having a pulse energy of ~ 200 mJ/pulse. The TOF data in the second column in each figure are taken with the laser linearly polarized in the direction of the detector but with the power reduced by a factor of ~7.

The polarization dependence of the primary dissociation channels can be qualitatively derived from the TOF spectra of I^+ and Br^+ at source to detector angles of 10° shown in Figures 23a and d and 24a and d. The TOF spectra at 10° are very nearly superimposable, independent of the polarization of the laser. The signal from IBr elimination to form stable IBr product rising near 500 μsec in both sets of 10° TOF data spans a wide range of c.m. angles. The Newton diagram in Figure 25 shows the angle between the electric vector of the light and the c.m. recoil direction of the observed IBr product ranges from 26° to beyond 90°. The c.m. angular distribution with respect to the molecular beam-detector plane is necessarily isotropic for the data taken with unpolarized light as the direction of the electric vector is isotropic in that plane. The fact that the shape of the TOF signal from IBr product does not change when the light is polarized shows that the c.m. angular distribution of the stable IBr product is nearly isotropic. The same argument can be applied to the broad underlying

signal attributed to the dissociation to CH_2 + I + Br extending from 400 μsec to 900 μsec in the 10° TOF data in Figures 23 and 24. One can also see from this data that the overlapping fast signals from CH_2Br, CH_2I, I, and Br also show no strong polarization dependence. In fact, the TOF data shown in Figures 23d-e and 24d-e are fit with all components assumed to have an isotropic angular distribution. It is evident from the Newton diagram in Figure 25 that the range of c.m. angles between these fast products detected at 10° and the electric vector of the polarized light is small, between 5 and 15°. In this case one does not expect a large difference in the shape of the TOF spectra of the fast products, because the c.m. scattering angle does not change much across the spectra, but one does expect a large change in the relative intensity of any anisotropic fast signal compared to signal that is isotropic. If the c.m. angular distribution of I or Br resulting from C-I or C-Br bond fissions were perpendicular, for instance, signal from I or Br in the polarized light data should disappear almost entirely in the polarized light TOF data relative to the slow isotropic IBr signal. Thus all the primary processes observed at 193 nm have close to an isotropic c.m. angular distribution.

The identification of signal from the secondary dissociation of fragments may also be made by examining the data in Figs. 23 and 24. If the absorption transition of a fragment for a 193 nm photon is not saturated, then signal from "fragments of fragments" should decrease linearly with respect to the primary product signal when the laser power is decreased. There are a few obvious features in the I^+

and Br^+ TOF spectra of Figures 23 and 24 a-c that substantially decrease in intensity relative to the primary fragment signal when the laser power is decreased. The very fast peaks in the I^+ and Br^+ TOF spectra arriving at 200 and 140 μsec respectively in the 20° TOF spectra are easily assigned to some IBr product absorbing a photon and dissociating to I + Br by inspection of their arrival times.[6] The obvious broad hump in the I^+ spectrum at 20° (Figure 23b) rising near 240 μsec and extending underneath the primary dissociation signal is assigned to the I from $CH_2I \xrightarrow{193\ nm} CH_2 + I$. The Br product from the secondary dissociation of CH_2Br is noticeable just to the fast side of the primary Br atom peak at 20° (Figure 24b) at ~ 200 μsec and clearly extends through the primary signal, as evidenced by the difference between the two 30° Br^+ TOF spectra in Figure 24 (the underlying secondary signal becomes more important at wider angles in the laboratory frame of reference). The corresponding low power TOF data show the expected substantial decrease in the secondary photodissociation signal. The CH_2 fragment in the secondary photodissociation of CH_2I and CH_2Br would partially overlap the CH_2 product from primary IBr elimination. This signal is apparent in the CH^+ TOF spectrum shown in Figure 26.

The identification of the portion of the slow signal in the data of Figs. 23 and 24 which does not correspond to IBr product may now be discussed. At both 193 nm and 210 nm, the energy of one photon is sufficient to break both C-halogen bonds in the molecule, producing CH_2 + I + Br. A priori, the net chemical reaction may proceed via

CH_2I, CH_2Br, or IBr intermediates which are internally excited above their dissociation limits or via a one-step three-body dissociation where only the net linear momenta of the three products must sum to zero (reaction 8). The considerations discussed in II.B and C suggest little CH_2I or CH_2Br is formed which undergoes spontaneous secondary dissociation, leaving reaction (8c) or (8d) to produce the slow signal in the I^+ and Br^+ spectra. Although it is easiest to suggest that the signal is due to IBr formed above the dissociation limit decaying spontaneously, the IBr $^3\Pi_1$ state cannot be a true metastable intermediate as it correlates to ground spin-orbit state products. (If any IBr were produced in the energetically allowed $^3\Pi_0{}^+$ state, this state could serve as an intermediate, as it correlates to I + $Br(^2P_{1/2})$). It is thus probable that the three products are formed in one process with no true intermediate. In the absence of coincidence measurements of all three fragments, however, a three body dissociation is not uniquely defined; only the individual translational energies of the I and Br fragment may be determined. For the purpose of attempting a unique analysis, primary CH_2 + IBr formation releasing very little translational energy such that the CH_2 is primarily a spectator will be assumed, so the momenta of I and Br must be matched as they would if a true slow IBr intermediate were formed. The $P(E_T)$ derived is the probability of the total energy in translation of the I and Br fragments, neglecting the recoil of the CH_2 fragment. The data at 193 nm may be approximately fit under this constraint, but not the 210 nm data which will be discussed later.

Identification of the signal from reaction (8) in the I^+ and Br^+ spectra of Figures 23 and 24 is made by subtracting the known velocity distributions of products from C-I fission, C-Br fission and IBr elimination from the spectra, leaving the signal from formation of CH_2 + I + Br. The deconvolution of the spectra into their components is somewhat flexible, particularly where primary product signal from C-I and C-Br bond fission overlaps the signal from reaction (8), but the process still yields valuable information. The shapes of the TOF signals from IBr, CH_2I, and CH_2Br at I^+ and Br^+ are determined by the shapes of their spectra in Figures 20, 16 and 18, assuming that no significant fraction of CH_2Br or CH_2I undergoes secondary unimolecular dissociation, so that the CH_2Br^+ and CH_2I^+ signal represent all the primary dissociation events. Thus three of the four curves used to fit the I^+ and Br^+ spectra are uniquely determined from other data. The remaining large broad signal indicated in long dashed line between 300 and 900 μsec arrival times in the I^+ and Br^+ spectra in Figures 23 and 24 is most likely from the spontaneous secondary dissociation of internally excited IBr or from three-body dissociation (reaction 8d). The relative intensity of the signal from C-I fission, C-Br fission and IBr elimination was varied to produce the best fit to the data while constraining the remaining broad I^+ and Br^+ signal to be smooth. The additional constraint that the signal attributed to secondary or three-body I and Br production be related by momentum conservation with CH_2 as a spectator was imposed to obtain the shape of the secondary or three-body dissociation signal shown in

long dashed line in Figures 23 and 24 d-f. The overlapping spectra clearly produce uncertainty in the fast portion of this signal.

An approximate $P(E_T)$ for the I and Br from dissociation to CH_2 + I + Br was obtained by fitting this remaining signal in the I^+ and Br^+ spectra and is shown in Figure 27. The mean energy released to translation of the I and Br fragments together is 2.9 kcal/mol. The CH_2 from three body dissociation could not be isolated in the congested CH^+ spectra (Fig. 26) so a full picture of this three body or secondary process could not be obtained.

F. Absence of $CH_2BrI \xrightarrow{193\ nm}$ CHI + HBr and

$CH_2BrI \xrightarrow{193\ nm}$ CHBr + HI.

These dissociation channels were excluded using exactly the same method as described for the photolysis at 248 nm in Section I.C. The HI^+ and HBr^+ spectra at 193 nm show no significant signal. The spectra of $CH^{81}Br^+$ and CHI^+ are identical to those of $CH_2{}^{81}Br^+$ and CH_2I^+, further establishing that no HI or HBr elimination occurs.

G. Branching Ratio Between C-I and C-Br Bond Fission

A branching ratio between the two bond fission channels at 193 nm can be obtained with no approximations for the fragment ionization cross sections by considering the spectra of Figures 23 and 24. Since secondary dissociation of IBr or three-body dissociation produces one of each halogen atom fragment, the signal from the secondary (or three body) dissociation channel can be used to calibrate the detector

sensitivity for Br and I atoms from C-Br and C-I bond fissions. With the deconvolution of the spectra as shown in Figures 23 and 24 and described in Section II.E and the anisotropy for each channel taken to be zero (see Section II.E) a C-Br to C-I branching ratio of 3.5:1 is obtained. The effects of the c.m. to lab transformation and number density sensitivity of the ionization process were accounted for here, as in the rest of the analysis.

III. Photodissociation of CH_2BrI at 210 nm[14]

A. Thermodynamic Constraint on the Stability of Dissociation Products

As at 193 nm, the energy of a 210 nm photon is greater than the energy required to promote the net chemical reaction $CH_2BrI \rightarrow CH_2 + I + Br$ (rxn. 8). At 210 nm, however, only the lowest electronically excited state of IBr is energetically allowed and correlates to ground state halogen atom products, so it may not serve as a metastable intermediate. The photon energy of 136 kcal/mol is only slightly above the endothermicity of the net reaction (8) of 130.4 kcal/mol, so any initial internal energy of the CH_2BrI parent molecule could have a noticeable influence on the energetic constraints. If one assumes the rotation of the parent molecule is completely relaxed in the supersonic expansion, but no vibrations relax, the average internal energy of the CH_2BrI parent at 140°C is found to be 1.5 kcal/mol. Thus, on the average, there is only 7.1 kcal/mol of energy for the relative translational and internal energies of the final $CH_2 + I + Br$ products of reaction (8).

Several conditions on the stability of dissociation products and the internal energies of the final products are immediately apparent: 1) the CH_2I or CH_2Br products from dissociation events forming spin-orbit excited Br or I atoms will not undergo secondary dissociation, 2) CH_2I, CH_2Br, or IBr from dissociation events channeling more than 7.1 kcal/mol to translation in the primary dissociation event (± ~1.5 kcal/mol due to the distribution of

internal energies of the parent) will not undergo secondary dissociation, and 3) any possible three-body dissociation (rxn. 8d) may not produce spin-orbit excited halogen product and may not channel more than about 7.1 kcal/mol to the relative translation of the products. (CH_2BrI parent with greater than the mean internal energy will raise the 7.1 kcal/mol limit correspondingly.)

B. $CH_2BrI \xrightarrow{210\ nm} CH_2I + Br$ (16)

The TOF spectrum of m/e = 141, CH_2I^+, at a 20° source to detector angle is shown in Fig. 28. The spectrum consists of a sharp spike from C-Br fission which tails off slowly at longer arrival times. The TOF spectrum of Br^+ at a 20° source to detector angle is shown in Fig. 29. The sharp spike in that spectrum corresponds to Br product that is momentum matched with the signal from CH_2I. The $P(E_T)$ for C-Br bond fission at 210 nm which gave the fit in solid line to the CH_2I^+ signal is shown in Fig. 30. This $P(E_T)$ correctly predicts the time of arrival of Br atoms from C-Br bond fission as shown in Fig. 29. The dissociation events releasing less than 5.6 kcal/mol to translation must have produced spin-orbit excited Br atoms or the CH_2I product would not have been stable. One would not expect to resolve the Br spin-orbit states in the TOF spectrum given the large range of internal energies of the CH_2I product, so some of the dissociation events may also produce ground state Br atoms. However the polarization study described in III.G indicates

the whole distribution has the same anisotropy; because transition at the curve crossing is less likely in C-Br dissociation than in C-I dissociation,[15] the anisotropy suggests that only $Br(^2P_{1/2})$ atoms are formed here.

C. Absence of $CH_2BrI \xrightarrow{210\ nm} CH_2Br + I$ (17)

The TOF spectra of m/e = 127, I^+, shown in Fig. 31 for source to detector angles of 10° and 20°, show no contribution from C-I fission, but only contributions from fragmentation of CH_2I and IBr in the ionizer and I atoms from three body dissociation, as explained below. No signal was detected at m/e = 95, $CH_2{}^{81}Br^+$. These results show there is no primary C-I fission to produce CH_2Br + I. Because primary C-I fission occurs along a repulsive surface releasing a large fraction of the total available energy to translation as in C-Br fission and because I is lighter than CH_2I, I atoms recoiling from CH_2Br in C-I bond fission are expected to have larger c.m. recoil velocities than CH_2I from C-Br fission. This expectation is confirmed experimentally at both of the other excitation wavelengths. Thus, I atom product from primary C-I fission should appear at slightly faster arrival times than CH_2I from C-Br fission. The shape of the signal from CH_2I product from C-Br fission which fragments to I^+ in the ionizer is obtained from the CH_2I^+ spectrum shifted by 2 μsec for the different ion flight times. When this shape is superimposed on the I^+ spectrum (Fig. 31, bottom

frame) one obtains a perfect fit to the fast side and peak of the fast signal. There is no signal in the I^+ spectrum which can be attributed to I atoms from primary C-I fission. As at 193 nm, the slow signal in the I^+ spectrum is from the net chemical reaction (8) and from fragmentation of IBr in the ionizer.

It is clear that the absence of any signal at CH_2Br^+ from the photodissociation of CH_2BrI monomer and the absence of any fast signal in the I^+ spectrum which does not precisely match the velocity of the CH_2I product from C-Br fission shows that CH_2BrI does not undergo primary C-I fission at an excitation wavelength of 210 nm.

D. $CH_2BrI \xrightarrow{210\ nm} CH_2 + IBr$ (18)

The TOF of m/e = 208, $I^{81}Br^+$, at a source to detector angle of 10° is shown in Fig. 32. The corresponding product velocities in the c.m are too small for the IBr to appear in the 20° I^+ and Br^+ spectra, but the I^+ spectrum at 10° shown in the top frame of Fig. 31 shows I^+ signal from IBr fragmenting in the ionizer. The signal at CH^+ was too small to be observable but a $P(E_T)$ for the concerted elimination giving CH_2 + IBr is easily derived from the IBr^+ data. The $P(E_T)$ is shown in Fig. 33; the corresponding fit is shown in solid line in Fig. 32. The shape of the $P(E_T)$ below ~4 kcal/mol in translation is not sensitive to fitting the IBr^+ data because the slower IBr product will not recoil out to 10°. The sharp

cutoff of the $P(E_T)$ near 13 kcal/mol is sensitive to the data; the cutoff again occurs near the total available energy corresponding to formation of only electronically excited IBr (see Section II.D) in the concerted elimination. A crude estimate of the probability for this dissociation channel indicates it accounts for less than 6 percent of the dissociation events.

E. Absence of $CH_2BrI \xrightarrow{210\ nm} CHI + HBr$ and $CH_2BrI \xrightarrow{210\ nm} CHBr + HI$

The TOF spectra of m/e = 128, HI^+, and m/e = 82, $H^{81}Br^+$, at source to detector angles of 20° show no signal from HI or HBr elimination. The I^+ and Br^+ spectra also indicate no evidence for these channels.

F. $CH_2BrI \xrightarrow{210\ nm} CH_2 + I + Br$ (8d)

The net reaction to form $CH_2 + I + Br$ produces the broad signal in the I^+ and Br^+ spectra which is not from stable IBr product. It accounts for roughly 1/3 of the dissociation events. There is no obvious metastable IBr state which can serve as an intermediate in a two step process. We attribute the slow signal in the I^+ and Br^+ spectra to simultaneous three-body dissociation for several reasons. These include first, the $^3\Pi_1$ state of IBr correlates to ground state I and Br atoms, while the energy of the system is not sufficient to produce much IBr in the $^3\Pi_{0+}$ state which could serve as an

intermediate, predicted to have its zero point vibrational level about 1500 cm^{-1} above the dissociation limit to ground state I and Br.[15b] Second, there is no CH_2Br product formed which can undergo secondary dissociation and give the slow signal detected at Br^+ and secondary dissociation of CH_2I would not give signal peaking as close to the c.m. as that observed in the I^+ spectra. The possibility of metastable electronically excited CH_2I or CH_2Br intermediates which all subsequently dissociate cannot be positively excluded, but because the electronic states of these radicals are not known we will not speculate further.

The distribution of translational energies imparted to the I atom and Br atom products in the three body dissociation events is derived from fitting of the slow signal in the I^+ and Br^+ TOF spectra in Figs. 31 and 29. The range of translational energies of the Br atom product is shown in the right frame of Fig. 34 and for the I atom product is shown in the left frame of Fig. 34. A total translational energy distribution for the three-body process cannot be arrived at without coincidence measurements of the velocities of the products. The fastest I atom velocities in the slow signal may only originate from dissociation of CH_2BrI with at least 2 kcal/mol of internal energy (unless the endothermicity of reaction (8) is overestimated).

G. Polarization Dependences of Dissociation at 210 nm

The polarization dependencies of each of the reactions observed at 210 nm were measured and are discussed in detail in Reference 6. The translational energy release was derived from the unpolarized data, only the anisotropy parameter β was varied to obtain a fit to the data taken with polarized light. The slow signal from three-body dissociation to CH_2 + I + Br shows a parallel angular distribution with β = approximately 1.0 ± 0.2 for I and β = 0.65 ± 0.25 approximately for Br. Reaction (16) producing CH_2I + Br also shows a parallel polarization dependence with β = 0.6, derived by comparison with the slow Br^+ signal from three-body dissociation. Due to the very low c.m. translation energies imparted to IBr from reaction (18), the IBr^+ TOF spectra are only weakly dependent on the anisotropy which lies in the range $0.8 > \beta \geq -1.0$.

DISCUSSION

I. Summary of Primary Experimental Results

Although several chemically distinct reactions, including C-Br and C-I bond fission and IBr, HBr, and HI elimination, are energetically allowed via excitation of CH_2BrI at all three wavelengths,[4] the dissociation channels that result are few and specific to the excitation wavelength. At 248 nm, only C-I and C-Br bond fission occur,

with C-I bond fission dominant by a ratio of more than 1.2 to 1. C-I bond fission produces both spin-orbit states of iodine with the same polarization dependence in a ratio of $^2P_{3/2}$:$^2P_{1/2}$=1.0:0.75. The anisotropies of the recoil of the I and Br atoms are each from a parallel transition with β equal to 1.0 and 0.6 respectively. The results at 248 nm are interpreted in terms of the excitation being in a region where the n $\longrightarrow$ σ^* transitions of I and Br overlap. At 193 nm, three dissociation channels occur, C-Br bond fission, C-I bond fission and IBr elimination with bond fission producing halogen atoms primarily (perhaps exclusively) in the spin-orbit excited $^2P_{1/2}$ state. C-Br bond fission dominates C-I bond fission by a ratio of 3.5:1. The concerted reaction apparently produces exclusively electronically excited IBr in the $^3\Pi_I$ and perhaps higher electronic states. The recoil of all the primary fragments is isotropic with respect to the electric vector of the light, suggesting they all result from excitation to an I atom Rydberg level which is predissociated on a time scale long with respect to the rotational period of CH_2BrI. Excitation at 210 nm, which is assigned to a n(Br) $\rightarrow$ σ^*(C-Br) transition, results in primary C-Br fission but no primary C-I bond fission. IBr elimination to produce probably exclusively electronically excited IBr also occurs. Dissociation to CH_2 + I + Br is energetically allowed and occurs at the two shorter wavelengths; whether this occurs as a very fast two step process or as a three-body dissociation is not certain. The experimental results are summarized in Table 1.

II. Bond Selective Fission of the C-Br Bond over the Weaker C-I Bond in CH_2BrI

The possibility of inducing specific dissociation or isomerization pathways in a molecule by varying the nature of the initial excitation has been of interest to many workers in the field of photochemistry and unimolecular reaction dynamics. For the dissociation of vibrationally excited molecules in the ground electronic state, theories[16] in which the energy in vibrations and active rotations of the molecule is assumed to be distributed statistically throughout the molecule are extremely successful in modeling experimental results. Elegant selective excitation studies of unimolecular reaction dynamics in which vibrational energy is deposited into a particular local C-H or O-H stretch in the molecule[17] have shown that, at the low energies studied, vibrational energy redistribution occurs on a time scale fast with respect to isomerization or dissociation, so overall rates and branching ratios between dissociation pathways are successfully predicted with statistical theories. Dissociation pathways following electronic excitation of a molecule, however, are shown in this work to be critically sensitive to the electronic nature of the initial excitation and not just the energy of the exciting photon, as suspected in an earlier study by Bersohn and coworkers.[1]

If one deposits energy in CH_2BrI by heating it slowly, the weakest bond in the molecule, the C-I bond, will break preferentially. Branching ratios at a particular excitation energy E are determined

from the ratio of the dissociation rate constants, approximately $k=A\cdot\exp(-E_a/E)$. As the preexponential A factors for simple bond fission reactions are similar, the activation energies, E_a, which are in this case roughly the C-X bond energies, would determine the branching ratio between C-I and C-Br bond fission; C-I bond fission would thus dominate in this statistical framework. Photochemistry texts have generalized the results of previous experiments on the primary photodissociation pathways of polyhaloalkanes at excitation wavelengths $\geq$2000 Å as "the dominant split in the photolysis ruptures the weakest C-halogen bond",[18] implying that the results might be similar to thermal decomposition. However, excitation in this region is to $n \rightarrow \sigma^*$ states which are purely repulsive in the respective C-halogen bond. Dissociation lifetimes have been estimated from the anisotropy of product angular distributions to be much less than a picosecond. The concept of statistical distribution of energy in the molecule on such a short time scale is not reasonable. Thus, contrary to a statistical description, the experimental results show that excitation of CH_2BrI at 210 nm of a transition assigned to $n(Br) \rightarrow \sigma^*(C\text{-}Br)$ results in C-Br fission but no primary C-I fission.

The previous photolysis experiments which led to the conclusion that the weakest C-halogen bond ruptures preferentially are easily reinterpreted on the basis of selective fission of the C-X bond corresponding to the particular $n(X) \rightarrow \sigma^*(C\text{-}X)$ transition excited. The absorption bands corresponding to these transitions for X=Cl or F do not peak until the vacuum ultraviolet region. Of the twelve

molecules studied no system contained both C-Br and C-I bonds.[19] At wavelengths $\geq$2000 Å the n(Cl) $\rightarrow$ σ^*(C-Cl) transition is expected to be at least an order of magnitude weaker than the corresponding C-Br or C-I transition. The weakest bond broke in these molecules because the n-σ^* transition for that bond was the strongest at wavelengths >2000 Å. This picture is consistent with the interpretation given by Bersohn of his recent experimental results on CH_2BrI[1] irradiated primarily in the n(I) $\rightarrow$ σ^*(C-I) absorption band. Here he attributes the small fraction of C-Br fission to the photolysis bandwidth partially overlapping the n(Br) $\rightarrow$ σ^*(C-Br) transition.

Still, this is oversimplified, as is evident from the results of photodissociation of 1,2-C_2F_4BrI by Krajnovich et al.,[2] in which selective C-Br fission was not observed, and the occurrence of the IBr elimination channel in addition to C-Br bond fission in CH_2BrI excited at 210 nm. One might begin to think about these differences as follows. The similarity in the positions and shapes of the absorption bands, despite the dissimilarity in intensities, of CH_2BrI (or C_2F_4BrI) to the corresponding features in the spectrum of CH_3I and CH_3Br (or C_2F_5Br and C_2F_5I) give plausibility to the assignment of the transition as still being local. The spectra do not show the broadening and splitting found in the spectra of CH_2I_2 and CH_2Br_2 when the unperturbed orbitals of the C-X bond lie at the same energies and so mix and split. Given the truth of the assumption that one is exciting essentially a n(Br) $\rightarrow$ σ^*(C-Br) transition in CH_2BrI at 210 nm and in

1,2-C_2F_4BrI at 193 nm, any processes other than C-Br fission must be the result of intramolecular energy transfer that is fast enough to compete with rapid C-Br bond dissociation. The formation of IBr from CH_2BrI might result from the predissociation of the σ^*(C-Br) state by one that correlates to excited state IBr. It is probably not the result of internal conversion because dissociation of vibrationally excited ground state CH_2BrI should give an overwhelmingly high fraction of C-I fission relative to IBr elimination. That the n(Br) $\rightarrow$ σ^*(C-Br) state of 1,2-C_2F_4BrI is not also predissociated to form some IBr follows easily from the geometric separation of the I and Br atoms in that molecule. However, the other difference in the dissociation pathways of the two bromo-iodo compounds is not so simply explained. The observation of an effect described as fast intramolecular electronic energy transfer occurring in 1,2-C_2F_4BrI at 193 nm, leading to a 1.7:1 ratio of C-I:C-Br fission, but not occurring in CH_2BrI allowing selective fission of the C-Br bond over the C-I bond at 210 nm, warrants more careful inspection.

The mechanism for the fast intramolecular electronic energy transfer in 1,2-C_2F_4BrI from the initial n $\rightarrow$ σ^* excitation on the C-Br bond to one on the C-I bond is not certain, but several clues can be inferred from the experimental results. The anisotropy of the products is parallel, β=1.8, so assuming the initial excitation is correctly assigned as an n(Br) $\rightarrow$ σ^*(C-Br) local excitation (as indicated by the similarity of the absorption spectrum in that region to C_2F_5Br) the initial transition moment is parallel to the C-Br

bond. The translational energy distribution of the I atom product following intramolecular energy transfer is fast and narrow, indicating the C-I bond stretches on an electronic surface that is repulsive in the C-I bond. In addition, the present results on CH_2BrI have indicated that the fraction of the total available energy (corrected by subtracting off any energy in spin-orbit excitation of I or Br product) partitioned to translation is the same for C-I fission and C-Br fission at each wavelength (~0.3 at 248 nm for C-I or C-Br fission and 0.2 at 193 nm). This result indicates that the I atoms and the Br atoms from 1,2-C_2F_4BrI at 193 nm are probably both spin-orbit excited, as only then is the partitioning to translation the same in both fissions, f=0.37 (see Table 3 of Ref. 2). A repulsive surface that correlates to $I(^2P_{1/2})$ is the $^3Q_0$ [20] surface on the C-I bond. Thus we have a fast intramolecular electronic energy transfer from the repulsive $^3Q_0$ n(Br) $\rightarrow$ σ^*(C-Br) surface to a repulsive surface on the C-I bond, possibly the $^3Q_0$ (C-I) surface. The energy transfer must be fast enough to compete with dissociation of the C-Br bond.

An obvious model for such an energy transfer was suggested in Ref. 2 and will be clarified here. As the C-Br bond stretches along the repulsive electronic surface, some of the electronic energy will be converted into kinetic energy associated with C-Br separation. At some C-Br separation, the electronic energy remaining localized on the C-Br bond will become equal to the energy required to excite the n $\rightarrow$ σ^* transition on the C-I bond and a near resonant electronic

energy transfer could occur. The new state would roughly consist of a locally electronically excited C-I bond and a vibrationally excited C-Br bond. The question of what interaction would lead to such an energy transfer is raised. Two types of interactions which have been extensively studied in terms of electronic energy exchange are electron exchange and dipole-dipole interactions.[21] The C-I and C-Br bonds are spatially separated in 1,2-C_2F_4BrI, so a short range electron exchange interaction is probably not indicated, but a dipole-dipole interaction is a strong possibility. Both transitions are dipole allowed and the transition moments are roughly parallel.[22] Dipole-dipole electronic energy exchange is known to be very efficient with cross sections in some cases on the order of 10-100 $Å^2$.[21] The expectation that dipole-dipole electronic energy exchange could compete with C-Br dissociation was confirmed with a crude calculation of the time required for a dipole-dipole transition from the σ^*(C-Br) surface to the σ^*(C-I) surface.[6] Because the C-I and C-Br bonds are fixed at a certain distance in the molecule, analogy was made to Forster energy transfer[21] and the dipole-dipole interaction between the two chromophores was assumed to be constant over the time for which the electronic energy left over in the stretching C-Br bond was equal to the energy region of the $n \rightarrow \sigma^*$(C-I) transition (a gross approximation). Applying the simplified dipole-dipole interaction formulae of Ref. 21 to this system we obtained a rate of 1.5×10^{11} transitions$\cdot sec^{-1}$ for electronic energy transfer from the C-Br chromophore to the C-I chromophore.[6] Thus if the C-Br bond takes on

the order of a picosecond to stretch through the region where the electronic energy in the C-Br excitation is equal to the energy required to excite to the repulsive C-I surface, energy transfer can take place and C-I fission can result from an initially local C-Br excitation.

This model is difficult to extend to the case of CH_2BrI to explain why intramolecular electronic energy transfer does not occur here, thus allowing us to selectively dissociate the C-Br bond. The angular factor in the dipole-dipole interaction would strongly inhibit the transfer in CH_2BrI as the angle between the C-Br and C-I bonds (to which the transition moments are parallel) is strongly bent in CH_2BrI and would approach 90° as Br recoiled from C. However, the distance between I and Br is much closer and is expected to overwhelm the angular factor in favor of transfer in CH_2BrI. In fact, it is not at all clear that the interaction in CH_2BrI is well described by the simplified dipole-dipole interaction expression which relies on the assumption that the distance between the two transition dipoles is large. We are left with no clear indication of why electronic energy transfer does not occur in CH_2BrI but does occur in 1,2-C_2F_4BrI. Participation of low frequency vibrational modes in 1,2-C_2F_4BrI in facilitating a near-resonant energy transfer is possible.

III. Concerted Elimination of Electronically Excited IBr from CH_2BrI at 210 and 193 nm

The product translational energy distributions for the formation of IBr + CH_2 at both 210 and 193 nm cut off sharply at energies corresponding to the total available energy if only electronically excited IBr were formed in the concerted reaction. In addition, no concerted reaction occurred following excitation at 248 nm. Formation of ground state IBr + CH_2 is energetically allowed at 248 nm, but formation of electronically excited IBr($^3\Pi_1$) is not. These two experimental results lead to the conclusion that the electronic states of CH_2BrI resulting from excitation at 193 and 210 nm are predissociated by a state which correlates specifically to electronically excited IBr (hereafter referred to as IBr*).

The result that only IBr* is formed from electronic excitation of CH_2BrI may shed light on previous experimental results on CF_2Br_2 and CH_2I_2. Although Krajnovich et al.[9] found that no concerted elimination of Br_2 occurred from CH_2Br_2 following excitation at 248 nm, an older experiment by Simons and Yarwood[23] indicated that Br_2 was formed when CF_2Br_2 was irradiated with light extending down to wavelengths of 2000 Å. Leone and coworkers[24] detected fluorescence from I_2 after photolyzing CH_2I_2 at 193 nm as did Style and Ward[25] photolyzing in the VUV. Broad-band photolysis experiments reviewed briefly in Ref. 18a report concerted elimination of Br_2, BrF and Cl_2 from a variety of polyhalomethanes at short

wavelengths, but the electronic states of the diatomic fragment are not identified. It appears that concerted elimination of X_2(X_2 = Br_2, I_2 or IBr) from substituted methanes following excitation in the UV may produce exclusively electronically excited X_2, and cannot occur when the photon energy is too small to produce electronically excited X_2.

The exclusive production of IBr* is consistent with a simple LCAO-MO description of the dissociation in which the reaction proceeds along a least motion path and spin is conserved.[26] The evolution of the reaction under this model is shown in Fig. 35. Following excitation, the C-Br coordinate is repulsive and the C-Br bond will stretch; the CH_2I portion of the molecule will rotate to reduce the Br-C-I angle as the C recoils from Br, better aligning the orbitals labeled as p_z on the halogen atoms which will combine to form σ and σ^* orbitals of IBr. One immediately sees there are three electrons in the two p_z orbitals; when the IBr product is formed one of these electrons will be forced to the σ^*(IBr) orbital. Thus no ground state IBr may be formed along this least motion path, consistent with our experimental results. This model is readily applied to the photodissociation of CH_2I_2 and CH_2Br_2. It would explain why Br_2 elimination was not observed at 248 nm[9] but was observed at shorter excitation wavelengths[23] and it suggests that the I_2 fluorescence observed by Leone[24] and by Style and Ward[25] is representative of all the I_2 formed in the reaction. The first group[24] suggested

study of the $I_2(B)$ and $I_2(X)$ channels; this model shows the $I_2(X)$ channel probably does not occur.

The model suggests an interesting possibility. If the electron spin is conserved during the evolution of the reaction, then only a ^1Q [18] excitation can correlate to $CH_2(^3B_1)$ + $IBr(^3\Pi_1)$ (the singlet products not being together energetically allowed here). The $^3Q_0$ excitation may only correlate to one triplet and one singlet product. One might then postulate that excitation to the ^1Q surface results in IBr elimination and excitation to the ^3Q surface results in C-Br fission (the lowest energy elimination path not being spin allowed). This hypothesis is consistent with the parallel angular distribution of the Br atom from C-Br bond fission because excitation to the $^3Q_0$ surface is via a transition moment parallel to the C-Br bond. In this case the branching ratio between C-Br fission and IBr elimination might be controlled by tuning the excitation wavelength through the n(Br) $\rightarrow$ σ^*(C-Br) absorption band where the oscillator strengths of the $^1Q_1$ and $^3Q_0$ transitions should vary. One would also expect that all the Br atoms would be formed in the $^2P_{1/2}$ spin-orbit excited state.[20,27]

IV. Product Energy Partitioning in the Simple Bond Fission Channels

The simple bond fission reactions resulting from the UV excitation of CH_2BrI in this work occur via electronically excited surfaces which are repulsive in the respective C-X bond. Even the excitation at 193 nm is to a Rydberg state which is predissociated by repulsive electronic surfaces.[27] Breaking of a C-X bond on such a repulsive surface is amenable to modeling with very simple classical impulsive models.[28] Particularly at the higher energy excitation wavelengths where the repulsive potential is very steep, one would expect an impulsive force approximation to be good. The partitioning of the total available energy to translation, rotation, and vibration may be predicted under one of two very simple impulsive force models originally suggested by Wilson.[28] Derivations of the expressions for energy partitioning in the hard and soft radical impulsive models are outlined in Appendix 1 of Reference 6; it was found that the expression for partitioning between vibration and rotation given by Wilson is dependent on there being no geometry changes in the radical formed. A more general expression is derived in Ref. 6 and specific calculations for CH_2BrI are presented. The soft radical impulsive model predicts that 20.3 percent of the available energy is channeled to translation in C-I fission and 20.4 percent is channeled to translation in C-Br fission. The results summarized in Table 1 show that the soft radical model correctly predicts the average fraction of the energy partitioned to translation in C-X fission at 193 nm. At the

lower excitation energies the portion of the repulsive potential reached is not so steep and the heavy X atom recoils away not just from the light carbon atom, but from the whole radical, resulting in a larger fraction of the energy being partitioned to translation.

The calculations also suggest that the rotational excitation of the CH_2I or CH_2Br fragments is quite large, ~54 percent of the total available energy in the soft radical approximation. Unlike many previously studied haloalkanes such as CH_3I, CF_3I, C_2F_5I, or CH_3Br, bond fission in CH_2BrI occurs with the fragments leaving each other at a large impact parameter, resulting in the radical having rotational energies predicted to be as great as 37 kcal/mole for CH_2I from the C-Br fission observed at 193 nm. Whether the orbital motion of the separating collision partners can couple effectively with the molecule's spin and orbital angular momenta and affect the dissociation pathway is an interesting question.

Finally, consideration of the constraint on the exit impact parameter imposed by conservation of energy and angular momentum provides a partial explanation for our observation of such reduced values of the anisotropy parameter β for C-I and C-Br fission at 248 nm following presumed purely parallel excitations. In a classical picture, when two fragments depart with exit impact parameter b and relative translational energy E_T, conservation of angular momentum requires that

$$E_{rot} = \frac{1}{2} I\vec{\omega}^2 = \frac{1}{2} \frac{\vec{L}^2}{I} = \frac{1}{2} \frac{\mu^2 \vec{v}_{rel}^{\,2} b^2}{I} = E_T \frac{\mu b^2}{I}$$

where μ is the reduced mass of the two fragments and I is the moment of inertia of the radical R formed in dissociation. Since the sum of the rotational and translational energies must be less than or equal to the total available energy one easily derives that

$$b \leq [\frac{I}{\mu} (\frac{E_{avail}}{E_T} - 1)]^{1/2} .$$

For C-I bond fission in CH_2BrI at 248 nm where 12.5 kcal/mole is released to translation, near E_T, and $I(^2P_{1/2})$ is formed, the exit impact parameter must be $\leq$ 1.26 Å (I for CH_2Br is taken as 45.53 $Å^2$ g/mol). The equality is realized only if $E_{vib} = 0$. If the molecule dissociated from its equilibrium configuration with a repulsive force along the C-I bond the exit impact parameter would be much greater, ~1.5 Å. Thus, to undergo C-I fission to $CH_2Br+I(^2P_{1/2})$ with 12.5 kcal/mol in translation the molecule must distort significantly during dissociation, resulting in a reduced anisotropy in the angular distribution of the scattered product following an absorption parallel to the C-I bond.

In this work, we have investigated the dissociation processes resulting from excitation to three different electronic surfaces in CH_2BrI. Several results were of particular interest. An excitation assigned as n(Br) -> σ*(C-Br) to a surface repulsive in the the C-Br bond allowed prompt fission of that bond over a weaker bond in the molecule.[29] The detailed investigation of such selective processes

and the intramolecular energy transfer processes which inhibit such selectivity in other systems[2] must now be undertaken. In addition, the concerted elimination of solely electronically excited IBr at the two higher energy excitation wavelengths and no IBr at the lowest energy wavelength highlights the importance of asking more detailed questions about the photochemical decomposition of polyatomic molecules. Although a molecule may not dissociate to certain products when only their ground electronic states are energetically allowed, those products may be formed when there is enough energy to form them in excited electronic states. Here this phenomena was explained via a simple LCAO-MO least motion path for the dissociation. Clearly, the decomposition pathways of an electronically excited polyatomic molecule can be sensitive to both the interactions between electronic states in the molecule and the nuclear dynamics of the dissociation and their continued study will further our understanding of chemical reactions.

ACKNOWLEDGEMENT

This work was supported by the Director, Office of Energy Research, Office of Basic Energy Sciences, Chemical Sciences Division of the U.S. Department of Energy under contract No. DE-AC03-76SF00098. The molecular beam apparatus used for this research was funded by the Mechanics Division of the Office of Naval Research under Contract No. N00014-83-K-0069. The EMG 102E Lambda Physik excimer laser used in this work was borrowed from the San Francisco Laser Center, supported by the National Science Foundation, NSF Grant No. CHE-83-03-208 and the National Institute of Health, NIH Grant No. P41 RR01613-03, awarded to the University of California in collaboration with Stanford University.

REFERENCES

1. S. J. Lee and R. Bersohn, J. Phys. Chem. 86, 728 (1982).

2. D. Krajnovich, L. J. Butler, and Y. T. Lee, J. Chem. Phys. 81, 3031 (1984).

3. L. Cavalli, J. Mag. Resonance 6, 298 (1972).

4. The heats of formation of a variety of chemical species used to calculate the enthalpies shown in Fig. 1 were obtained from: H. M. Rosenstock, K. Draxl, B. W. Steiner, and J. T. Herron, J. Phys. Chem. Ref. Data 6, Suppl. 1, I-774 (1977). The heat of formation of CH_2BrI, 17.338 kcal/mole at 0 K, is calculated in S. A. Kudchadker and A. P. Kudchadker, J. Phys. Chem. Ref. Data 7, 1285 (1978). In addition, the C-I and C-Br bond fission energies in CH_2BrI were assumed to be the same as in CH_3I and CH_3Br respectively. Calculation of the HI and HBr elimination channel endoergicities also required the assumption that the energy required to remove H from CH_2Br or CH_2I is the same as required to remove it from CH_3. C-H bond fission and H_2 elimination are not included as we are not sensitive to these channels in our experiment.

5. ONR/NRL Workshop on Energetic Materials Initiation Fundamentals, 30 October-1 November 1984.

6. L. J. Butler, Ph.D. Thesis, University of California, Berkeley 1985.

7. This is a result of both sets of products recoiling down a similar repulsive energy surface except for the difference in final product energies. The complete or partial resolution in TOF spectra of products from carbon-halogen bond fission producing two spin-orbit states of halogen atom product has been previously observed by several workers cited in Ref. 6.

8. M. D. Barry and P. A. Gorry, Mol. Phys. 52, 461 (1984).

9. D. Krajnovich, Z. Zhang, L. Butler, and Y. T. Lee, J. Phys. Chem. 88, 4561 (1984).

10. R. N. Zare, Mol. Photochem. 4, 1 (1972).

11. Y. B. Band, K. F. Freed, and S. J. Singer, J. Chem. Phys. 84, 3762 (1986), and references by Band, Freed, et al. within.

12. D. J. Krajnovich, Ph.D. thesis, University of California, Berkeley, California, Appendix B, 1983.

13. V_{00} = 12255 cm^{-1} for the $A^3\Pi_1$ state of IBr is obtained from K. P. Huber and G. Herzberg, Molecular Spectra and Molecular Structure IV: Constants of Diatomic Molecules (Van Nostrand Reinhold Co., New York, 1979).

14. This work was published in preliminary form as a communication. L. J. Butler, E. J. Hintsa, and Y. T. Lee, J. Chem. Phys. 84, 4104 (1986).

15. (a) See Ref. 27 and (b) M. S. Child and R. B. Bernstein, J. Chem. Phys. 59, 5916 (1973).

16. a) P. J. Robinson and K. A. Holbrook, Unimolecular Reactions, (Wiley-Interscience, New York, 1972), b) I. W. M. Smith, Kinetics and Dynamics of Elementary Gas Reactions (Butterworth, London/ Boston, 1980).

17. F. F. Crim, Ann. Rev. Phys. Chem. 35, 657 (1984).

18. a) J. G. Calvert and J. N. Pitts, Jr., Photochemistry (John Wiley and Sons, Inc., New York, 1966), Chap. 5, p. 522-528.; b) R. P. Wayne, Photochemistry (American Elsevier Publishing Co., Inc., New York, 1970) Chap. 3, p. 66-67.

19. See Calvert and Pitts of Ref. 18, Chap. 5, p. 526.

20. Electronic levels in iodoalkanes are derived with analogy to HI, see R. S. Mulliken, Phys. Rev. 51, 310 (1936), related papers, and ibid. 47, 413 (1935) as well as the review given in Ref. 2.

21. J. T. Yardley, Introduction to Molecular Energy Transfer (Academic Press, New York, 1980).

22. Transitions dipole moments to the $^3Q_0$ surfaces of the $n \rightarrow \sigma^*$ transitions are parallel to each bond (Ref. 19) and the C-I and C-Br bonds are parallel to each other before the Franck-Condon excitation. The molecules are cooled in the expansion and the molecular ground state is lowest in energy in the trans configuration by 1.15 kcal/mol according to Ref. 3.

23. J. P. Simons and A. J. Yarwood, Nature 192, 943 (1961).

24. W. H. Pence, S. L. Baughcum, and S. R. Leone, J. Phys. Chem. 85, 3844 (1981).

25. D. W. G. Style and J. C. Ward, J. Chem. Soc., 2125 (1952).

26. The description is analogous to the least motion reaction path shown for a more restricted case where the two halogens have the same identity and the initial transition is not localized on one of the bands by S. R. Cain, R. Hoffman, and E. R. Grant, J. Phys. Chem. 85, 4046 (1981).

27. G. N. A. van Veen, "Excited Species from Photofragmentation," Ph.D. Thesis, Amsterdam (1984).

28. G. E. Busch and K. R. Wilson, J. Chem. Phys. 56, 3626 (1972).

29. Such a result was first suggested in Ref. 1 and selective fission of the C-H bond over the C-I bond in CH_3I was observed by M.R. Levy and J.P. Simons, J. Chem. Soc. Faraday Trans. 2 71, 561 (1975).

Table 1: Summary of primary experimental results.

Reaction	Wavelength	$\bar{E}_T$ (kcal/mol)	FWHM (kcal/mol)	$E_T(max)$[a] (kcal/mol)	β	E_{avail}[b] (kcal/mol)	$f_T = \frac{\bar{E}_T}{E_{avail}}$
$CH_2BrI \rightarrow CH_2Br + I(^2P_{3/2})$	248.5	18.6	4.3	--	1.0 ± 0.1	60.0	.31
$\rightarrow CH_2Br + I(^2P_{1/2})$	248.5	12.4	4.5	--	1.0 ± 0.1	38.3	.32
$\rightarrow CH_2I + Br(^2P_{3/2}, \underline{^2P_{1/2}})$[c]	248.5	11.1	8.2	--	0.6 ± 0.1	(47.4, <u>36.8</u>)[c]	(.23, <u>.30</u>)[c]
$CH_2BrI \rightarrow CH_2I + Br(^2P_{3/2}, \underline{^2P_{1/2}})$[c]	210	15.0	9.2	--	(||)[d]	(68.5, <u>57.9</u>)[c]	(.22, <u>.26</u>)[e]
$\rightarrow CH_2 + IBr(^3\Pi_1)$[e]	210	5.5	7.1	13.6	--	12.5[e,f]	.44[e]
$CH_2BrI \rightarrow CH_2Br + I(^2P_{1/2})$	193.3	14.1	8.5	--	~0	71.1	.20
$\rightarrow CH_2I + Br(^2P_{1/2})$	193.3	14.1	10.0	--	~0	69.7	.20
$\rightarrow CH_2 + IBr(^3\Pi_1)$[e]	193.3	11.7	19.0	23.7	~0	24.3[e]	.48[e]

a) $E_T(max)$ is the maximum energy in translation for those processes in which a sharp cutoff is observed.

b) E_{avail} for this table = $E_{h\nu} - \Delta E_{rxn} - E_{elec}$; e.g. for C-Br fission to form spin-orbit excited Br $\Delta E_{rxn} = D_0(C\text{-}Br)$ and E_{elec} = 10.54 kcal/mol, the spin-orbit splitting of Br. The initial internal energy of the parent is not included here but is discussed in the text.

c) The more likely spin-orbit state of the Br product is underlined, see text.

d) (||) signifies a parallel angular distribution, here $\beta = 0.6 \pm 0.3$.

e) The electronic state of the IBr product is assumed to be solely $^3\Pi_1$ for this table. The experiment only determined that some of the IBr is formed in the $^3\Pi_1$ state and none is formed in the ground state. Some fraction of the IBr may be formed in the $^3\Pi_0$ state if energetically allowed.

f) Note the $E_T(max)$ is greater than E_{avail} because the internal energy of the CH_2BrI parent of ~1.5 kcal/mol was not included in the E_{avail}.

FIGURE CAPTIONS

Fig. 1. UV absorption spectra of gaseous CH_2BrI (Cary spectrometer).

Fig. 2. Energetically allowed dissociation channels of CH_2BrI excited at 193 and 248 nm. The C-I and C-Br bond dissociation enthalpies are assumed to be the same as those of CH_3I and CH_3Br calculated from heats of formation given in Ref. 4. The HI and HBr elimination channel endothermicities were calculated using the C-I and C-Br energies estimated above, the H, I and Br heats of formation from Ref. 4 and the assumption that the enthalpy of $CH_2X \rightarrow CHX + H$ (X=I,Br) is the same as that for $CH_3 \rightarrow CH_2 + H$ calculated from Ref. 4. The enthalpy for $CH_2BrI \rightarrow CH_2 + I + Br$ was calculated using $\Delta H_{f,0}$ from Rosenstock et al. (see Ref. 4) for the products and the enthalpy of formation of CH_2BrI at 0 K calculated by Kudchaker and Kudchaker (see Ref. 4). The IBr elimination channel enthalpy is calculated from the above value and the enthalpy of $I + Br \rightarrow IBr$ from Rosenstock et al. The energetically allowed C-H bond fission and H_2 elimination channels are not shown. An asterisk indicates the atom is formed in the $^2P_{1/2}$ spin-orbit excited state.

Fig. 3. 248 nm: Product TOF spectra taken at m/e=95, $CH_2{}^{81}Br^+$, at a source to detector angle of 20°. o Experimental points, ———— best fit to the data, obtained by adding the two components ——— — ——— of CH_2Br product from reactions 1a and 1b which are calculated from the two component $P(E_T)$ shown in Fig. 5, an anisotrcpy of β=1.0 for each channel, and a branching ratio of rxn 1b:1a of 0.75:1.

Fig. 4. 248 nm: Product TOF spectra taken at m/e=127, I^+, at source to detector angles of 10°, 20°, and 30°. o Experimental data, ———— fit calculated as the sum of the individual contributions of $I(^2P_{3/2})$ (——— — ———, shorter arrival time), $I(^2P_{1/2})$ (——— – ———, longer arrival time) (rxns. 1a and 1b) and I product from CH_2I secondary dissociation (— — —). The contributions from rxns. 1a and 1b are calculated from the two component $P(E_T)$ shown in Fig. 5 which was derived from the CH_2Br TOF spectrum (Fig. 3). The secondary dissociation contribution was calculated from a $P(E_T)$ shown in Ref. 6, see Section I.G. The two 20° TOF's shown differ only in that signal was accumulated during 2 μsec time intervals for one and 3 μsec time intervals for the other.

Fig. 5. Center-of-mass product translational energy distribution for $CH_2BrI \xrightarrow{248\ nm} CH_2Br + I$. The two component $P(E_T)$'s shown as ——— show the shape of each component channel (see text) producing I ($^2P_{1/2}$) (lower translational energies) and I ($^2P_{3/2}$) (higher translational energies). This $P(E_T)$ was derived from forward convolution fitting of the CH_2Br^+ TOF shown in Fig. 3 and was used to fit the I contribution from primary dissociation in the I^+ TOF spectra of Fig. 4. The branching ratio for formation of $I(^2P_{1/2}):I(^2P_{3/2})$ is found to be 0.75:1 from the relative areas under each $P(E_T)$ given the same anisotropy for each channel of $\beta = 1.0$.

Fig. 6. 248 nm: Product TOF spectra taken at m/e=141, CH_2I^+, at a source to detector angle of 20°. o Experimental points. ——— fit to the data calculated for CH_2I product from rxn. 2 from the $P(E_T)$ shown in Fig. 8.

Fig. 7. 248 nm: Product TOF spectra taken at m/e=81, $^{81}Br^+$, at source to detector angles of 10°, 20°, and 30°. o Experimental points. ——— shape of Br product contribution from C-Br primary bond fission (rxn. 2) calculated from the $P(E_T)$ shown in Fig. 8.

Fig. 8. Center-of-mass product translational energy distribution for $CH_2BrI \xrightarrow{248\ nm} CH_2I + Br$. Derived from forward convolution fitting of the CH_2I product TOF of Fig. 6.

Fig. 9. 248 nm: Product TOF spectra taken at m/e=140, CHI^+, top, and m/e=94, $CH^{81}Br^+$, bottom, at a source to detector angle of 20°. o Experimental points.

Fig. 10. 248 nm: Product TOF spectra taken at m/e=206, 208, $I^{79,81}Br^+$ at a source to detector angle of 10°. The assumed shape of the signal shown in (— — —) was used to calculate the shape of the signal that would be observed at CH^+ (see Fig. 11) if the IBr^+ signal were due to concerted elimination of IBr. o Experimental points. Signal is proposed to be from fragmentation of dimers. See text.

Fig. 11. 248 nm: Product TOF spectra taken at m/e=13, CH^+, at a source to detector angle of 20°. o Experimental points. ——— total fit, sum of contributions from CH_2I (— — —) and CH_2Br (—— – ——), calculated from the $P(E_T)$'s shown in Figs. 5 and 8. The hump at short arrival times (—— – – – ——) shows where one would expect CH_2 from $CH_2BrI \rightarrow CH_2 + IBr$ if the signal observed in Fig. 10 were IBr product. The fast data shown without a fit is attributed to CH_2 from the secondary photodissociation of CH_2Br and CH_2I products (see Sections I.F and I.G).

Fig. 12. 248 nm: Product TOF spectra taken with a lower seeding ratio to reduce clusters in the beam. Top, taken at m/e=127, I^+, at a source to detector angle of 10°. Middle, taken at m/e=81, $^{81}Br^+$, at a source to detector angle of 10°. Bottom, taken at m/e=94, $CH^{81}Br^+$, at a source to detector angle of 20°. o Experimental points.

Fig. 13. 248 nm: Product TOF spectra taken at m/e=81, $^{81}Br^+$, at two different laser pulse energies ~200 mJ/pulse and ~35 mJ/pulse at a source to detector angle of 20°. (Laser focused to 1 mm x 3 mm, 17 nsec pulse width.)

Fig. 14. 248 nm: a) (top) Polarization Dependence of I atom signal from C-I bond fission. o Experimental points. ———— best fit calculated using the $P(E_T)$ for C-I fission of Fig. 5 and an anisotropy of β=1.0 in expression (7). Fits showing confidence in the value of β are — — — β=1.1 and —·—·— β=0.9. (Data and all fits normalized to highest point = 1.0). Bottom left corner shows velocity vector diagram that indicates that the I signal intensity peaks when the electric vector is aligned parallel to the c.m. recoil direction of the fragment. Error in angle is ±2°. b,c) (left frames) Fits to m/e=127, I^+, TOF spectra taken at a source to detector angle of 20° with the polarization vector of the light at 0° and at 100° (see Fig. 14a for diagram). o Experimental points. ———— total fit to the data assuming each channel (—— – ——), rxn's 1a and b, independently has an anisotropy of 1.0 and using the

$P(E_T)$ derived from the unpolarized TOF data. d,e) (right frames) Fits to the same I^+ data as in b,c) assuming the channel producing $I(^2P_{1/2})$ has a β of 2.0 and that producing $I(^2P_{3/2})$ has a β of 0.5. The weighting of the two channels is chosen so the unpolarized light data (Fig. 4) and the total I atom signal intensity vs polarization (Fig. 14a) would still be fit. The poor fits obtained show the two channels do not have different anisotropies.

Fig. 15. 248 nm: a) (top) Polarization Dependence of CH_2I fragment signal from C-Br fission. o Experimental points. ———— best fit calculated using the $P(E_T)$ for C-Br fission of Fig. 8 and an anisotropy of β=0.6 in expression (7). Fits showing confidence in the value of β are — — — β=0.7 and —— – —— β=0.5 (data and all fits normalized to highest point = 1.0). Fits assume that the same anisotropy is representative of the whole $P(E_T)$. Newton diagram shown in bottom left.
b,c) Fits to the m/e=141, CH_2I^+, TOF spectra taken at a source to detector angle of 20° with the polarization vector of the light at 0° (middle) and at 100° (bottom). o Experimental points. ———— fit to the data assuming the whole $P(E_T)$ is for dissociation events with an anisotropy of β=0.6.

Fig. 16. 193 nm: Product TOF spectrum taken at m/e=141, CH_2I^+, at a source to detector angle of 20°. o Experimental points. ———— fit to the surviving CH_2I product signal calculated from the $P(E_T)$ shown in Fig. 17.

Fig. 17. Center-of-mass translational energy distribution for $CH_2BrI \xrightarrow{193\ nm} CH_2I + Br$, for which the CH_2I is left with little enough internal energy to be stable. The $P(E_T)$ was derived from fitting the CH_2I signal in Fig. 16. The $P(E_T)$ probably corresponds to formation of all $Br(^2P_{1/2})$. See text.

Fig. 18. 193 nm: Product TOF spectra taken at m/e=95, $CH_2{}^{81}Br^+$.
a) (top), o Experimental points. ———— fit to the signal from stable CH_2Br product from C-I bond fission of the monomer CH_2BrI. Fit was calculated from the $P(E_T)$ in Fig. 19.
b) (bottom), o Experimental points obtained under molecular beam conditions which reduce the ratio of clusters to monomer CH_2BrI in the beam.

Fig. 19. Center-of-mass product translational energy distribution for $CH_2BrI \xrightarrow{193\ nm} CH_2Br + I$ for which CH_2Br is left with little enough internal energy to be stable. The $P(E_T)$ was derived from fitting of the signal from dissociation of CH_2BrI monomer giving CH_2Br product in Fig. 18. The $P(E_T)$ probably corresponds to formation of all $I(^2P_{1/2})$. See text.

Fig. 20. 193 nm: Product TOF spectra taken at m/e=206,208, IBr^+, at source to detector angles of 10° (top) and 20° (bottom).
o Experimental points. ———— fit calculated from the $P(E_T)$ shown in Fig. 22.

Fig. 21. 193 nm: a) Top left, product TOF spectrum taken at m/e=127, I^+ at a source to detector angle of 20°. o Experimental points. ———— shape of signal from IBr product fragmenting to I^+ in the ionizer obtained from the IBr^+ TOF spectrum of Fig. 20 and the precalibrated ion flight time. Shading shows hump in data where the signal from IBr is evident. b) Bottom left, product TOF spectrum of m/e=81, Br^+, at a source to detector angle of 20°. o Experimental points. ———— shape of signal from IBr fragmenting to Br^+ in the ionizer obtained from the IBr^+ TOF spectrum and ion flight time difference. Shading shows hump in data where the signal from IBr is evident. c,d) Product TOF spectra of m/e=127, I^+ (top right) and m/e=81, $^{81}Br^+$ (bottom right) at a source to detector angle of 20° under molecular beam conditions where the ratio of clusters to monomers in the beam is reduced. Note features in these spectra corresponding to IBr product are just as intense relative to their signal in Fig. 21a and b. o Experimental points.

Fig. 22. Center-of-mass product translational energy distribution for $CH_2BrI \xrightarrow{193\ nm} CH_2 + IBr$, for which the IBr survived secondary dissociation to I + Br. IBr may be lost via predissociation if it has enough internal energy or via absorption of a 193 nm photon. The shape of the $P(E_T)$ below ~4 kcal/mol (shown as — — —) is not sensitive to the data as then the c.m. recoil velocity of the IBr is too small for detection at 10°.

Fig. 23. 193 nm: Product TOF spectra of m/e=127, I^+, at source to detector angles of 10, 20, and 30°. a,b,c) Left top, middle, and bottom, taken with the laser unpolarized and high power ~200 mJ/pulse. o Experimental points. d,e,f) Right top, middle, bottom, taken with laser polarized at 0° and the laser power reduced by a factor of 6 to 8. o Experimental points. ———— total fit to the data, sum of contributions from CH_2I from C-Br fission (short dashed, — — —) I from C-I fission (—— – ——), IBr from the concerted elimination (—— – – – ——), and I atoms from $CH_2BrI \longrightarrow CH_2 + Br + I$ (long dashed, —— ——). The first 3 contributions were obtained from other TOF spectra, see text. Each component fit is calculated from the corresponding $P(E_T)$ (Figures 17, 19, 22, and 27 respectively) and an anisotropy of β=0.

Fig. 24. 193 nm: Product TOF spectra of m/e=81, $^{81}Br^+$, at source to detector angles of 10, 20, and 30°. a,b,c) Left top, middle, bottom taken with the laser unpolarized and high power ~200 mJ/pulse. o Experimental points. d,e,f) Right top, middle, bottom taken with laser polarized at 0° and the laser power reduced by a factor of 6 to 8. o Experimental points. ———— total fit to the data, sum of contributions from Br from C-Br fission (short dashed, — — —), CH_2Br from C-I fission (—— – ——), IBr from concerted elimination (—— – – – ——) and Br atoms from $CH_2BrI \longrightarrow CH_2 + Br + I$ (long dashed, —— ——). The first three contributions were

obtained from other TOF spectra, see text. Each component fit is calculated from the corresponding $P(E_T)$ (Figures 17, 19, 22 and 27 respectively) and an anisotropy of $\beta=0$.

Fig. 25. 193 nm: Velocity vector diagram showing the range of c.m. recoil angles of the IBr, CH_2I, and Br fragments detected at a source to detector angle of 10°.

Fig. 26. 193 nm: Product TOF spectra of m/e=13, CH^+ at a source to detector angle of 20°. o Experimental points. — — — expected time-of-arrival of CH_2I product at CH^+, —— – —— expected time-of-arrival of CH_2Br product at CH^+, —— – – – —— expected time-of-arrival of CH_2 product momentum-matched with IBr product; scaling is arbitrary. Leftover signal is due to secondary photodissociation of mostly CH_2I and some CH_2Br product and reaction (8) $CH_2BrI \rightarrow CH_2 + I + Br$.

Fig. 27. 193 nm: Center-of-mass product translational energy distribution for IBr (product) (predissociation) $\rightarrow$ I + Br assuming the slow signal in the I^+ (Fig. 23) and Br^+ (Fig. 24) TOF spectra can be described by a two step process (see text). The translational energies for I atoms or Br atoms respectively (for comparison with Fig. 31) are $\frac{80}{207}$ and $\frac{127}{207}$ times the energies shown.

Fig. 28. 210 nm: Product TOF spectrum of m/e=141, CH_2I^+, at a source to detector angle of 20°. o Experimental points. ———— fit to the data calculated from the $P(E_T)$ shown in Fig. 30.

Fig. 29. 210 nm: Product TOF spectrum of m/e=81, $^{81}Br^+$, at a source to detector angle of 20°. o Experimental points, ———— total calculated fit to the data, sum of contributions of Br atoms from C-Br fission (— — —) and Br atoms from the triple dissociation $CH_2BrI \rightarrow CH_2 + Br + I$ (—— – – – ——). The former is calculated from the $P(E_T)$ shown in Fig. 30 derived from the TOF spectrum of the CH_2I product (Fig. 28) and the latter is the fit calculated from a distribution of translation energies (Fig. 34b) imparted to the Br fragment in the three-body dissociation.

Fig. 30. 210 nm: Center-of-mass product translational energy distribution for $CH_2BrI \xrightarrow{210\ nm} CH_2I + Br$. This $P(E_T)$ was derived from fitting of the CH_2I product TOF signal at CH_2I^+ shown in Fig. 28 and was used to fit the Br atom signal from primary C-Br fission shown in Fig. 29.

Fig. 31. 210 nm: Product TOF spectra of m/e=127, I^+, at source to detector angles of 10 and 20°. o Experimental points. ———— total fit to the data, the sum of contributions from CH_2I product of C-Br fission (— — —) and I atoms from the three-body dissociation $CH_2BrI \rightarrow CH_2 + Br + I$ (—— – – – ——) (some of the slow signal may be I atoms from spontaneous dissociation of CH_2I product). The former is calculated from the $P(E_T)$ shown in Fig. 30 (or from shifting the CH_2I spectrum at CH_2I^+ by the small difference in ion flight times) and the latter is the fit calculated from a distribution of translational

energies (Fig. 34a) imparted to the I fragment in three-body dissociation. (The 10° data also contains a contribution from slow IBr elimination product (long dashed, —— ——) calculated from the $P(E_T)$ shown in Fig. 33.) Each contribution is scaled for best total fit.

Fig. 32. 210 nm: Product TOF spectrum of m/e=208, $I^{81}Br^+$, at a source to detector angle of 10°. o Experimental points. ———— fit calculated from the $P(E_T)$ shown in Fig. 33.

Fig. 33. 210 nm: Center-of-mass product translational energy distribution from $CH_2BrI \xrightarrow{210} CH_2 + IBr$. The shape of the $P(E_T)$ below ~4 kcal/mol (divided at — — —) is not sensitive to the data as at those energies the c.m. recoil velocity of the IBr product is too small for it to be detected at 10°.

Fig. 34. 210 nm: Energies imparted to translation for two of the fragments from the reaction $CH_2BrI \xrightarrow{210} CH_2 + Br + I$. a) (left). Distribution of translational energies (c.m.) released to the I atom fragment; it is derived from fitting the slow signal in the I^+ 20° TOF spectrum (Fig. 31) assuming none of that signal is from spontaneous secondary dissociation of CH_2I product from C-Br fission (true if all $Br(^2P_{1/2})$ is formed). b) (right). Distribution of translational energies (c.m.) released to the Br atom fragment; it is derived from fitting the slow signal in the Br^+ TOF spectrum (Fig. 29).

Fig. 35. Schematic diagram of the LCAO-MO least motion path model for the concerted elimination of IBr from CH_2IBr. The path shown is one following a singlet excitation by the photon in which the CH_2 product is constrained to be triplet. A $^3\Pi$ IBr product is necessarily produced; no ground state IBr is formed in this model.

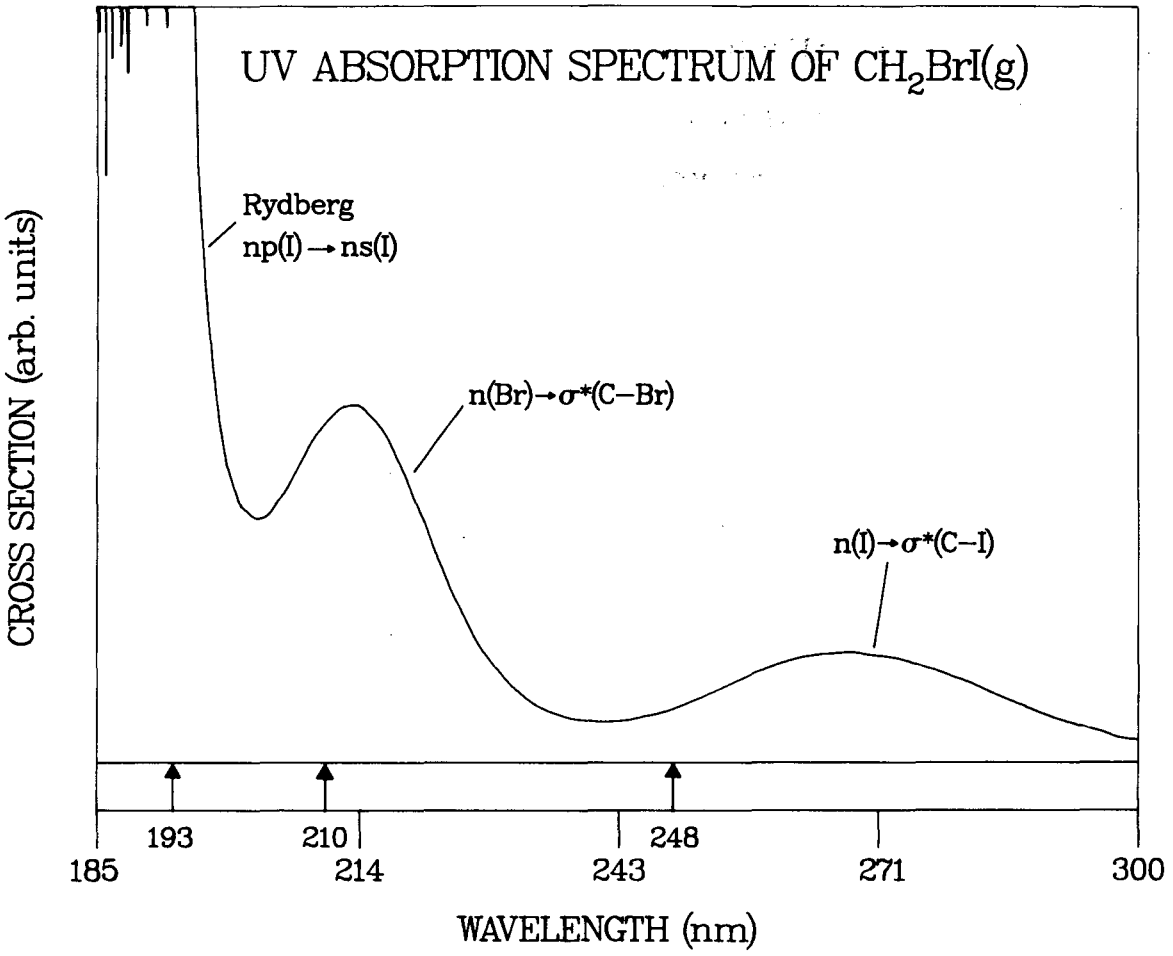

XBL 8510-4238

Fig. 1

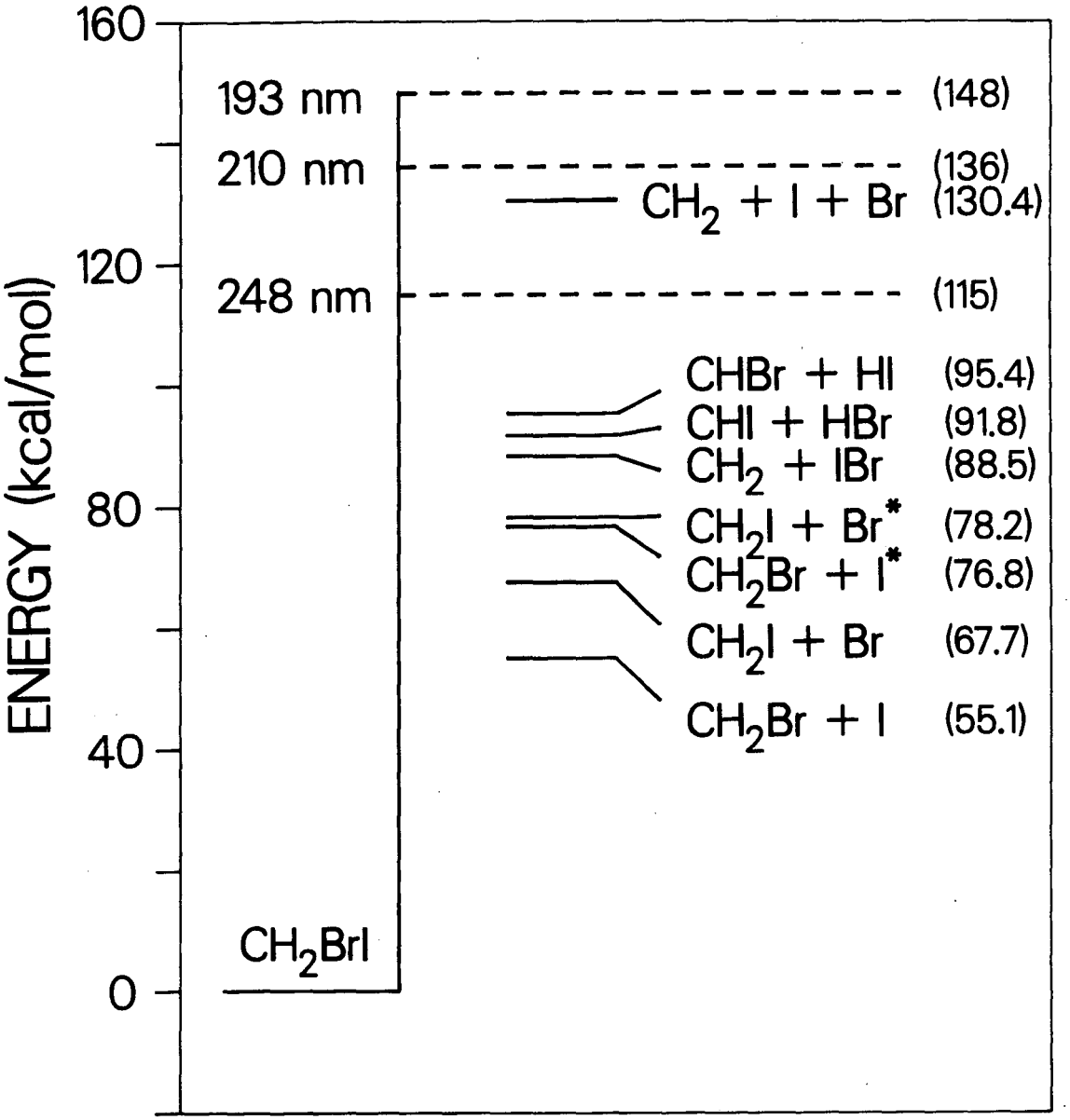

XBL 859 3871

Fig. 2

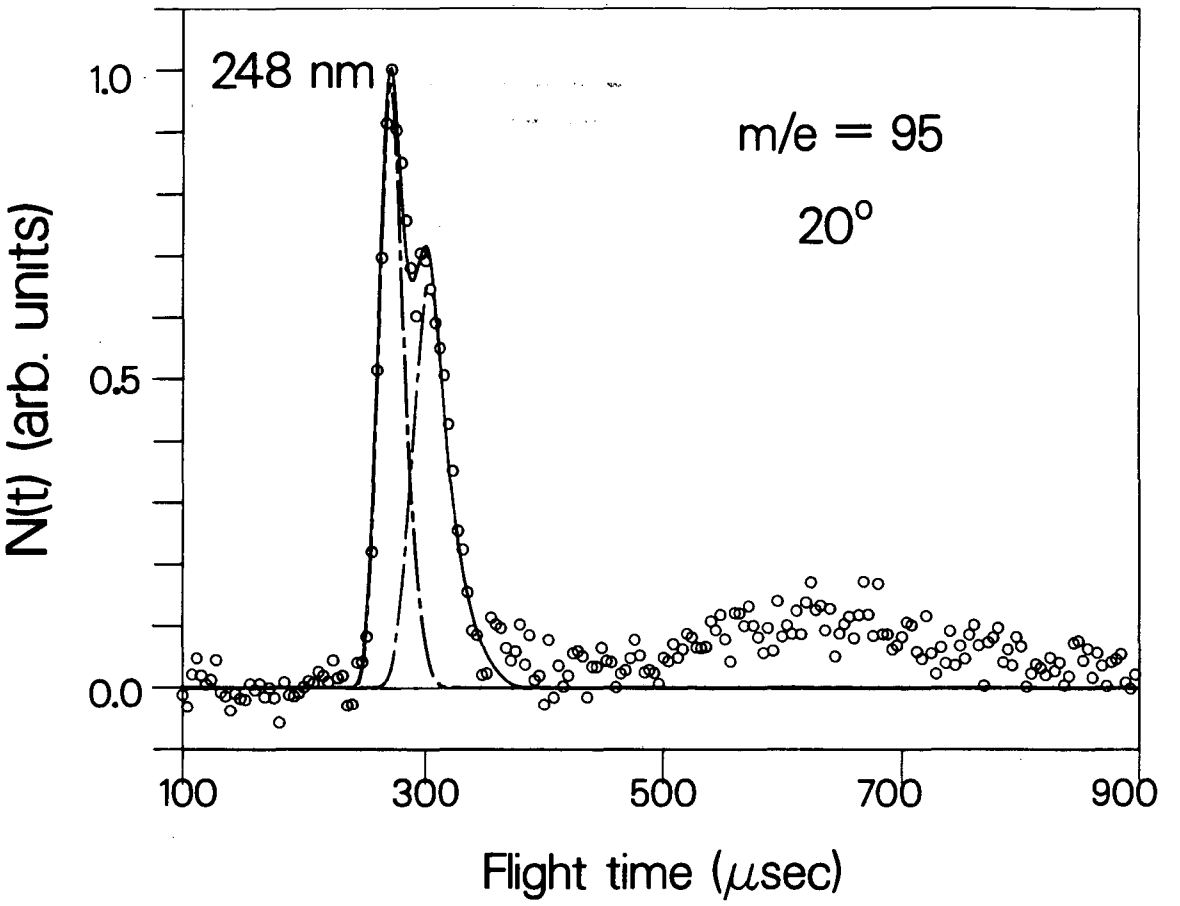

XBL 858 3721

Fig. 3

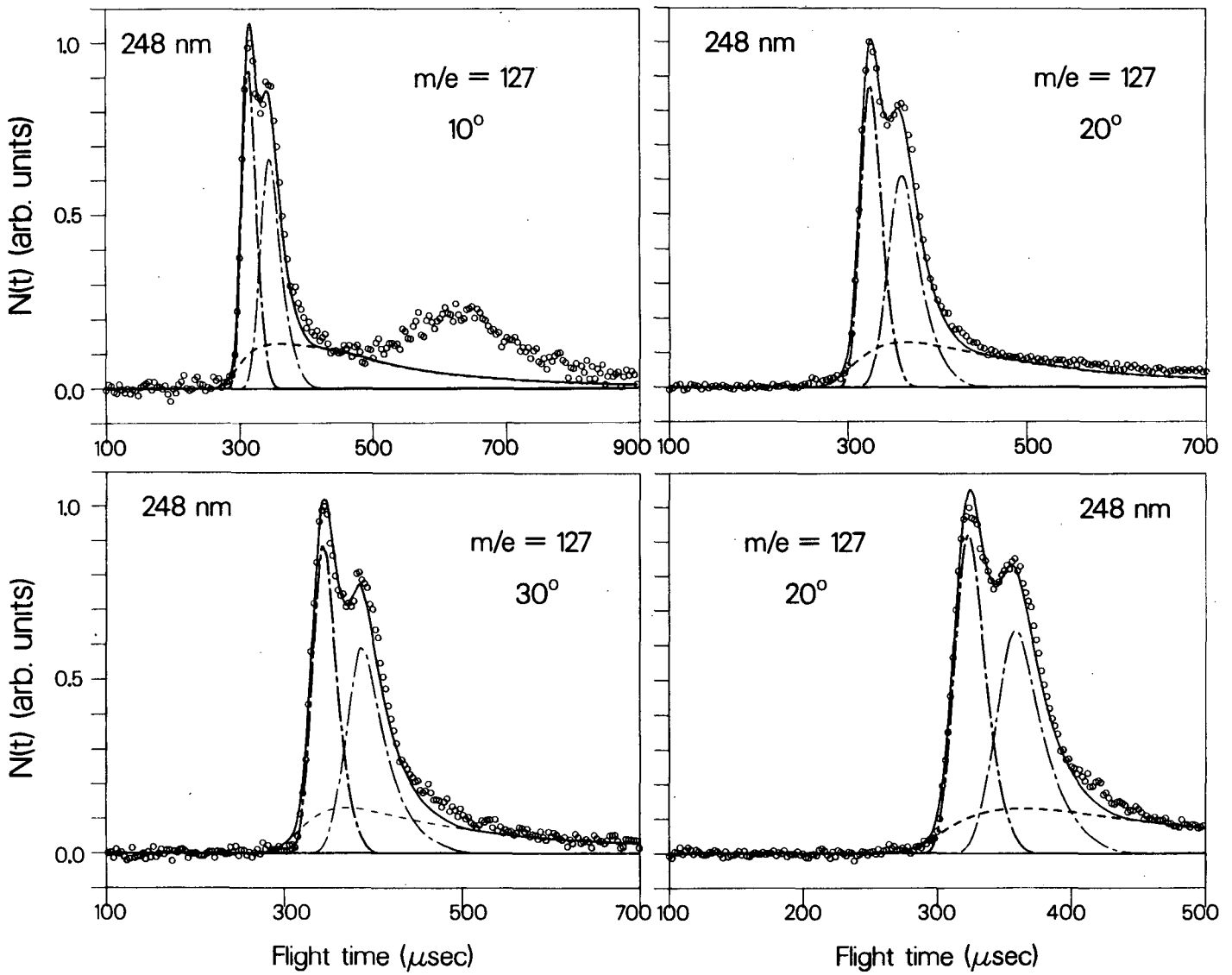

XBL 858 3728

Fig. 4

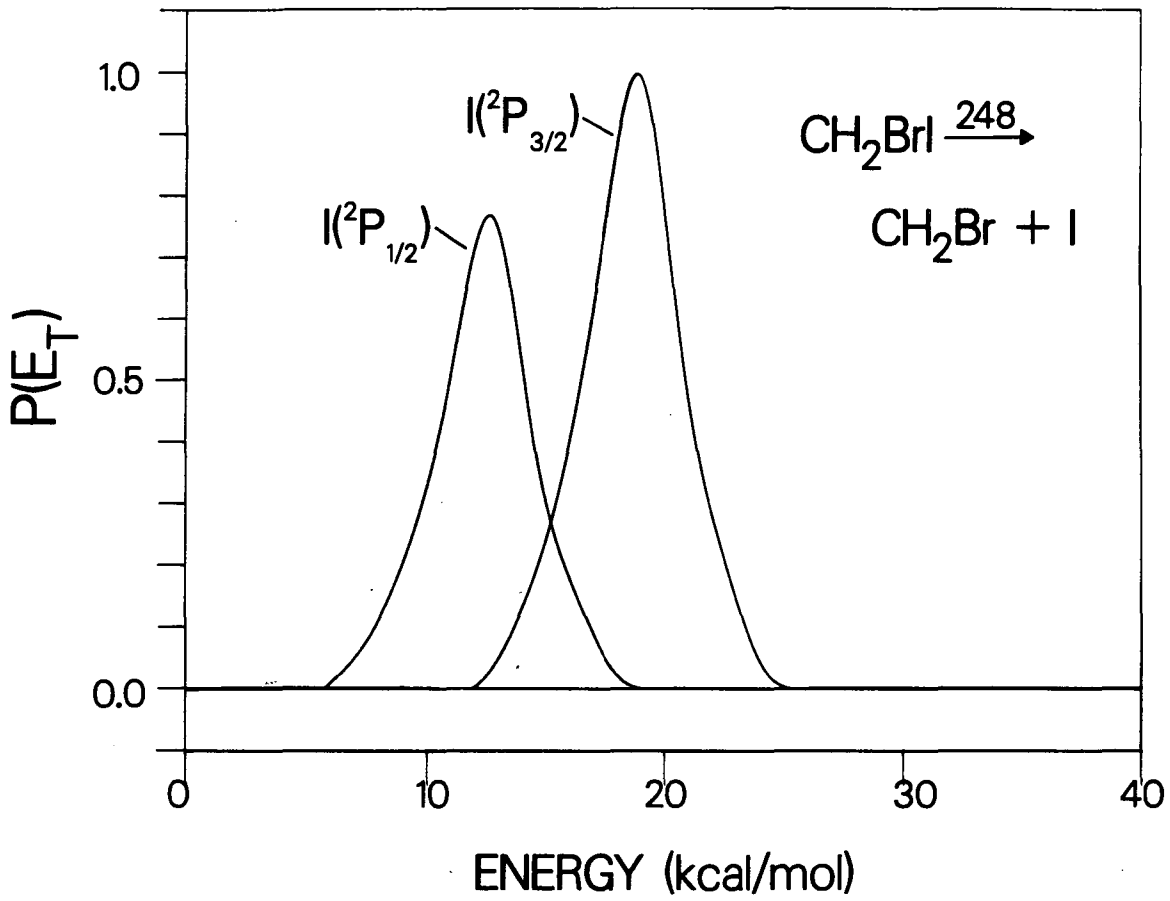

XBL 858 3722

Fig. 5

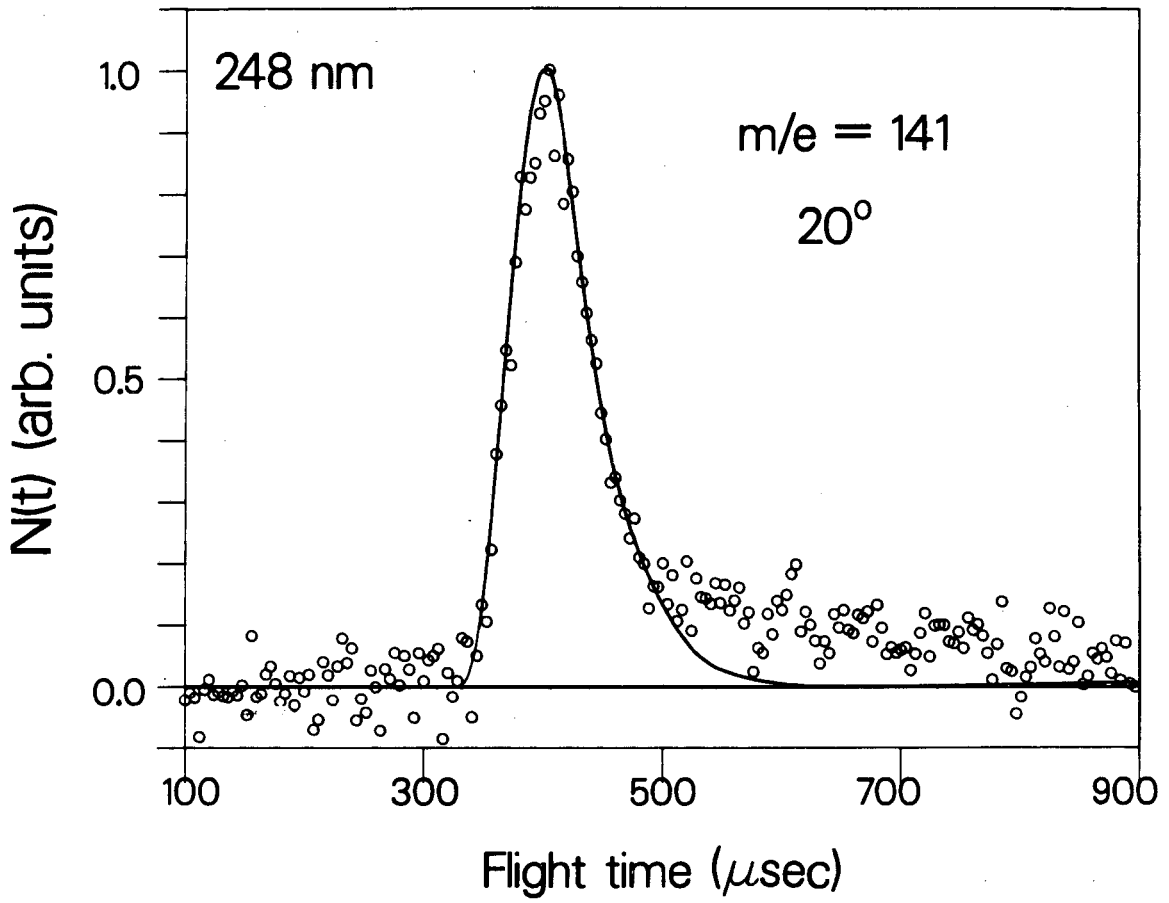

XBL 858 3727

Fig. 6

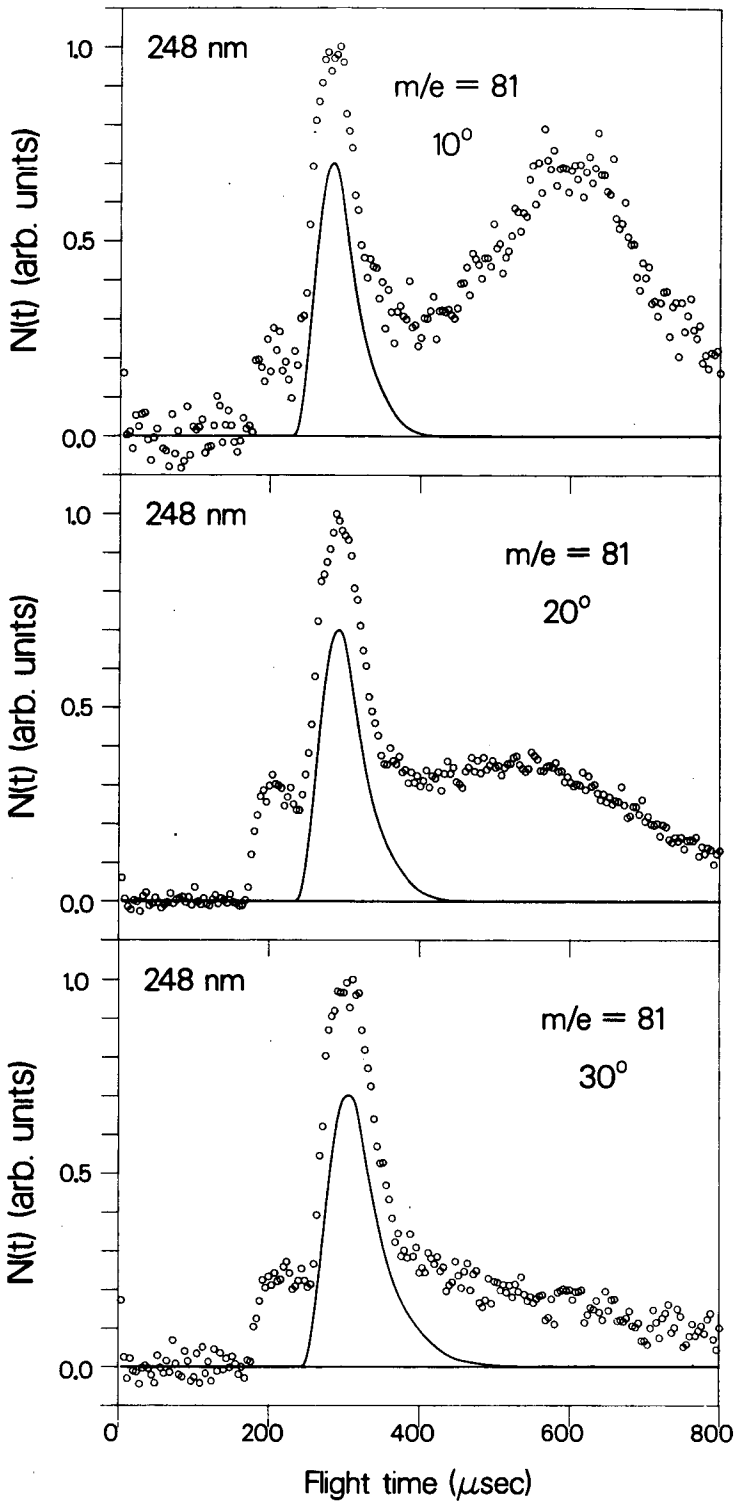

XBL859 3799

Fig. 7

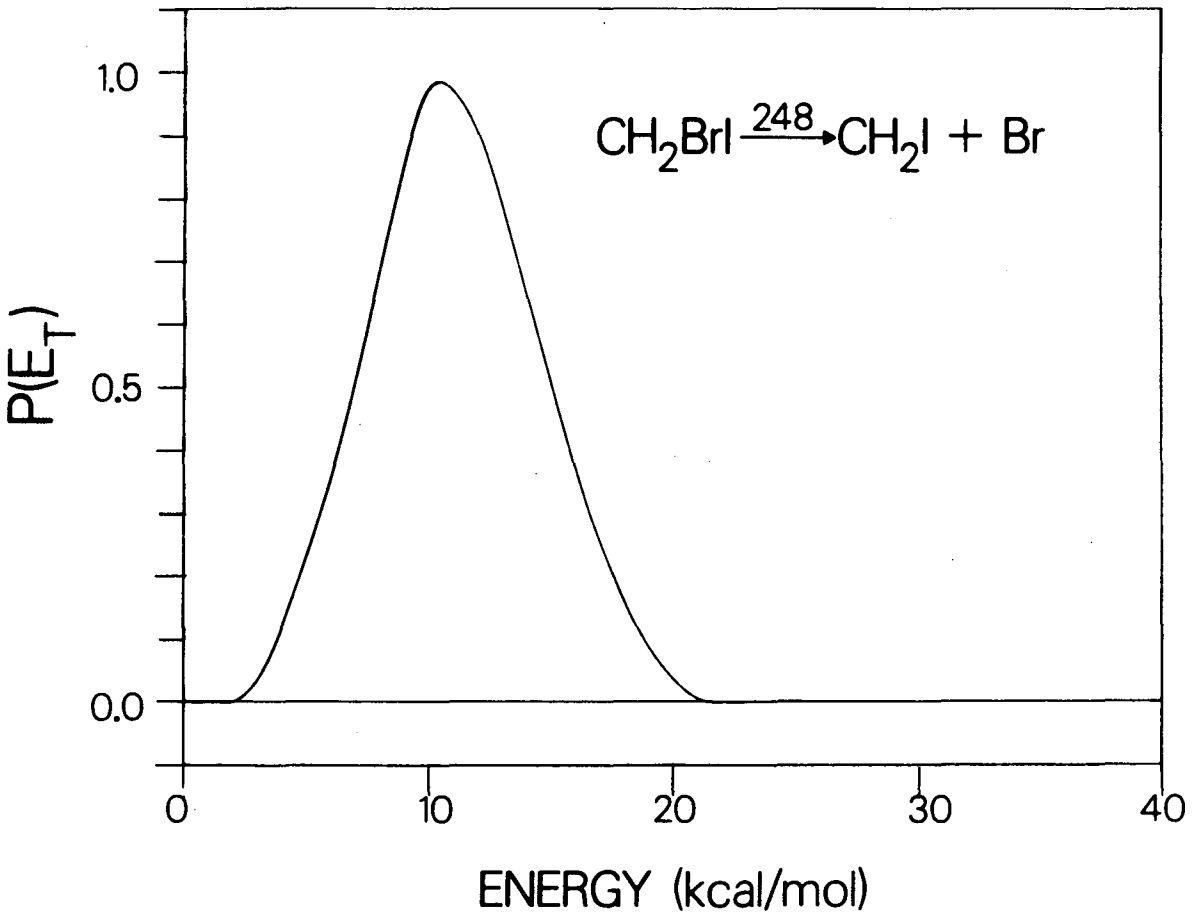

XBL 858 3731

Fig. 8

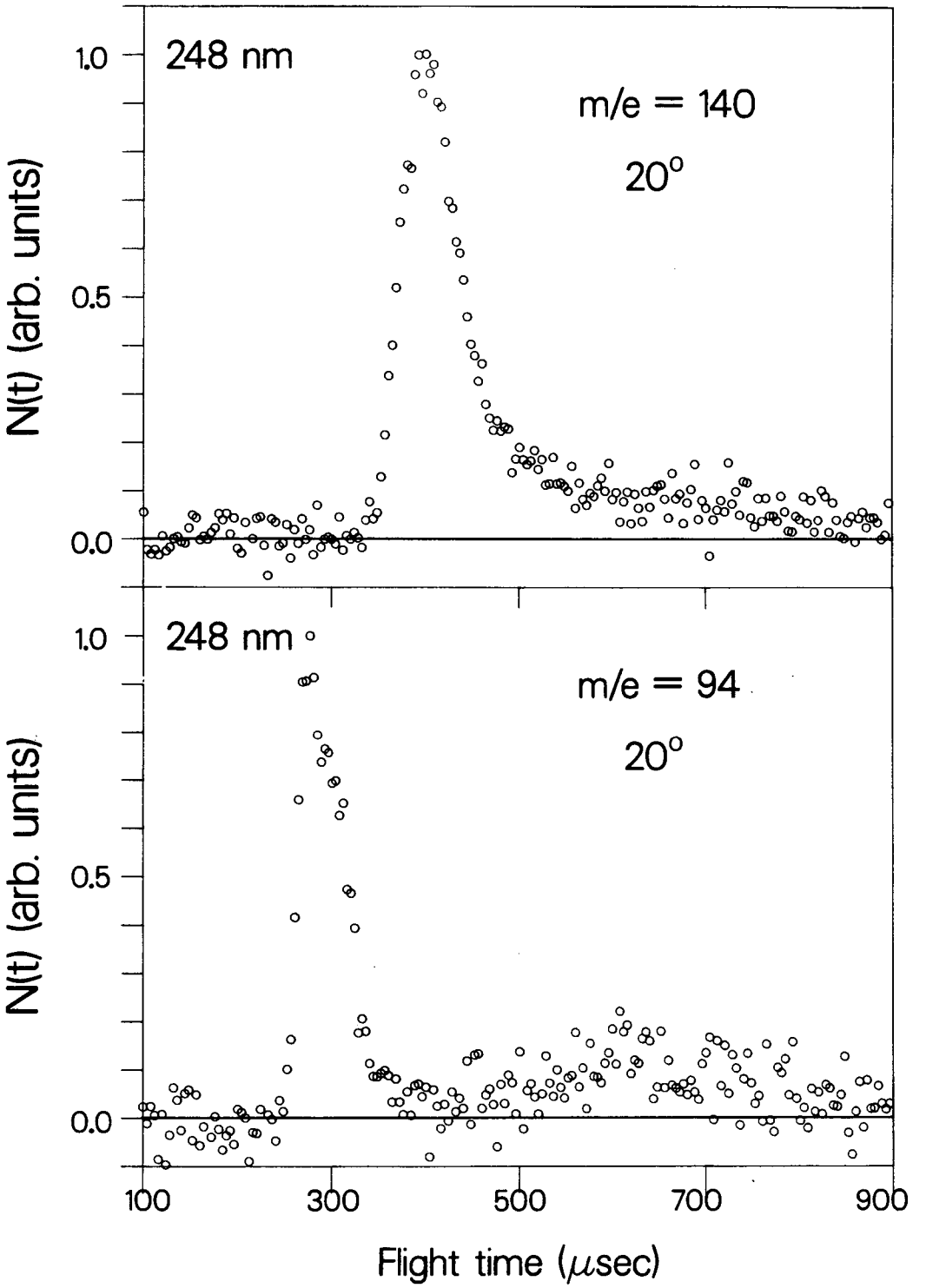

Fig. 9

XBL 858 3729

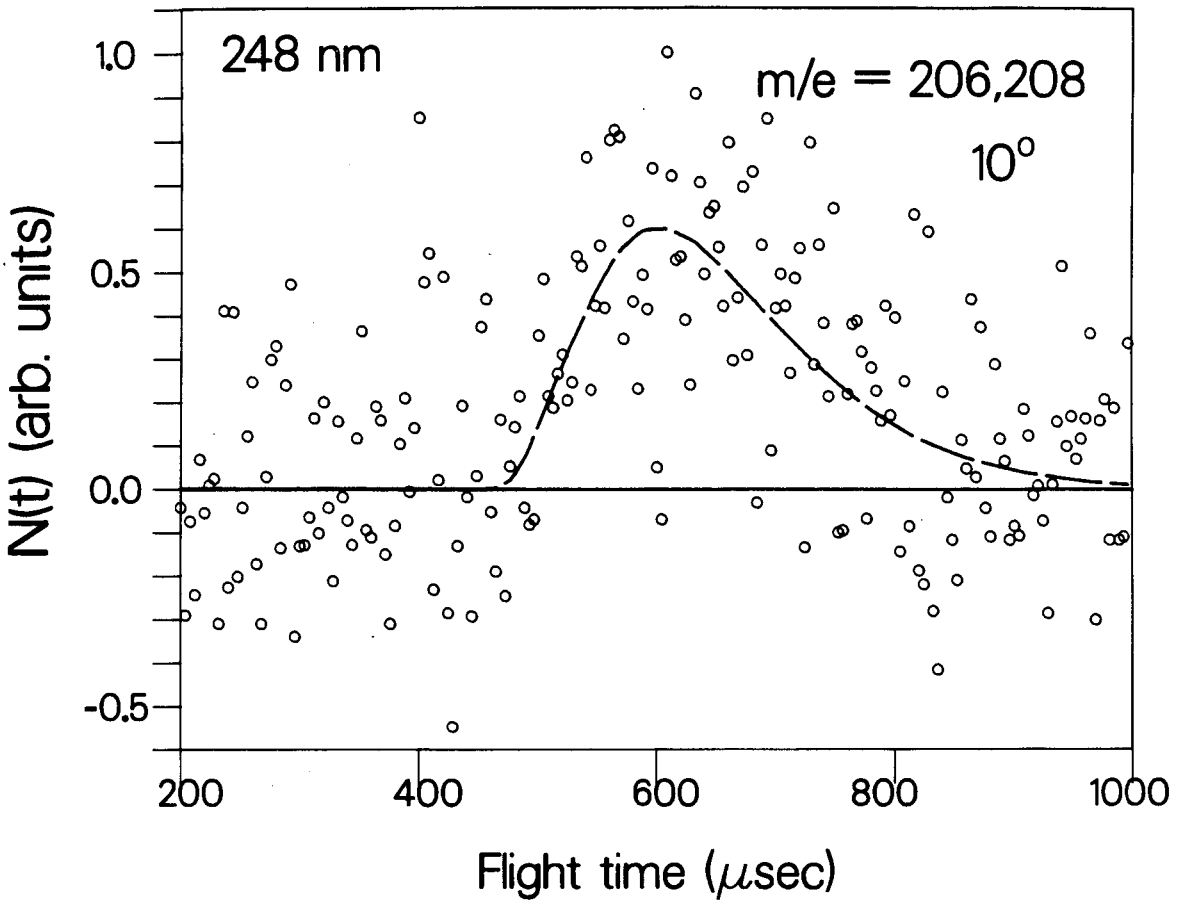

XBL 858 3724

Fig. 10

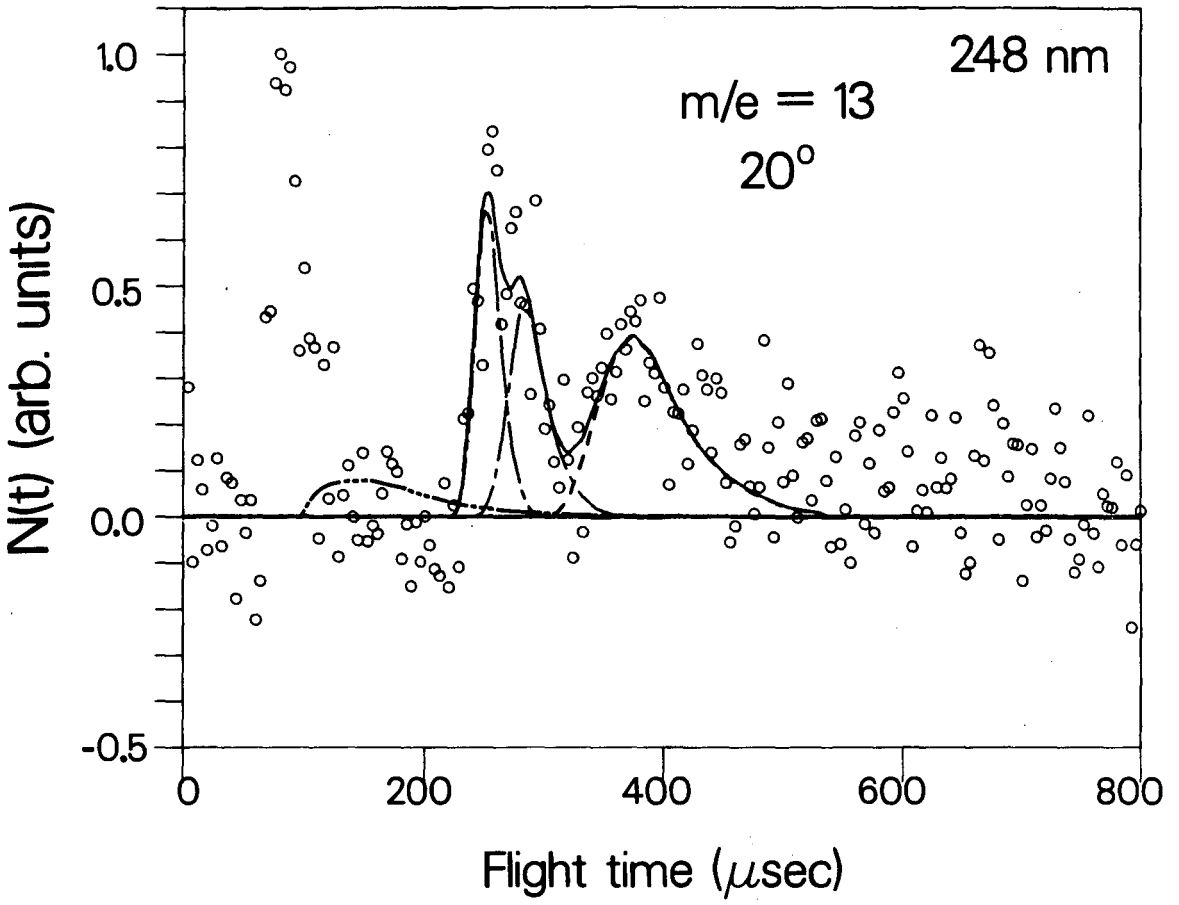

XBL 858 3723

Fig. 11

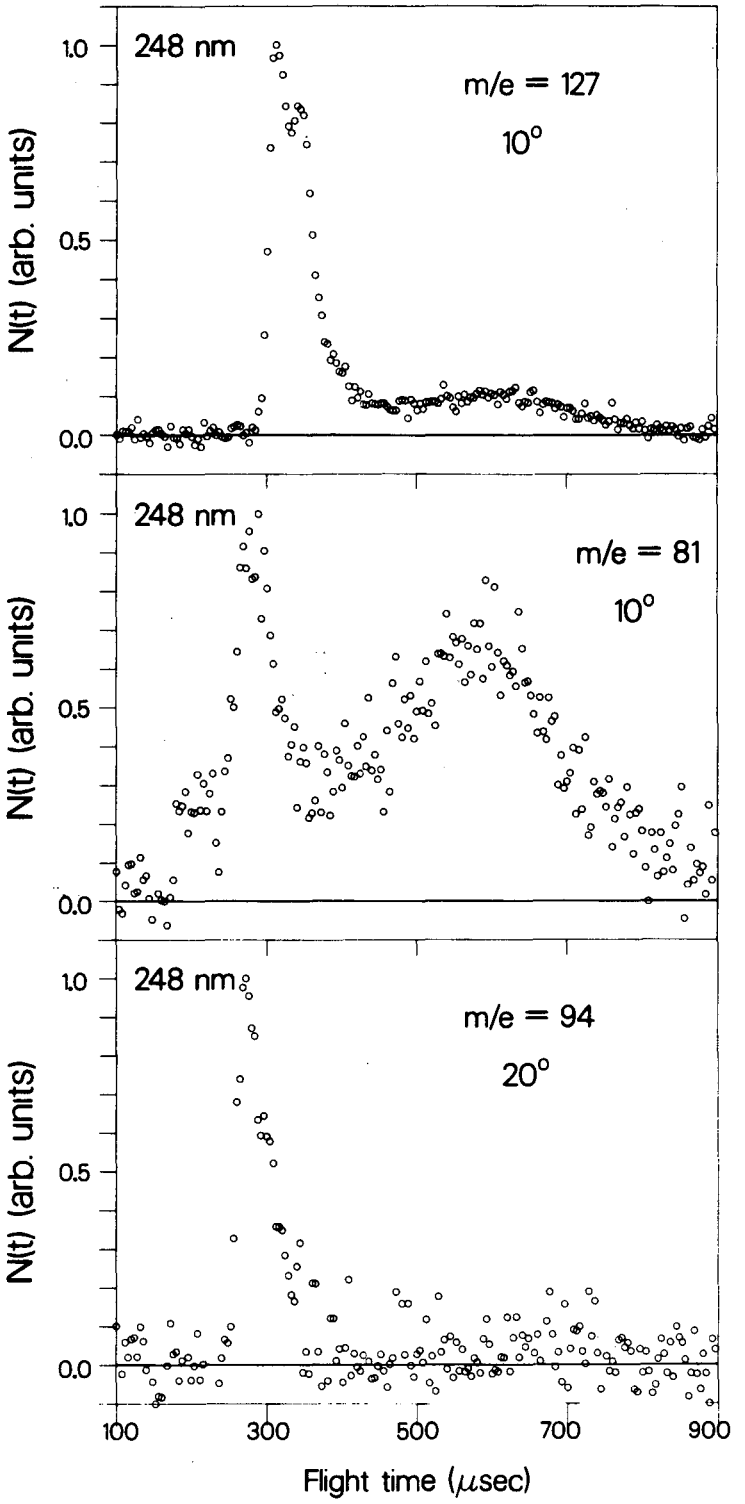

XBL 859 3800

Fig. 12

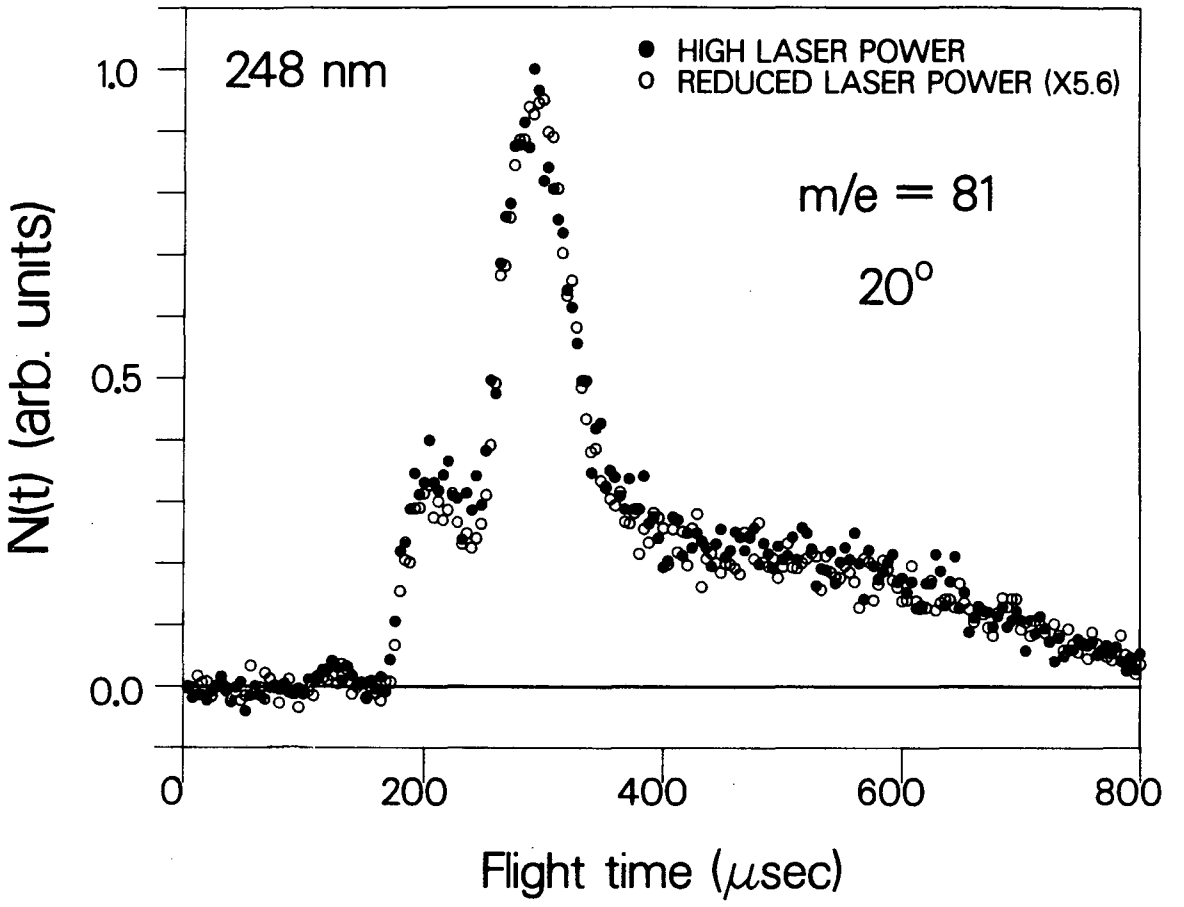

XBL 859 3795

Fig. 13

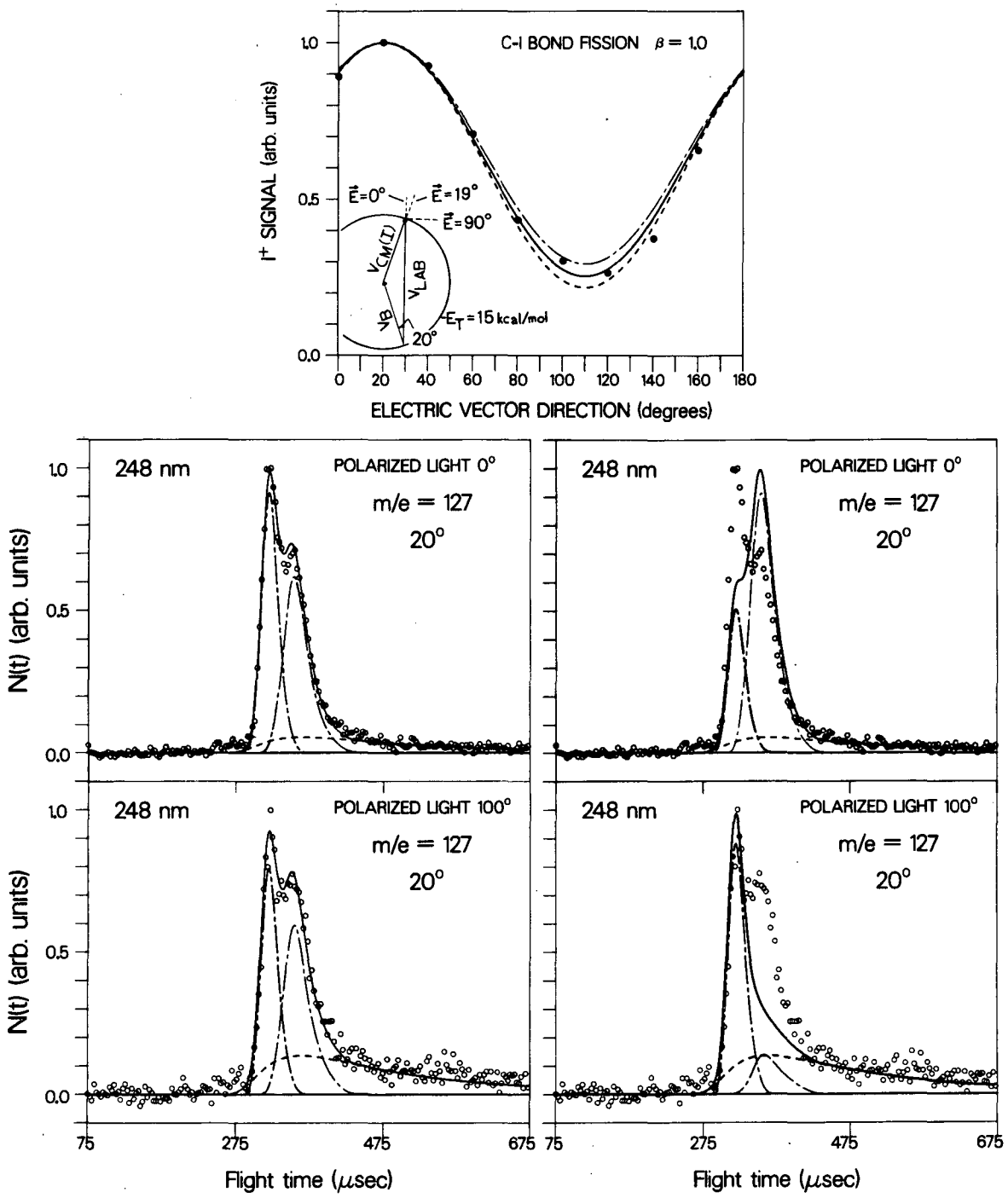

XBL 859 3798

Fig. 14

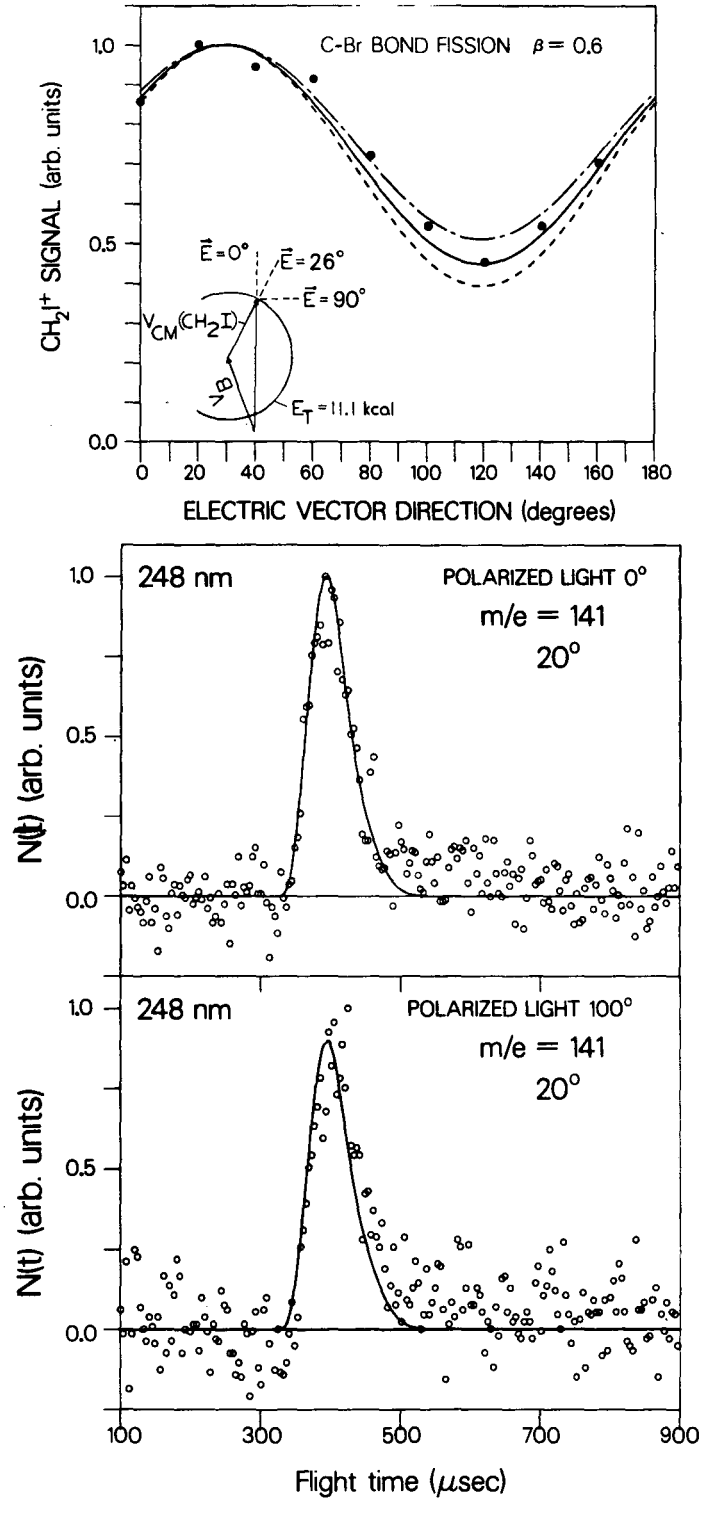

XBL 859 3971

Fig. 15

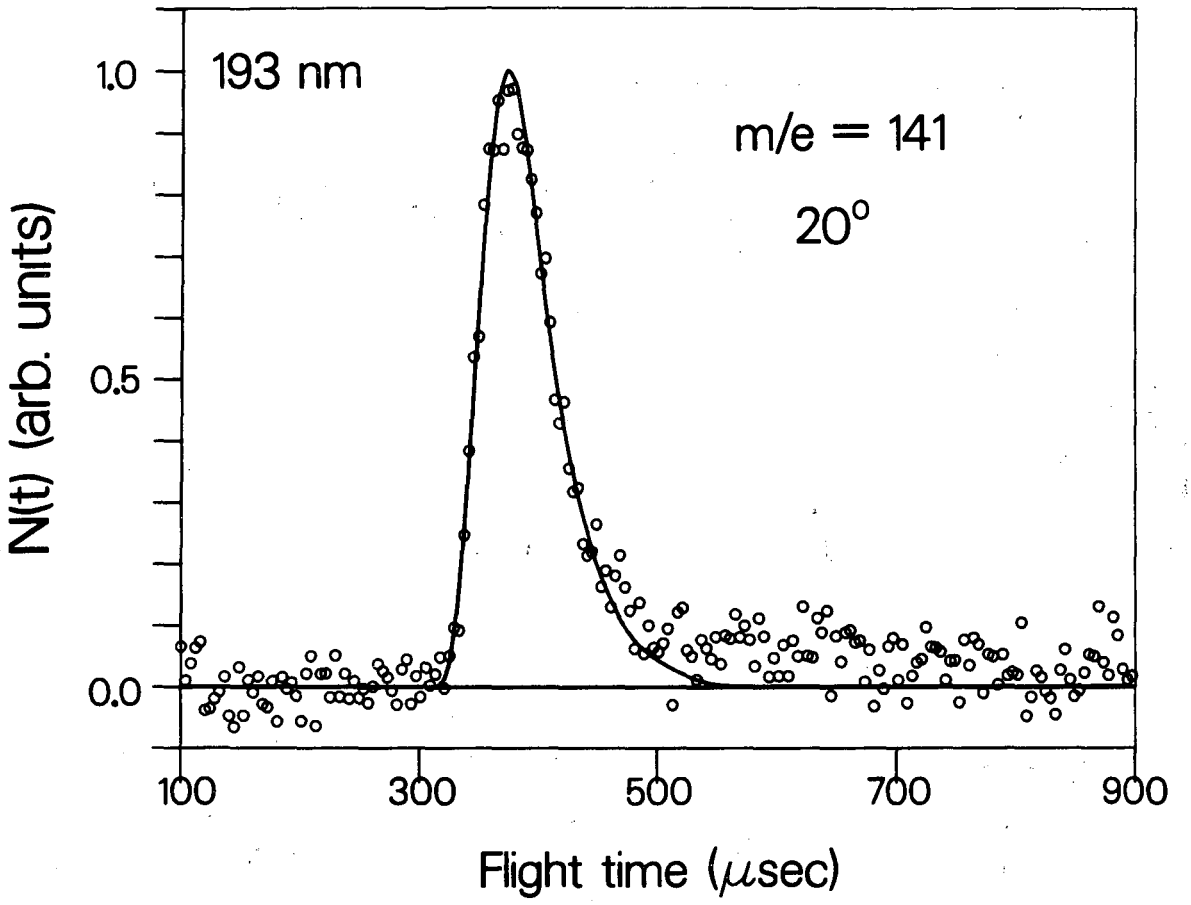

XBL 858 3725

Fig. 16

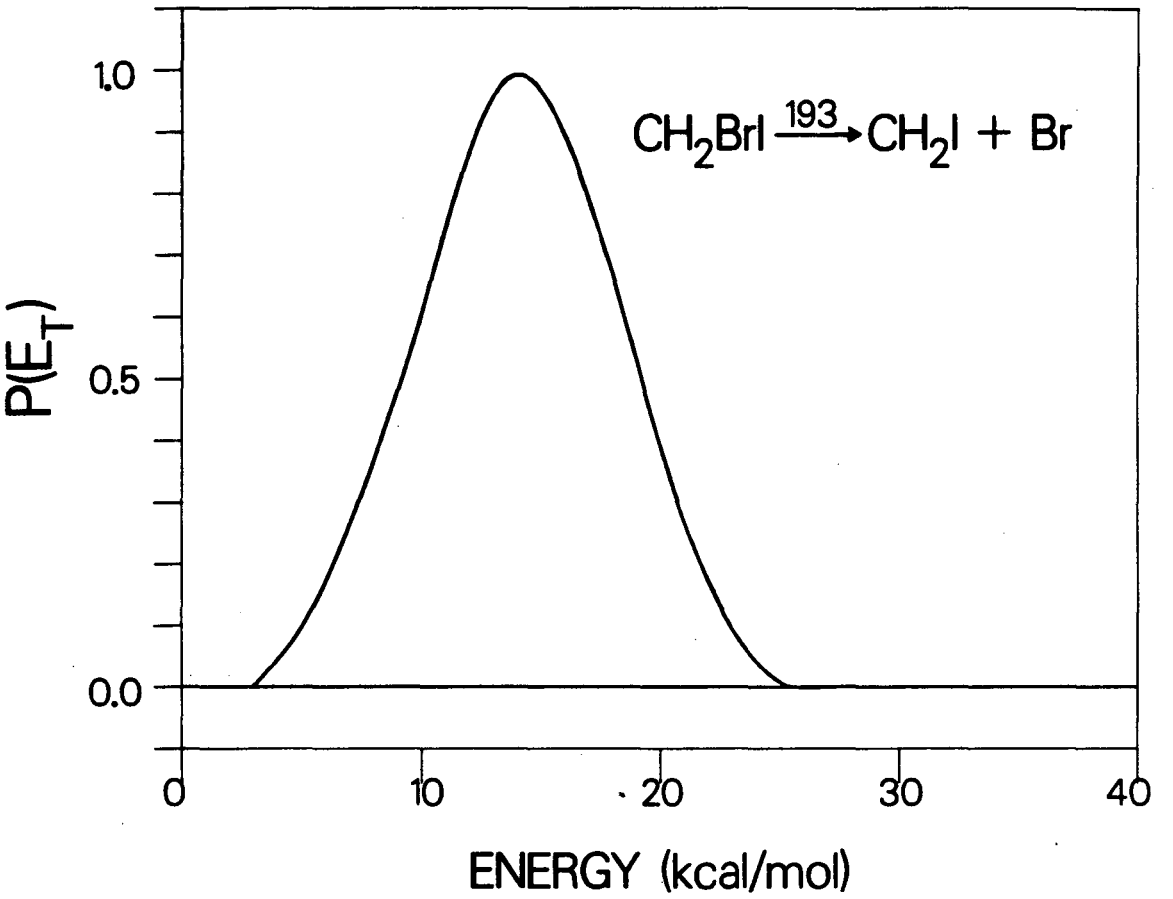

XBL 858 3730

Fig. 17

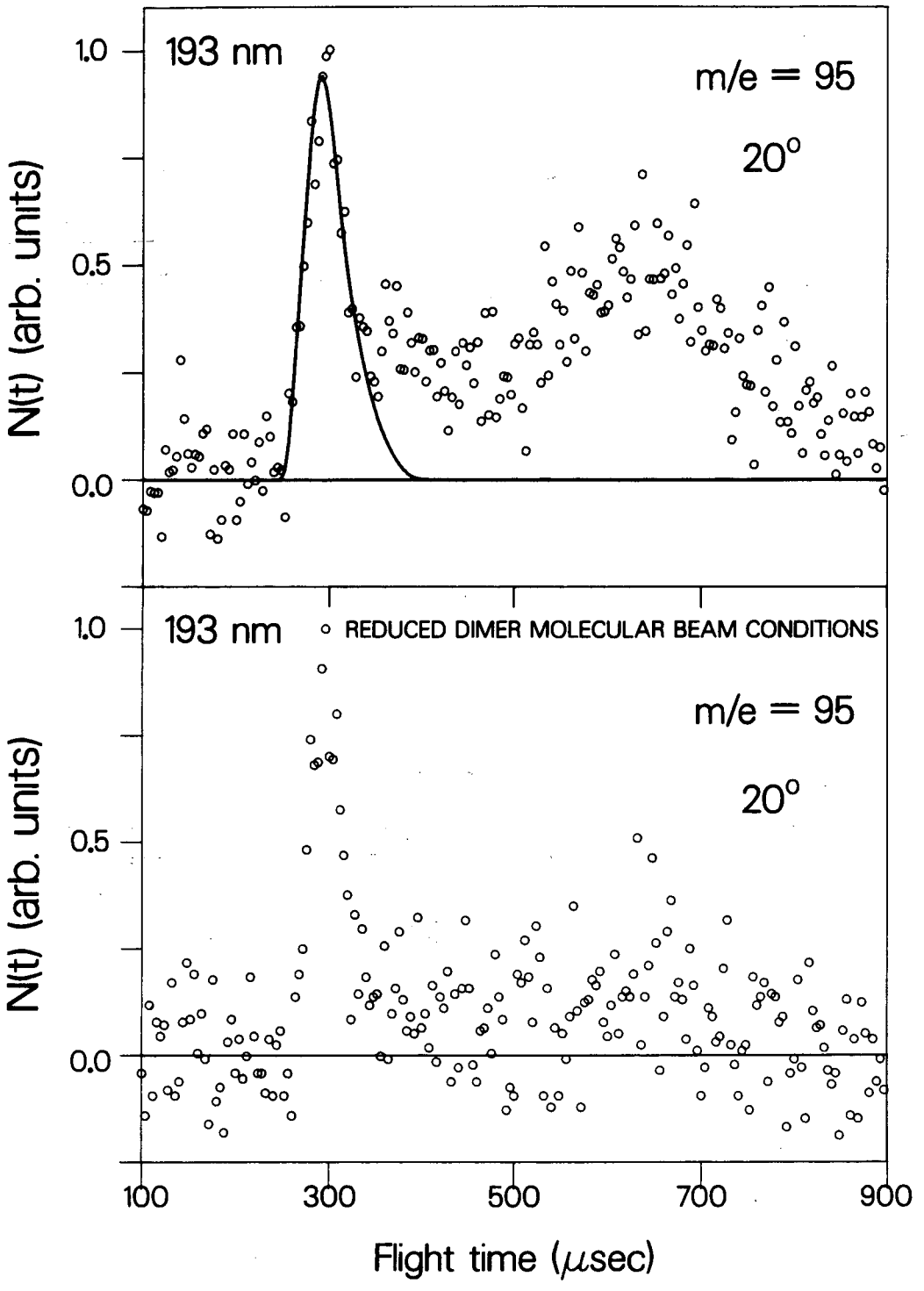

XBL 859 3797

Fig. 18

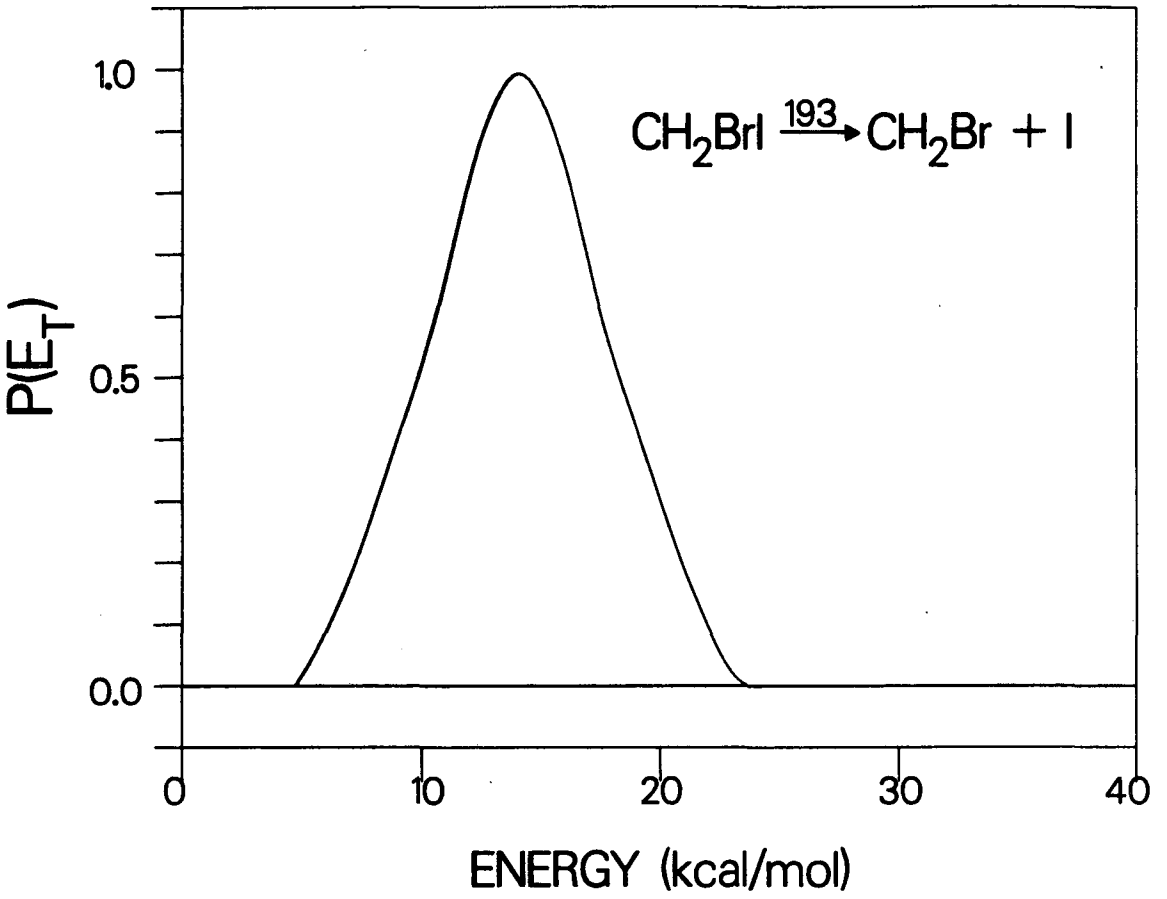

XBL 858 3726

Fig. 19

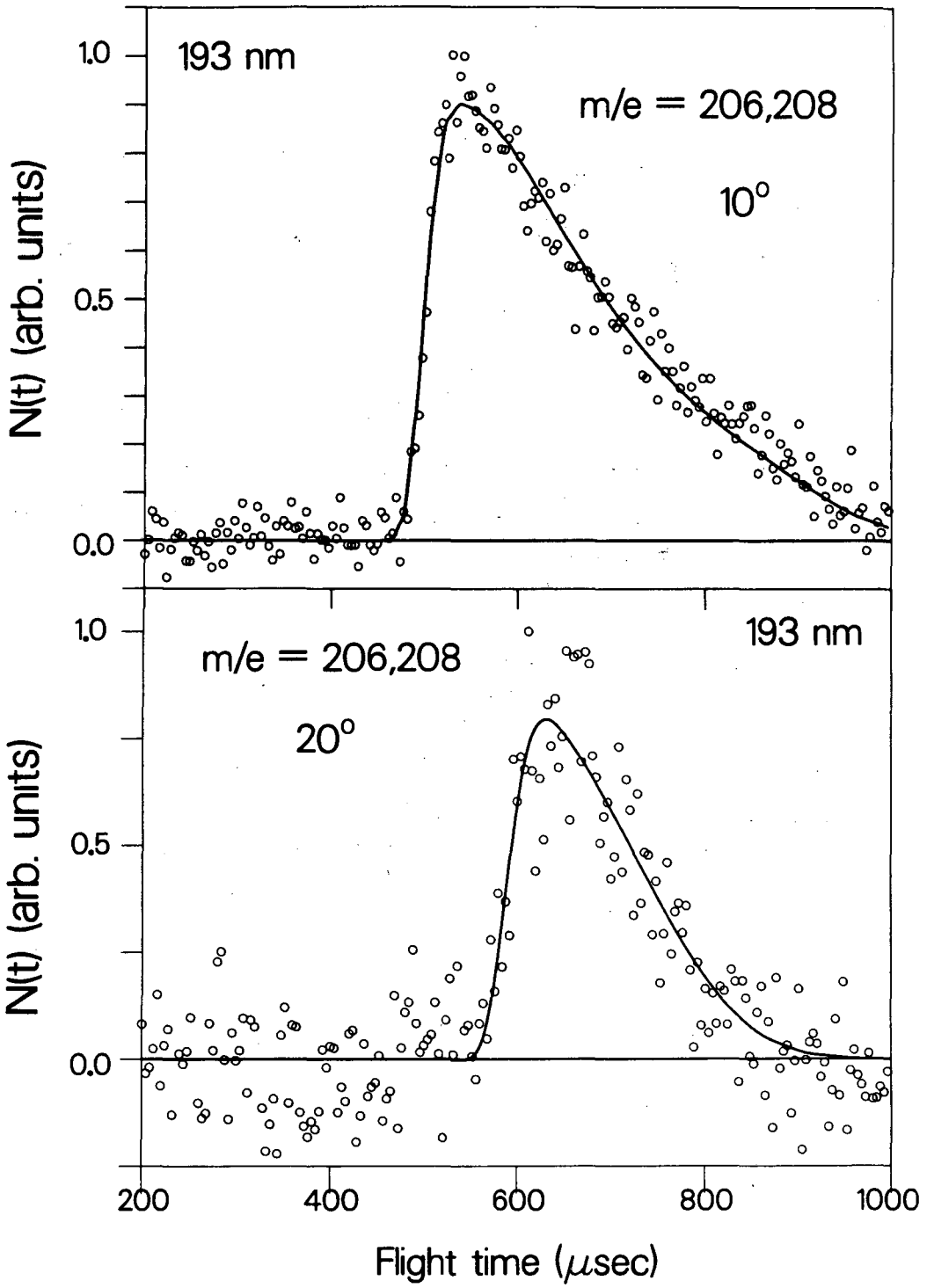

Fig. 20

XBL 859 3796

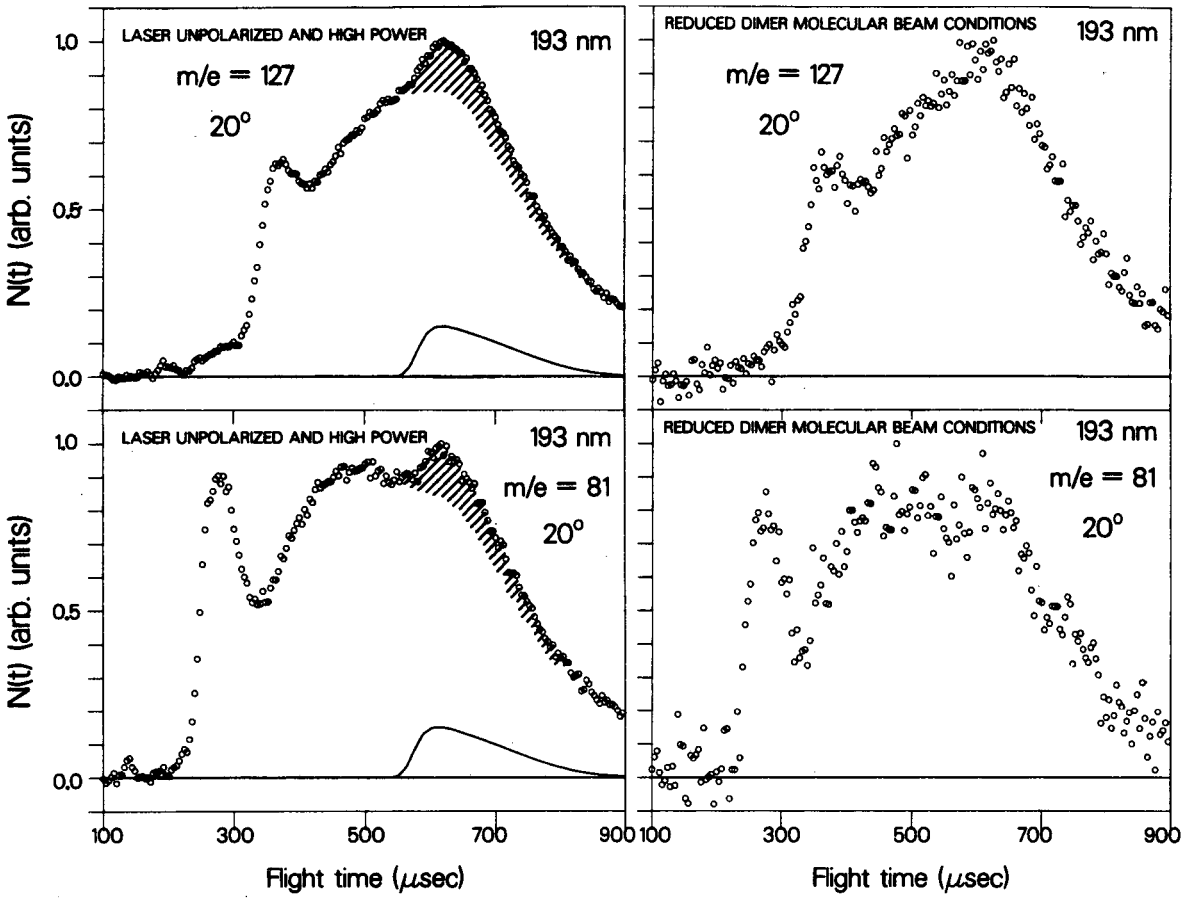

XBL 859 3802

Fig. 21

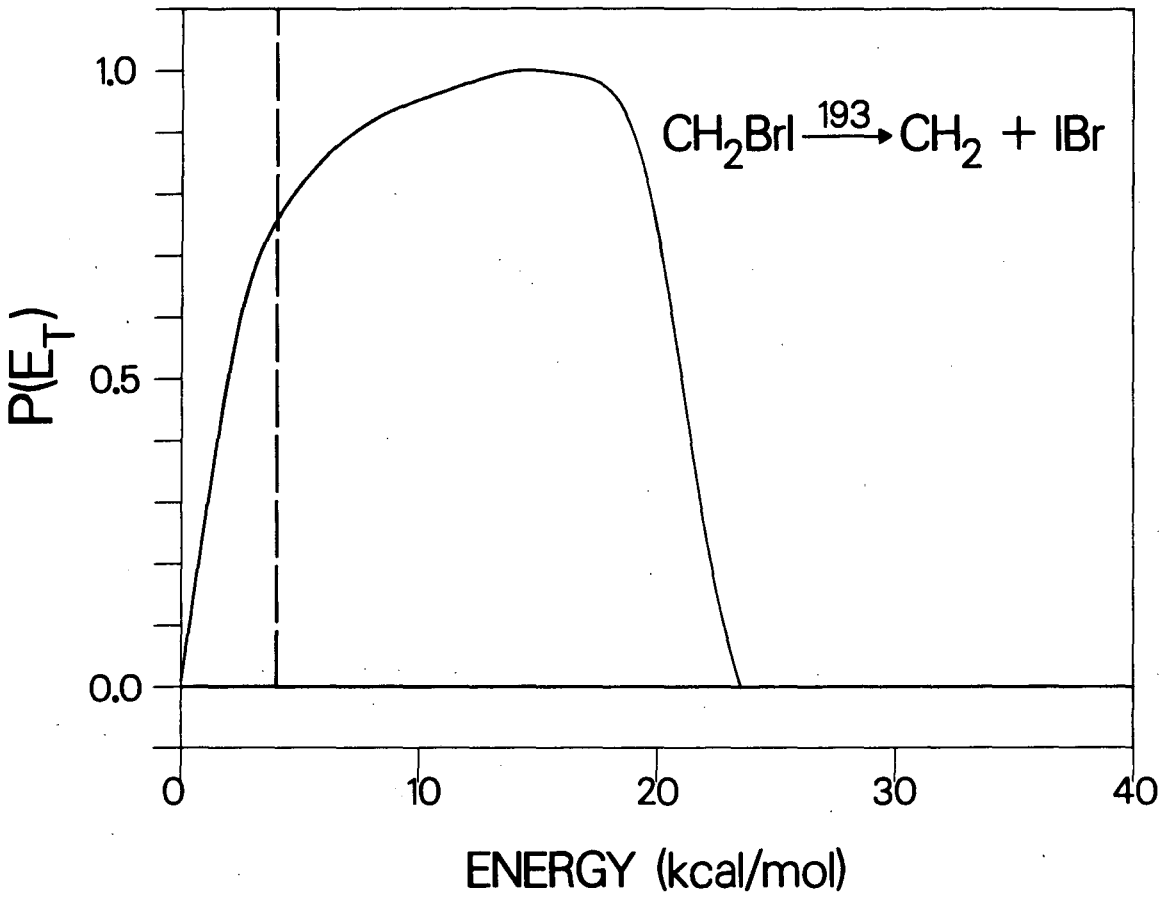

XBL 859 3794

Fig. 22

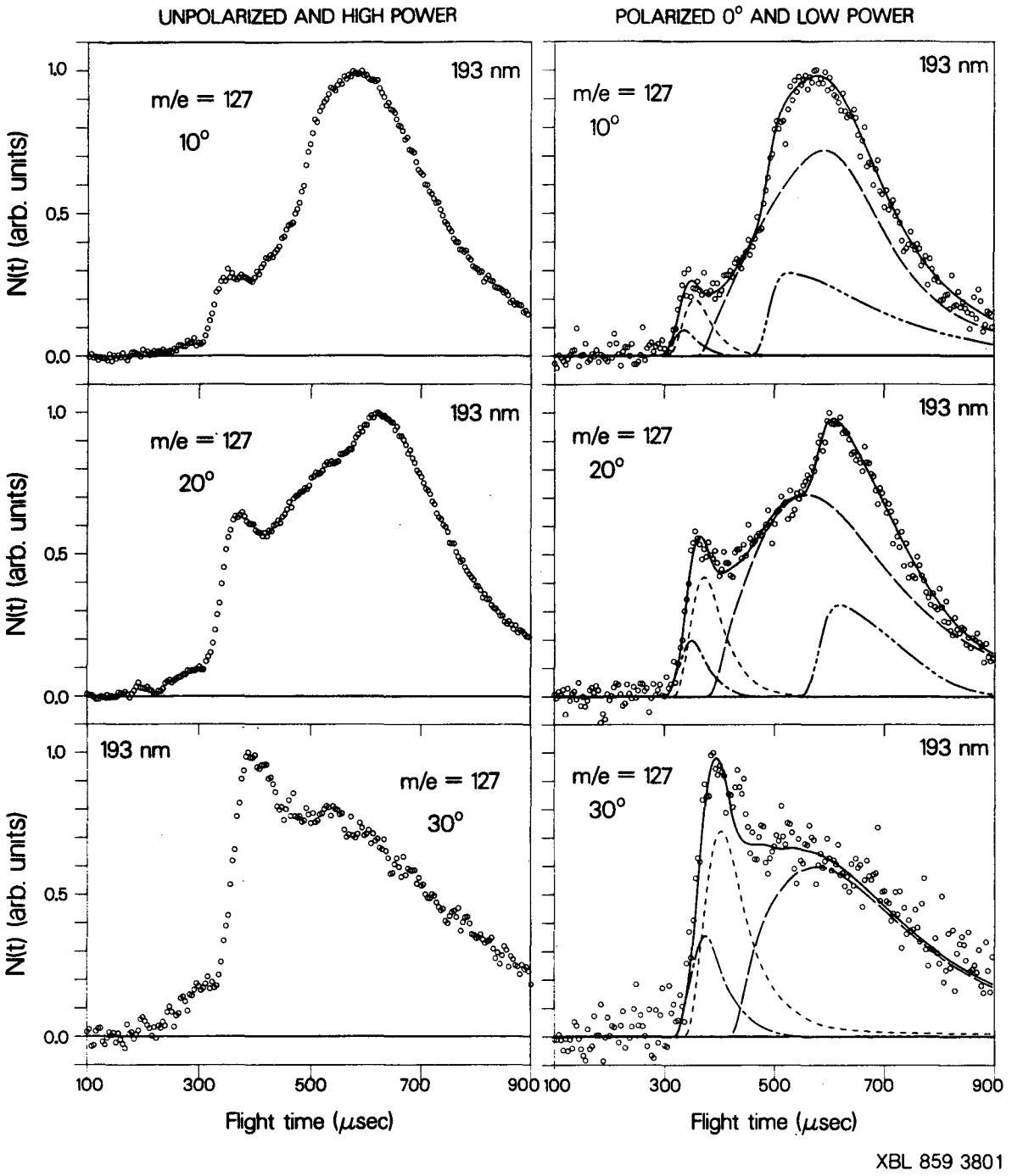
UNPOLARIZED AND HIGH POWER
POLARIZED 0° AND LOW POWER
193 nm
m/e = 127
10°
20°
30°
N(t) (arb. units)
1.0
0.5
0.0
100
300
500
700
900
Flight time (μsec)
XBL 859 3801

Fig. 23

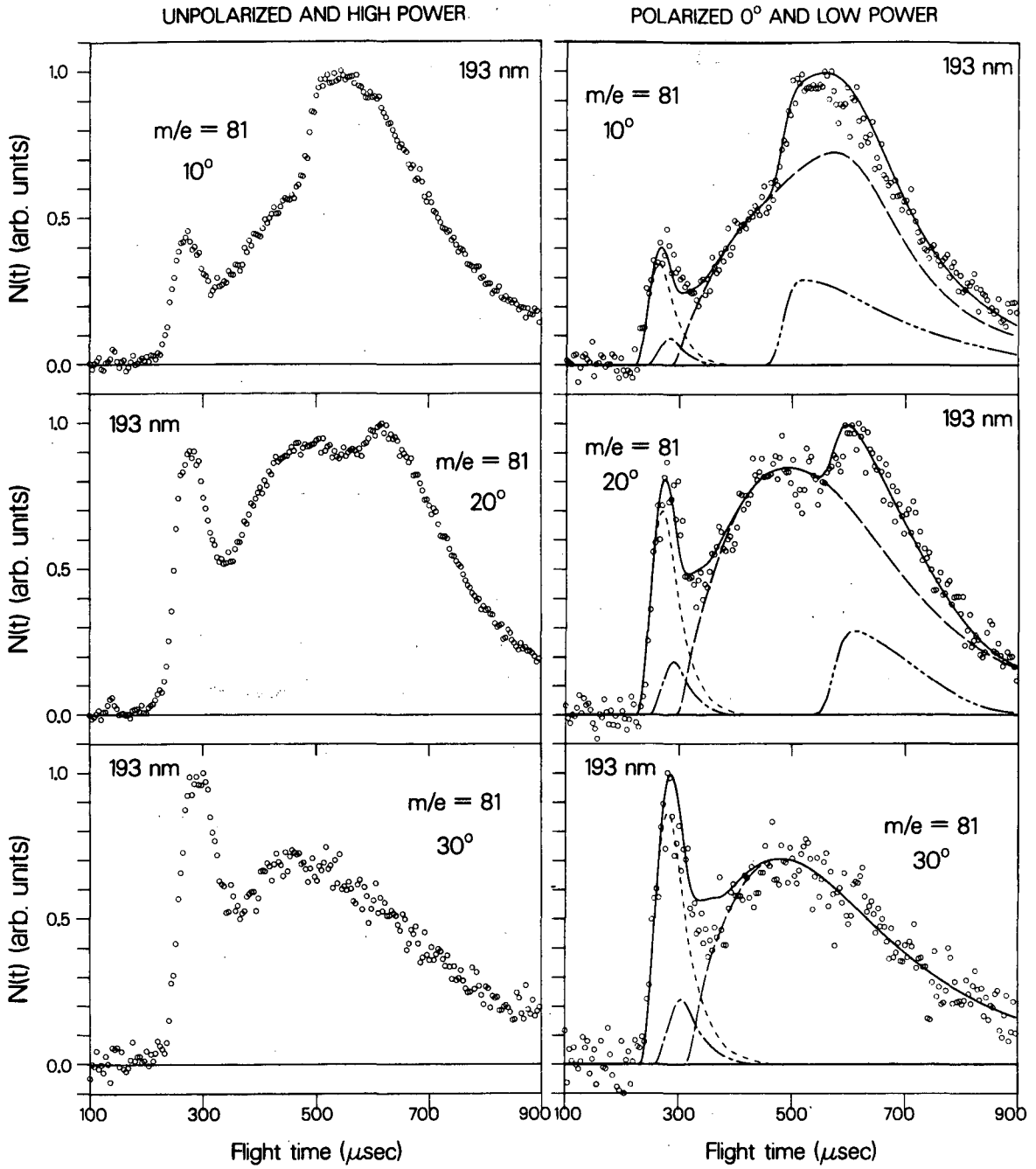

XBL 859 3824

Fig. 24

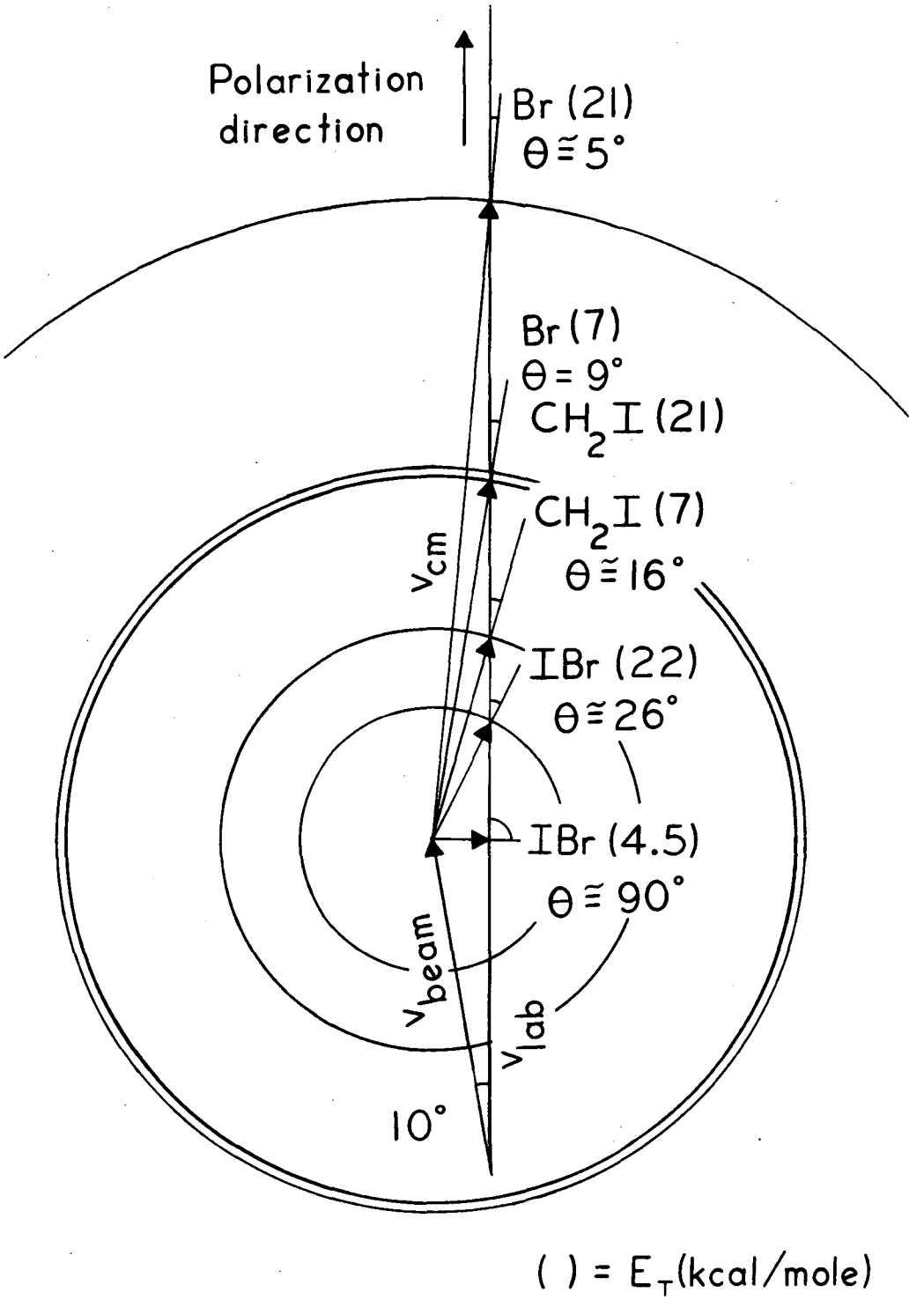

XBL 859-4101

Fig. 25

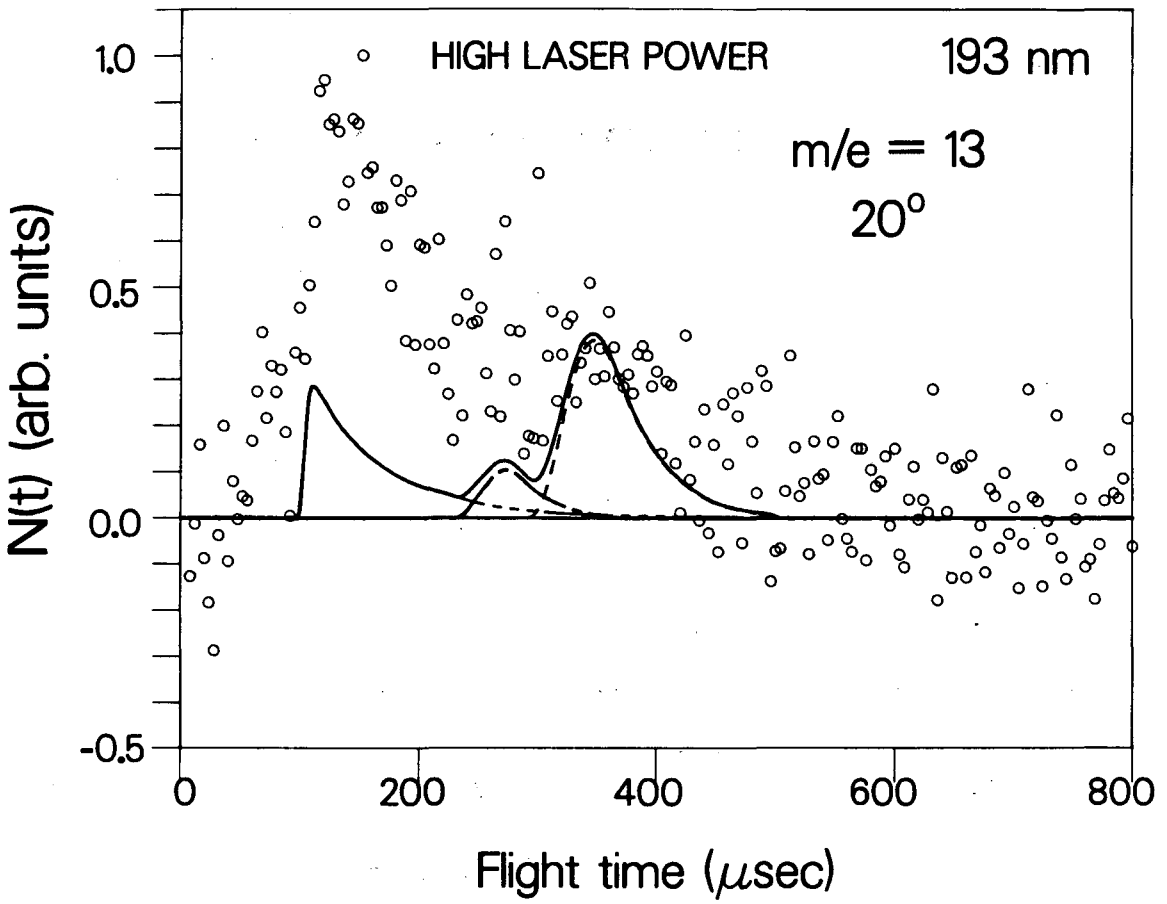

XBL 859 3826

Fig. 26

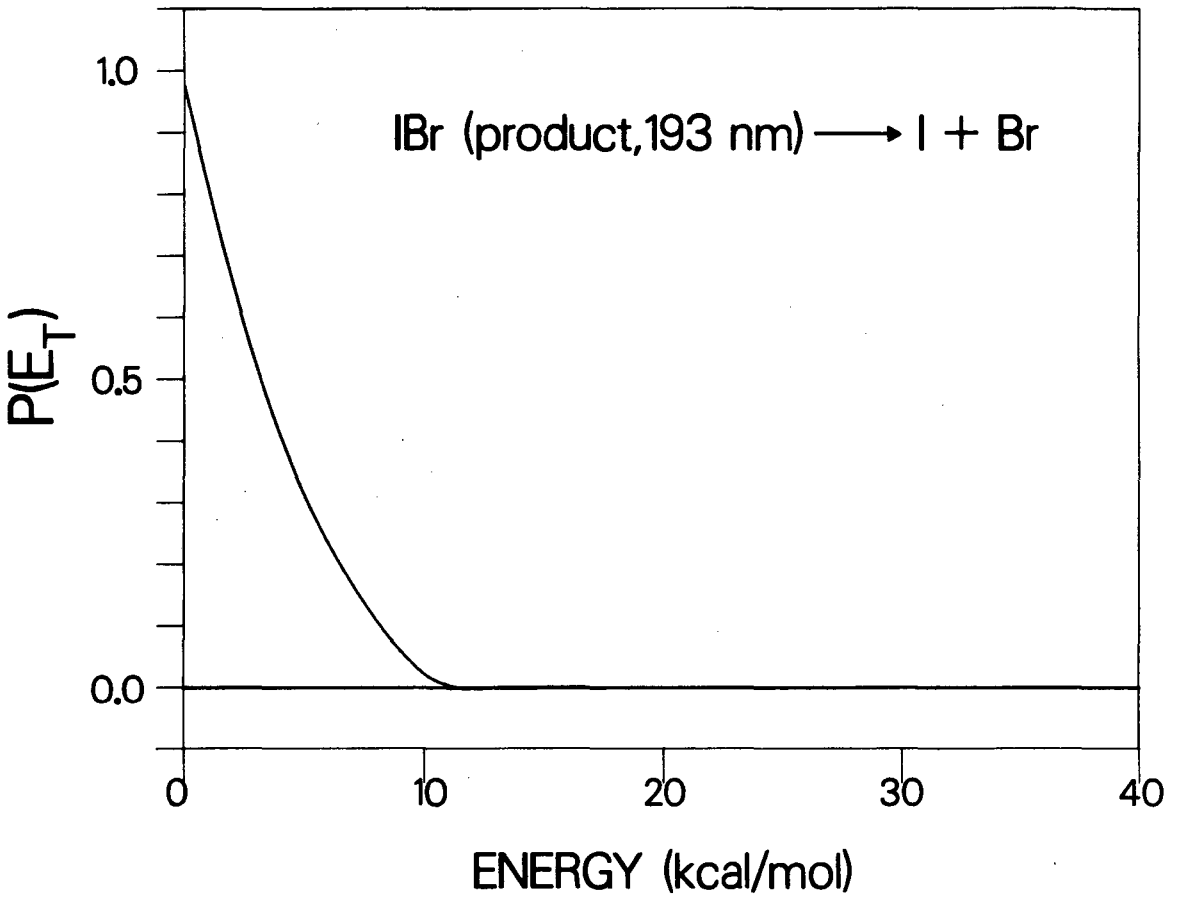

XBL 859 3828

Fig. 27

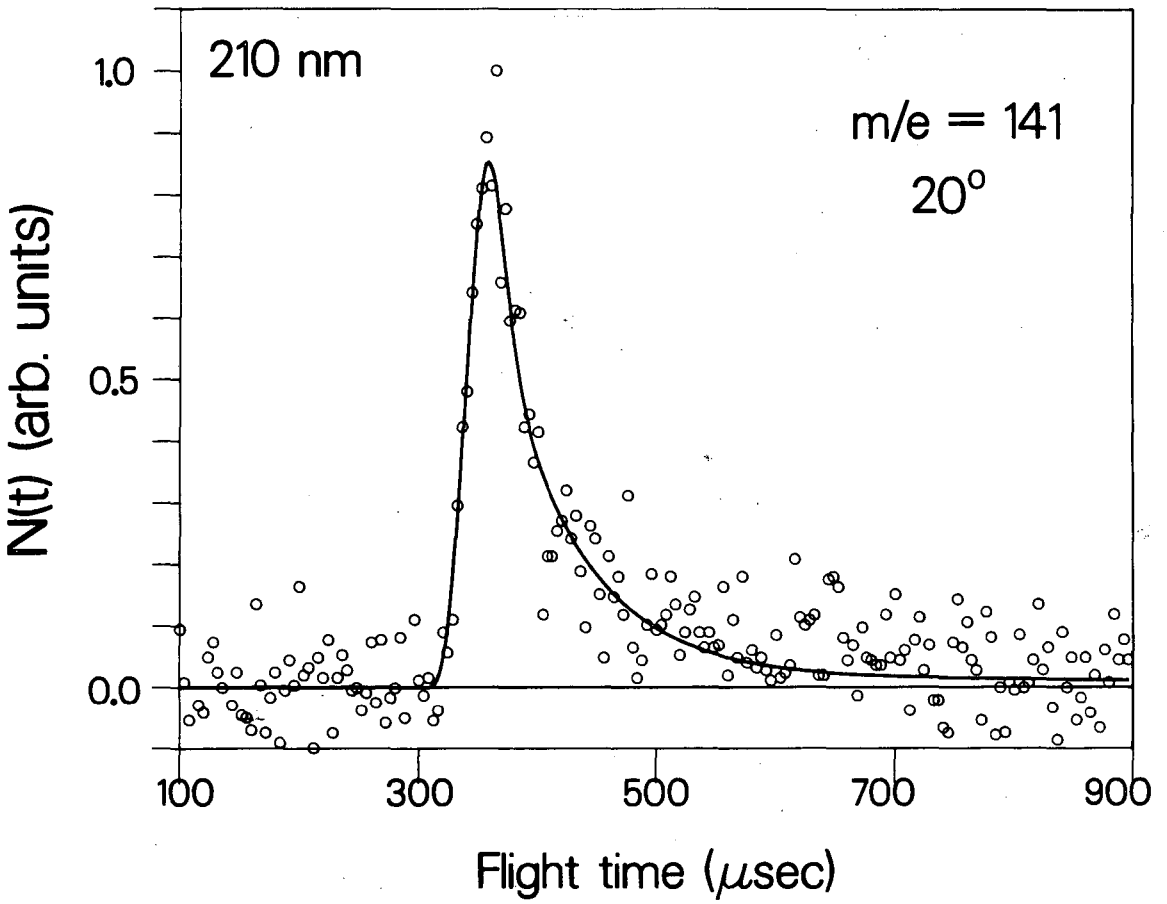

XBL 859 3827

Fig. 28

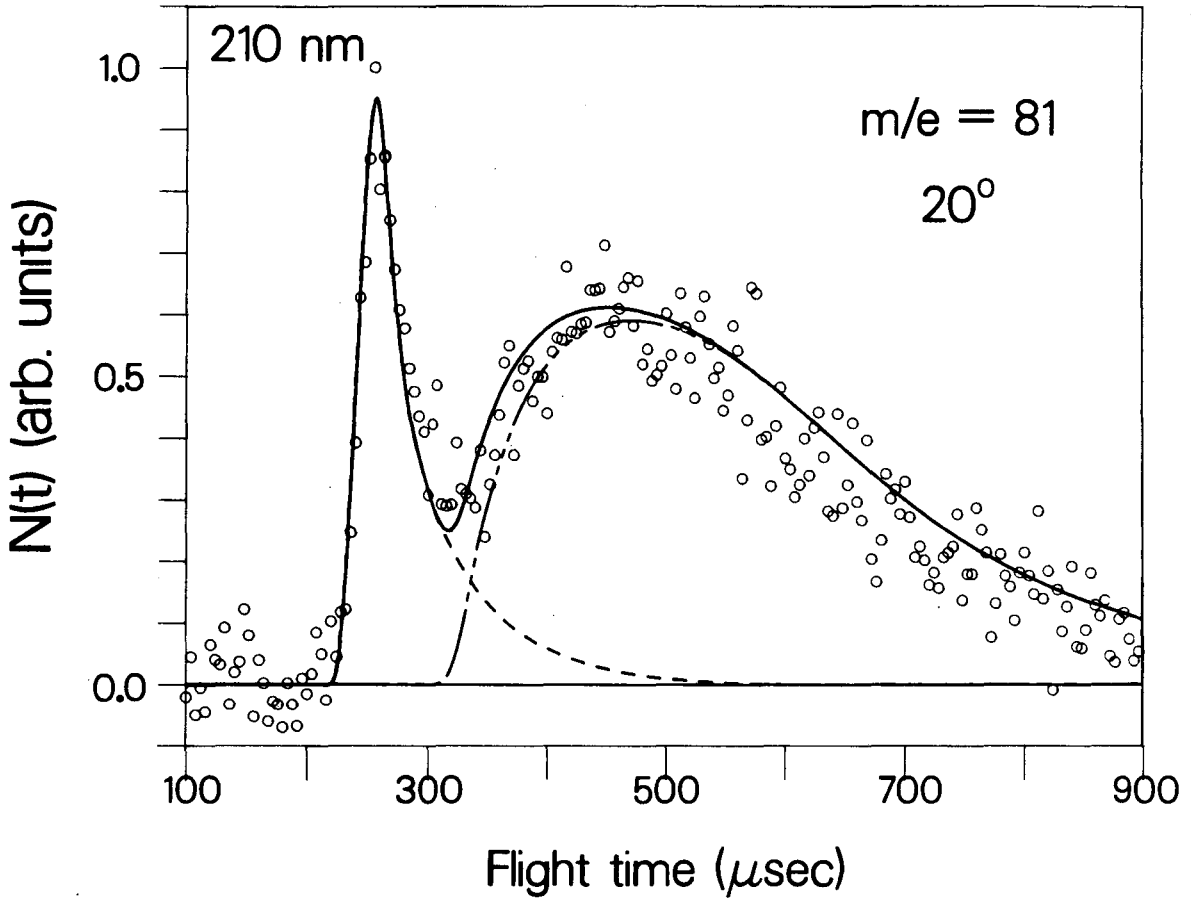

XBL859 3869

Fig. 29

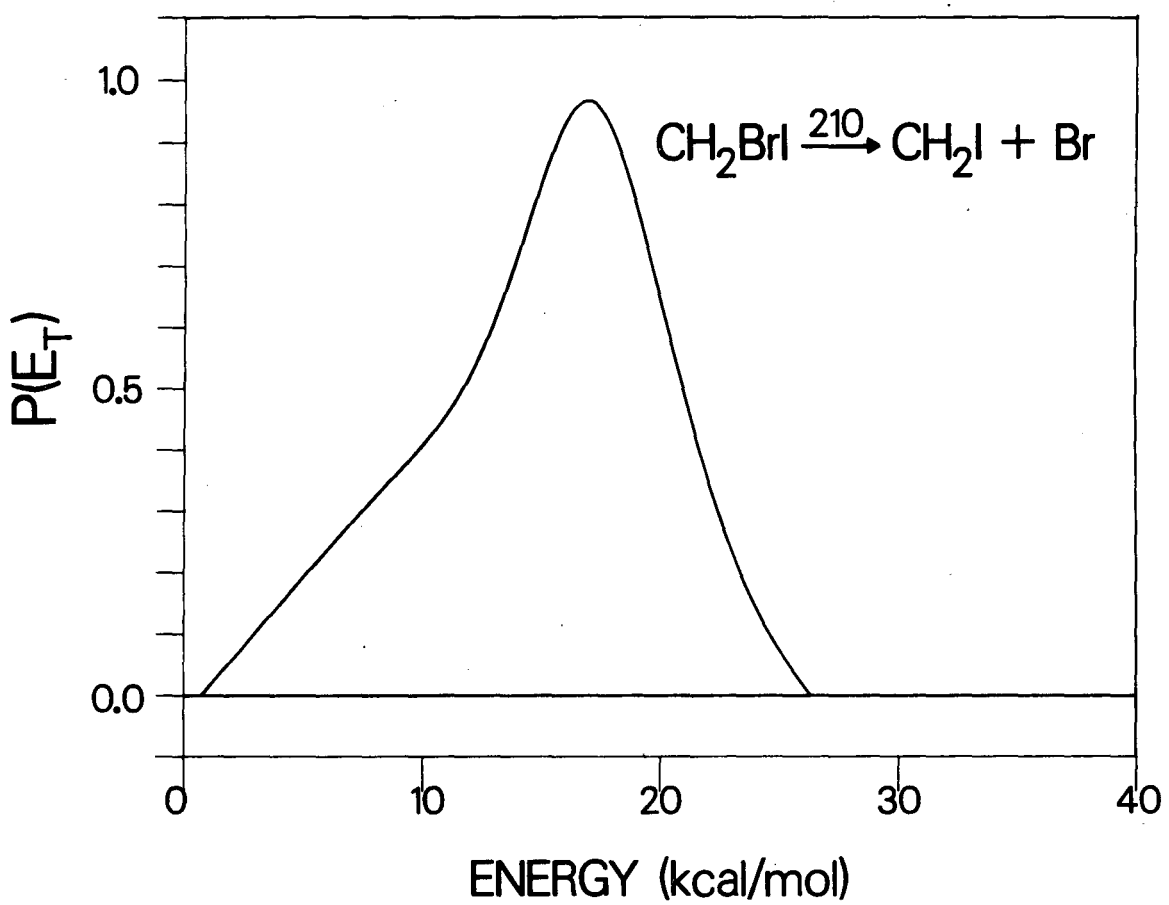

XBL 859 3829

Fig. 30

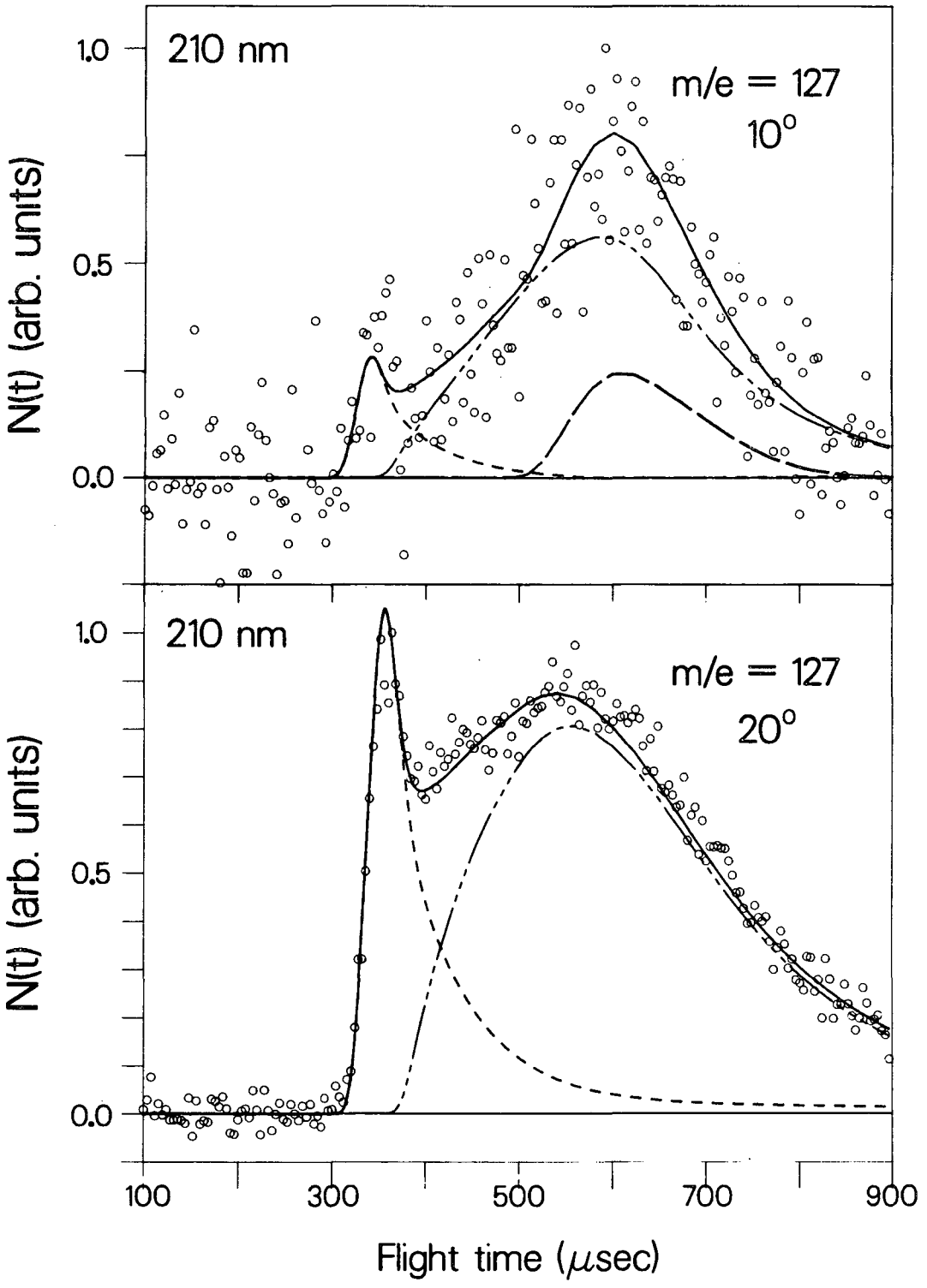

XBL 859 3865

Fig. 31

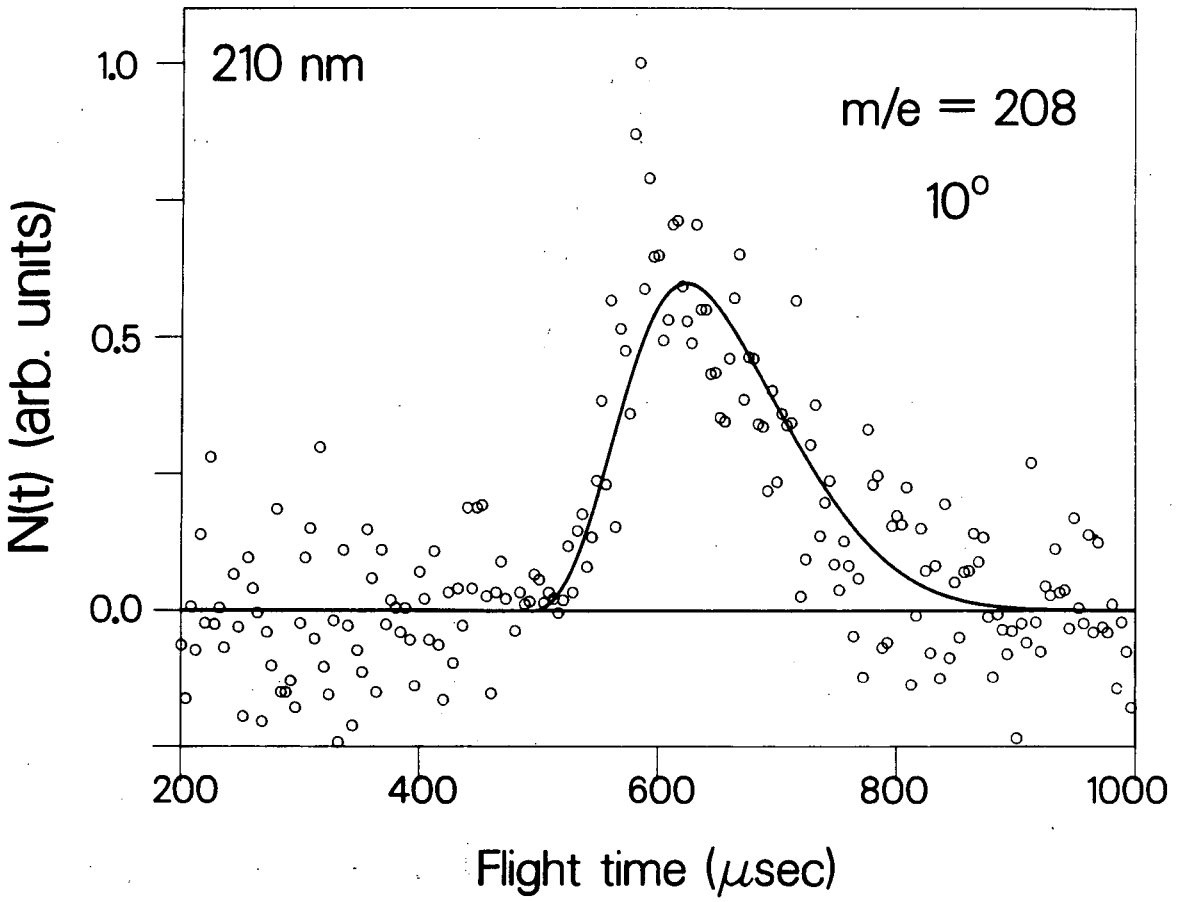

XBL 859 3868

Fig. 32

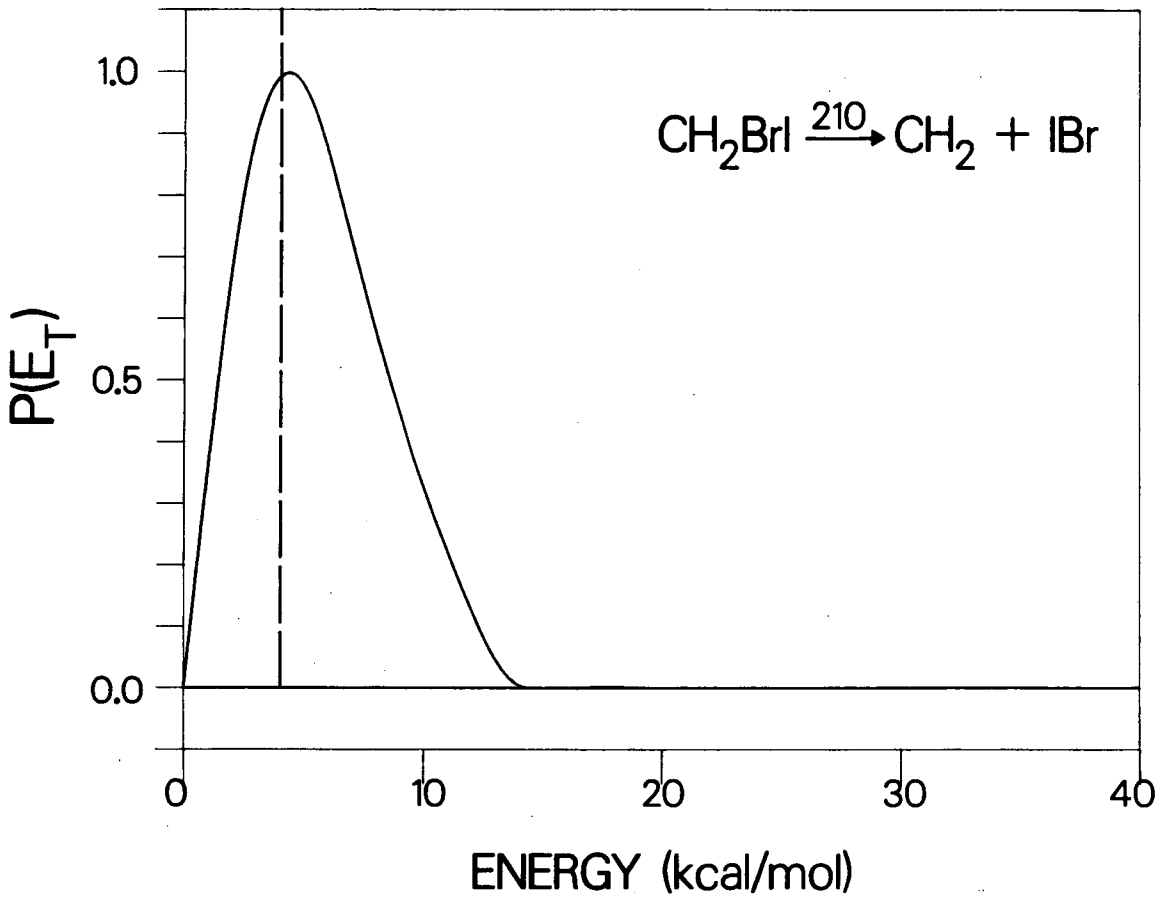

Fig. 33

XBL 859 3872

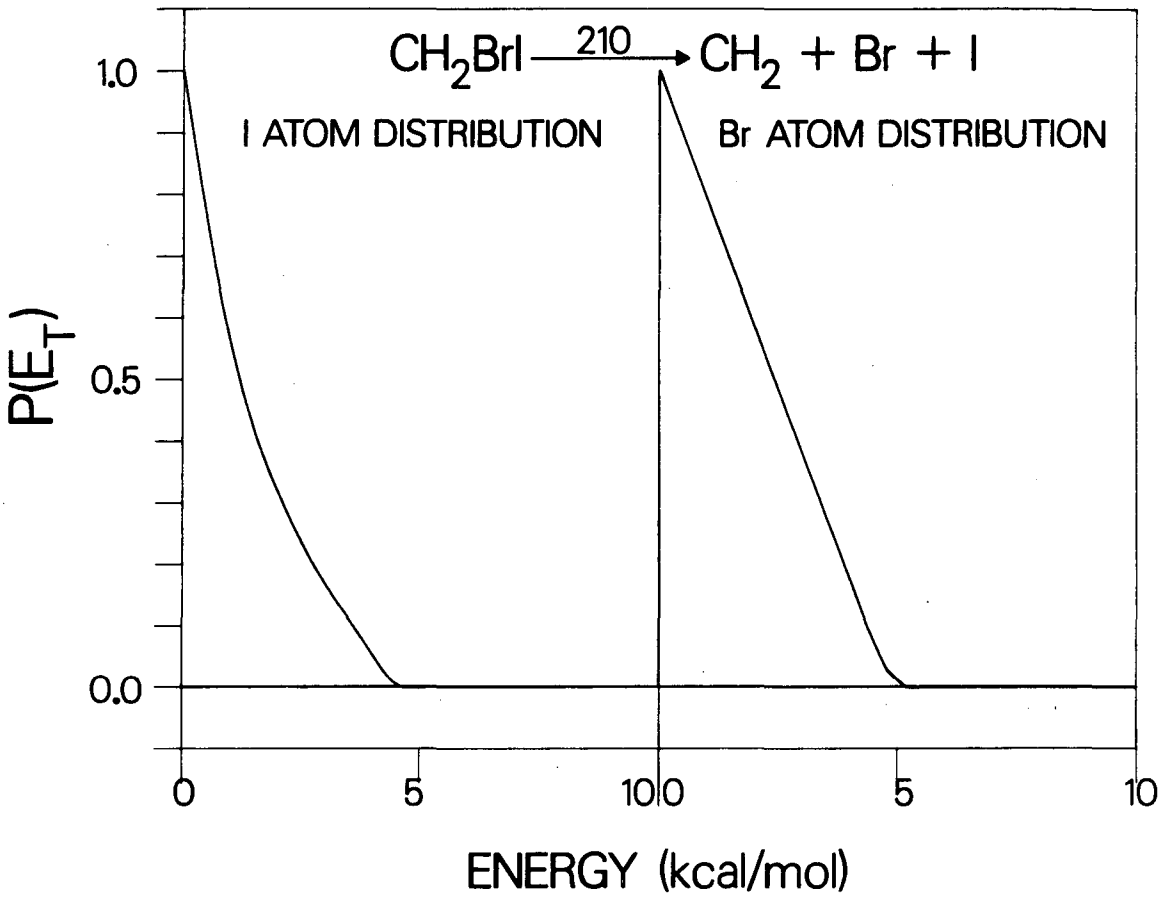

XBL 859 3867

Fig. 34

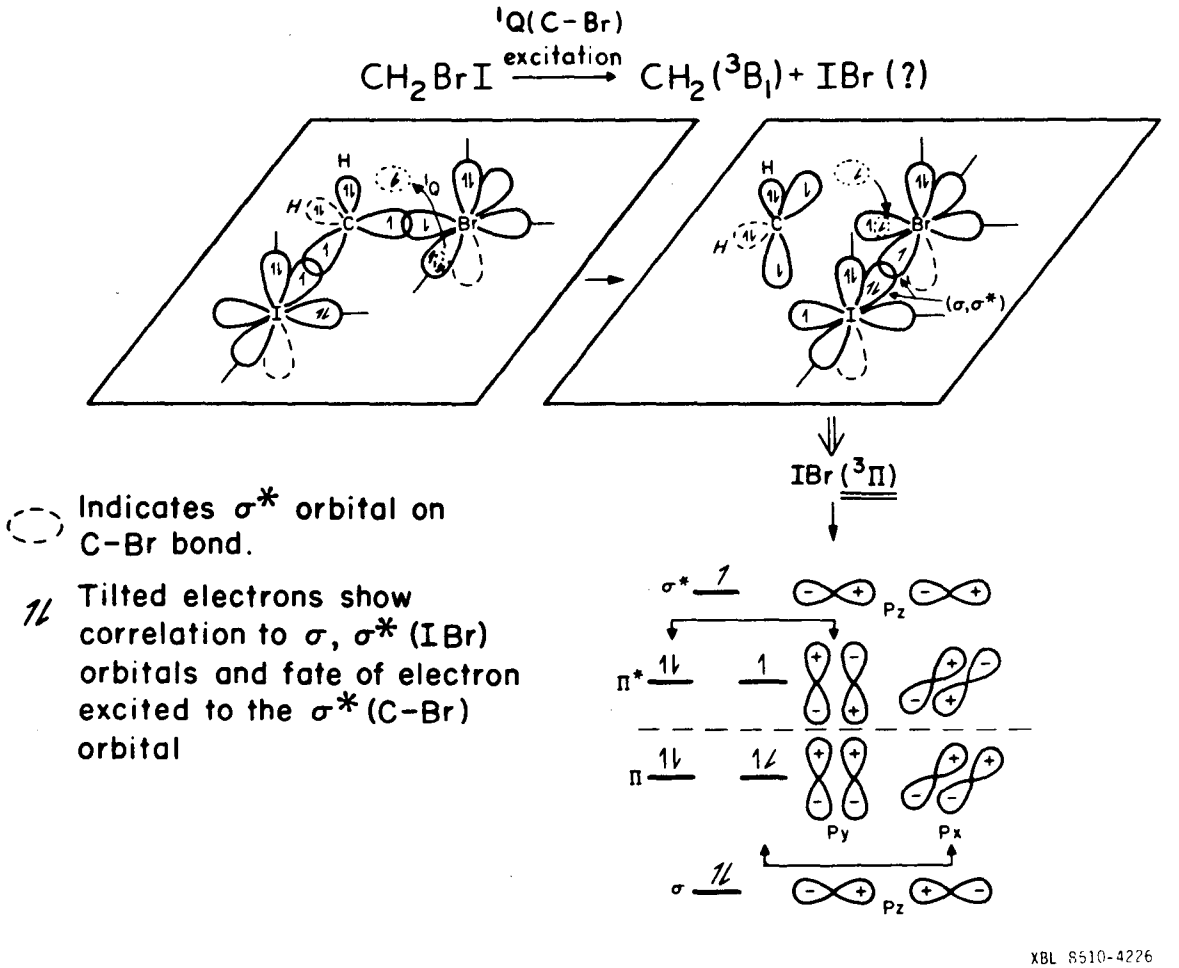
¹Q(C-Br)
CH2BrI excitation CH2(³B1) + IBr (?)
H
C
Br
I
(σ,σ*)
IBr (³Π)
σ*
Pz
π*
π
Py
Px
σ
Indicates σ* orbital on C-Br bond.
Tilted electrons show correlation to σ, σ* (IBr) orbitals and fate of electron excited to the σ* (C-Br) orbital
XBL 8510-4226

Fig. 35

This report was done with support from the Department of Energy. Any conclusions or opinions expressed in this report represent solely those of the author(s) and not necessarily those of The Regents of the University of California, the Lawrence Berkeley Laboratory or the Department of Energy.

Reference to a company or product name does not imply approval or recommendation of the product by the University of California or the U.S. Department of Energy to the exclusion of others that may be suitable.

LAWRENCE BERKELEY LABORATORY
TECHNICAL INFORMATION DEPARTMENT
UNIVERSITY OF CALIFORNIA
BERKELEY, CALIFORNIA 94720